Summer 8-13-2010

Combinatorial Polymer Synthesis and High-Throughput Screening Technology to Identify Optimal Approaches for Mineralized Tissue Engineering

Darren M. Brey
University of Pennsylvania, brey@seas.upenn.edu

Combinatorial Polymer Synthesis and High-Throughput Screening Technology to Identify Optimal Approaches for Mineralized Tissue Engineering

Abstract
The general tissue engineering approach is to combine cells, scaffolding, and signaling molecules in a manner that treats damaged or diseased tissues. Progress in the field has been made incrementally since changes to these inputs require meticulous iterative steps. However, recent advances in combinatorial chemistry and high through-put screening (HTS) technology have made available a wider range of potential scaffold materials with diverse properties, as well as new methods to accelerate the process of testing soluble factors or combinations of factors.

To this end, a library of poly(β-amino ester)s has been developed as the first combinatorial library of photopolymerizable and biodegradable materials. Polymers formed from this library were characterized with respect to changes in chemistry, macromer molecular weight, and macromer branching, which all affected the degradation, mechanics, and cellular interactions of the materials. Using set design criteria with respect to degradation and cellular interactions, the library was screened to identify an osteoconductive material for use in bone tissue engineering. The identified macromer, A6, was processed into porous scaffolds using a particulate leaching technique.

When implanted, A6 scaffolds had minimal inflammation and tissue readily invaded the porous structure, but no bone formation was observed with A6 scaffolds alone. However, in intramuscular and critical-sized cranial defect studies, the addition of BMP-2 led to the induction of bone formation throughout the scaffold, which surpassed control groups. Yet, in a femur window defect model, the empty defect healed equally to the A6 scaffold with BMP-2, illustrating the importance of a critical-sized defect in assessing tissue engineering approaches.

Using HTS techniques, a library of 1040 soluble factors was screened for promoters and inhibitors of osteogenesis in mesenchymal stem cells. 36 potential promoters and 20 potential inhibitors were identified, using statistical outcomes to identify hits that met criteria related to alkaline phosphatase activity and viability. Three of the promoters were investigated further using traditional culture to confirm their osteogenic behavior.

This work illustrates the importance of combinatorial libraries and HTS techniques in identifying new materials and soluble factors towards tissue regeneration applications and can be expanded to target a number of different tissues and diseases.

Degree Type
Dissertation

Degree Name
Doctor of Philosophy (PhD)

Graduate Group
Bioengineering

First Advisor
Jason A Burdick

Keywords
combinatorial library, high-throughput screening, mesenchymal stem cells, mineralization, bone tissue engineering

Subject Categories
Biomaterials | Molecular, Cellular, and Tissue Engineering

COMBINATORIAL POLYMER SYNTHESIS AND HIGH-THROUGHPUT SCREENING TECHNOLOGY TO IDENTIFY OPTIMAL APPROACHES FOR MINERALIZED TISSUE ENGINEERING

Darren M. Brey

A Dissertation in Bioengineering

Presented to the Faculties of the University of Pennsylvania

in Partial Fulfillment of the Requirements for the Degree of Doctor of Philosophy

2010

_____

Supervisor of Dissertation
Dr. Jason A. Burdick

_____

Graduate Group Chairperson
Dr. Susan S. Margulies

Dissertation Committee
Andrew Tsourkas, PhD
Kurt Hankenson, DVM, MS, PhD
Jonathan Garino, MD

ACKNOWLEDGEMENTS

I would first like to thank my advisor, Dr. Jason Burdick, who took me on as a transfer from Northwestern University after a few emails and a meeting at Starbucks. He has been there to guide, challenge, and goad me through this work the last five years. I am eternally grateful for all that he has taught me through discussions and his actions.

To the Burdick Lab: it has been a wonderful experience over the last 5 years watching the lab grow from scratch. I deeply appreciate the discussions, scientific and otherwise, with Dr. Cindy Chung and Jamie Ifkovits as we moved from a nomadic group of researchers to a bustling lab in Skirkanich Hall. And thanks to Josh Katz, whose expertise as a chemist, as well as being the only other married student in lab, were invaluable to me with my mechanical engineering background. To GABE, my Manayunk volleyball team, and the Philadelphia Central Board, I thank you for giving me athletic outlets.

I would like to acknowledge my thesis committee: Dr. Kurt Hankenson for providing laboratory equipment and expertise on bone regeneration, Dr. Jonathan Garino for surgical training and advice on the femur window defect, and Dr. Andrew Tsourkas, whose lab underwent some shared lab hopping beginnings, for chairing my thesis committee. I would be remiss if I did not thank Dr. Susan Margulies and Dr. David Meaney for providing bench space for me to start my work during the first year. And thanks also to Dr. Steve Nicoll, who not only provided space for me in his lab that first year, but was also responsible for meeting me on a cold call and putting me in contact

with Dr. Burdick. I am also very grateful for my funding sources, including National Institutes of Health and U.S. Department of Veterans Affairs.

Finally I would like to thank my family: my parents for their love and support, and my brothers, especially Eric, whose shared experience in getting a PhD has been an invaluable resource through many trials and tribulations. Most of all I would like to thank my lovely wife Jen, who over the last 12 years has shared in our many adventures in life that will soon include our fifth collegiate degree and fourth city to call home. Our most important adventure is the recent addition of our son Calvin, whose presence is constant source of joy.

ABSTRACT

COMBINATORIAL POLYMER SYNTHESIS AND HIGH-THROUGHPUT SCREENING TECHNOLOGY TO IDENTIFY OPTIMAL APPROACHES FOR MINERALIZED TISSUE ENGINEERING

Darren M. Brey

Advisor: Jason A. Burdick, Ph.D.

The general tissue engineering approach is to combine cells, scaffolding, and signaling molecules in a manner that treats damaged or diseased tissues. Progress in the field has been made incrementally since changes to these inputs require meticulous iterative steps. However, recent advances in combinatorial chemistry and high through-put screening (HTS) technology have made available a wider range of potential scaffold materials with diverse properties, as well as new methods to accelerate the process of testing soluble factors or combinations of factors.

To this end, a library of poly(β-amino ester)s has been developed as the first combinatorial library of photopolymerizable and biodegradable materials. Polymers formed from this library were characterized with respect to changes in chemistry, macromer molecular weight, and macromer branching, which all affected the degradation, mechanics, and cellular interactions of the materials. Using set design criteria with respect to degradation and cellular interactions, the library was screened to

identify an osteoconductive material for use in bone tissue engineering. The identified macromer, A6, was processed into porous scaffolds using a particulate leaching technique.

When implanted, A6 scaffolds had minimal inflammation and tissue readily invaded the porous structure, but no bone formation was observed with A6 scaffolds alone. However, in intramuscular and critical-sized cranial defect studies, the addition of BMP-2 led to the induction of bone formation throughout the scaffold, which surpassed control groups. Yet, in a femur window defect model, the empty defect healed equally to the A6 scaffold with BMP-2, illustrating the importance of a critical-sized defect in assessing tissue engineering approaches.

Using HTS techniques, a library of 1040 soluble factors was screened for promoters and inhibitors of osteogenesis in mesenchymal stem cells. 36 potential promoters and 20 potential inhibitors were identified, using statistical outcomes to identify hits that met criteria related to alkaline phosphatase activity and viability. Three of the promoters were investigated further using traditional culture to confirm their osteogenic behavior.

This work illustrates the importance of combinatorial libraries and HTS techniques in identifying new materials and soluble factors towards tissue regeneration applications and can be expanded to target a number of different tissues and diseases.

TABLE OF CONTENTS

LIST OF TABLES

LIST OF FIGURES

CHAPTER 1: *Introduction*

Tissue engineering involves the combination of cells, signaling factors, and 3-dimensional scaffolding to repair or replace damaged or diseased tissues [1]. This field has relied on the iterative development of the various components and advances have been slow and have not met previous expectations. Recently, the development and use of high-throughput and combinatorial techniques in tissue engineering has significantly enhanced this process through its efficient and productive platforms. Combinatorial techniques often eliminate or reduce tedious synthesis and purification steps, and techniques for more rapid assessment of these materials have improved, which can lead to more rapid polymer development [2]. High throughput assessment of combinatorial libraries of molecules, which has been used by pharmaceutical companies has translated more recently as a method of screening classes of soluble factors in order to identify stimulatory molecules for tissue repair [3]. As this field progresses, existing and new high-throughput techniques will be crucial in efficiently and rapidly developing ideal synergies between microenvironments and signaling factors for engineered tissues. These techniques will be reviewed in more detail in Chapter 3.

One area where these high throughput and combinatorial techniques may make an impact is in mineralized tissue repair. Bones are a dense connective tissue that provides structure, support, and protection to the body and organs. Despite their strong and seemingly rigid form, bones are highly vascularized and are constantly under a state of remodeling, where old bone is broken down only to be replaced with new bone [4].

These characteristics help explain why bones are also highly capable of healing following a normal fracture, through well studied stages. After an inflammatory period which forms a hemotoma in the first week after fracture, a soft callus is formed where osteoprogenitor cells begin to multiply and start creating extracellular matrix to support new mineralization. This callus hardens until around 4 months post fracture, in which the callus is then resorbed through bone remodeling processes.

Unfortunately, not all bone healing follows this paradigm. If a large section of bone is removed, such as during trauma or some cancers, a "non-union" occurs and the bone will never fully heal and the defect will only be filled with fibrous tissue growth [5, 6]. The standard treatment for these cases is bone graft surgeries. Annually there are around 500,000 bone graft surgeries in the United States and over 2.2 million worldwide [7]. The current state of the art for these surgeries are autografts, which requires harvesting healthy bone tissue from another part of the body to be implanted at the diseased or traumatized site. These approaches are not always ideal as they require a secondary surgery site (which can be painful and risks infection), as well as the limited bone tissue available if the defects are particularly large.

As an alternative, allografts utilize decellularized bone harvested from cadavers. These implants run the risk of being immunologically rejected and can transmit disease. Other alternatives include man made materials such as metals and ceramics, but these are subject to wear and stress shielding, which cause surrounding bone to degrade with time. However, our approach involves the use of biodegradable polymers, optimized for cellular interactions, which will stimulate natural bone regeneration using therapeutic molecule delivery. This route is advantageous over these other techniques in that the

scaffolding is not permanent, it requires only one surgery location, and is acellular so there is no rejection of non-native tissue. The significance of this research is that this composite material, if successful, can be used universally in bone loss applications, since use does not require patient-specific tissues.

Bone tissue engineering often involves one or more of the following components: (1) harvested osteoblast cells or osteoprogenitor cells, (2) osteoinductive signaling molecules, and (3) three-dimensional (3D) osteoconductive matrices to stimulate the body's natural healing processes [8, 9]. In recent years, a dearth of research has been conducted on bone tissue engineering, ranging from new scaffolding materials to the delivery of a wide range of cells. Our approach relies primarily on the development and optimization of biodegradable polymers for mineralized tissue formation.

The basic design criteria for polymeric scaffolding for mineralized tissue repair have been laid out by many researchers [9, 10]. In particular, the scaffolds should be readily available to surgeons, promote bone infiltration, degrade predictably as bone infiltrates, be adaptable to irregular shapes and fractures, possess correct mechanical and physical properties, not induce soft tissue growth at the bone-implant interface, and have pore sizes from 200-400 μm [9]. It may also be beneficial for these materials to promote the formation of extracellular matrix and serve as carriers for cells or growth factors[10].

Several polymers have been investigated for use as orthopaedic biomaterials due to their flexibility and range of physical properties. Polylactic acid (PLA) and polyglycolic acid (PGA) have long been used in the medical fields for such items as biodegradable sutures. However, the osteoconductive behavior of these materials has been demonstrated in 2D [11] and 3D [12] scaffolds. In critical size defects, PLA and

PLGA scaffolding have been shown to support bone tissue formation [13]. Poly(propylene fumarate)s (PPFs) have also been developed as in situ forming degradable polymers [14]. The double bonds in the backbone allow for thermal or photo polymerization with the addition of an initiator. The addition of β-tricalcium phosphate has been shown to make PPF osteoconductive [15] and bone tissue ingrowth has been demonstrated in non-critical sized calvarial defects [16]. Tyrosine-derived polycarbonates have been shown to possess good compatibly and cellular response in orthopaedic applications, and good osteoconductivity when implanted into bone tissue [17].

The use of osteoinductive factors is also important in bone tissue engineering paradigms. Many successful tissue regeneration approaches have involved the use of growth factors at an injury site. Several factors have been used, including transforming growth factor-β1 (TGF-β1) [18], platelet derived growth factor (PDGF) [19], and bone morphogenetic proteins (BMPs) [20-22]. BMP-2 has been shown in many cases to speed the healing of bones in a variety of animal models [22-24].

This dissertation is meant to characterize a new library of materials with diverse properties and develop screening techniques and tools to evaluate the materials, using bone tissue engineering as a representative application. Additionally, high-throughput screening techniques will be utilized to discover small molecules that influence osteogenesis in a range of cell types. These techniques will help speed up the development of new materials and molecules that may be useful in bone tissue engineering.

References:

[1] Langer R, Vacanti JP. Tissue Engineering. Science 1993;260(5110):920-926.

[2] Hoogenboom R, Meier MAR, Schubert US. Combinatorial methods, automated synthesis and high-throughput screening in polymer research: Past and present. Macromolecular Rapid Communications 2003;24(1):16-32.

[3] Goldberg M, Mahon K, Anderson D. Combinatorial and rational approaches to polymer synthesis for medicine. Advanced Drug Delivery Reviews 2008;60(9):971-978.

[4] Lieberman JR, Friedlander GE. Bone regeneration and repair : biology and clinical applications. Totowa, N.J.: Humana Press, 2005.

[5] Einhorn TA, O'Keefe RJ, Buckwalter JA. Orthopaedic Basic Science: Foundations of Clinical Practice. Third ed. Rosemont, IL: American Academy of Orthopaedic Surgeons, 2007.

[6] Miller MD. Review of Orthopaedics. Philadelphia: Saunders, 2004.

[7] Giannoudis PV, Dinopoulos H, Tsiridis E. Bone substitutes: An update. Injury-International Journal of the Care of the Injured 2005;36:20-27.

[8] Vacanti CA, Bonassar LJ. An overview of tissue engineered bone. Clinical Orthopaedics and Related Research 1999(367):S375-S381.

[9] Burg KJL, Porter S, Kellam JF. Biomaterial developments for bone tissue engineering. Biomaterials 2000;21(23):2347-2359.

[10] Agrawal CM, Ray RB. Biodegradable polymeric scaffolds for musculoskeletal tissue engineering. Journal of Biomedical Materials Research 2001;55(2):141-150.

[11] Ishaug SL, Yaszemski MJ, Bizios R, Mikos AG. Osteoblast Function on Synthetic Biodegradable Polymers. Journal of Biomedical Materials Research 1994;28(12):1445-1453.

[12] Ishaug SL, Crane GM, Miller MJ, Yasko AW, Yaszemski MJ, Mikos AG. Bone formation by three-dimensional stromal osteoblast culture in biodegradable polymer scaffolds. Journal of Biomedical Materials Research 1997;36(1):17-28.

[13] Winn SR, Schmitt JM, Buck D, Hu YH, Grainger D, Hollinger JO. Tissue-engineered bone biomimetic to regenerate calvarial critical-sized defects in athymic rats. Journal of Biomedical Materials Research 1999;45(4):414-421.

[14] Yaszemski MJ, Payne RG, Hayes WC, Langer R, Mikos AG. In vitro degradation of a poly(propylene fumarate)-based composite material. Biomaterials 1996;17(22):2127-2130.

[15] Peter SJ, Yaszemski MJ, Suggs LJ, Payne RG, Langer R, Hayes WC, et al. Characterization of partially saturated poly(propylene fumarate) for orthopaedic application. Journal of Biomaterials Science-Polymer Edition 1997;8(11):893-904.

[16] Vehof JWM, Fisher JP, Dean D, van der Waerden J, Spauwen PHM, Mikos AG, et al. Bone formation in transforming growth factor beta-1-coated porous poly(propylene fumarate) scaffolds. Journal of Biomedical Materials Research 2002;60(2):241-251.

[17] James K, Levene H, Parsons JR, Kohn J. Small changes in polymer chemistry have a large effect on the bone-implant interface: evaluation of a series of

degradable tyrosine-derived polycarbonates in bone defects. Biomaterials 1999;20(23-24):2203-2212.

[18] Beck LS, Deguzman L, Lee WP, Xu Y, McFatridge LA, Gillett NA, et al. Tgf-Beta-1 Induces Bone Closure of Skull Defects. Journal of Bone and Mineral Research 1991;6(11):1257-1265.

[19] Park YJ, Lee YM, Park SN, Sheen SY, Chung CP, Lee SJ. Platelet derived growth factor releasing chitosan sponge for periodontal bone regeneration. Biomaterials 2000;21(2):153-159.

[20] Boden SD. Bioactive factors for bone tissue engineering. Clinical Orthopaedics and Related Research 1999(367):S84-S94.

[21] Urist MR. Bone morphogenetic protein: The molecularization of skeletal system development. Journal of Bone and Mineral Research 1997;12(3):343-346.

[22] Yasko AW, Lane JM, Fellinger EJ, Rosen V, Wozney JM, Wang EA. The Healing of Segmental Bone Defects, Induced by Recombinant Human Bone Morphogenetic Protein (Rhbmp-2) - a Radiographic, Histological, and Biomechanical Study in Rats. Journal of Bone and Joint Surgery-American Volume 1992;74A(5):659-670.

[23] Peng HR, Usas A, Olshanski A, Ho AM, Gearhart B, Cooper GM, et al. VEGF improves, whereas sFlt1 inhibits, BMP2-induced bone formation and bone healing through modulation of angiogenesis. Journal of Bone and Mineral Research 2005;20(11):2017-2027.

[24] Li G, Cui YX, McIlmurray L, Allen WE, Wang HL. RhBMP-2, rhVEGF(165), rhPTN and thrombin-related peptide, TP508 induce chemotaxis of human

osteoblasts and microvascular-endothelial cells. Journal of Orthopaedic Research 2005;23(3):680-685.

CHAPTER 2: *Research Overview*

2.1 Specific Aims and Hypotheses

The field of tissue engineering has long searched for the proper combination of materials, soluble factors, and cellular therapies for a variety of clinical applications. These approaches have often involved narrowly focused studies on materials with only small variations, limited exposure to expensive growth factors or genetic therapies, or the use of different populations of multipotent stem cells. Recently, combinatorial libraries of biomaterials have largely increased the pool of potential materials for use as tissue engineering scaffolding. Although pharmaceutical companies have used combinatorial syntheses and screening techniques to identify potential drug therapies, these approaches are only now finding use within the field of tissue engineering. This technology may be very useful in identifying formulations for optimal tissue regeneration approaches, as long as they are easily developed and screened.

In this dissertation, a new library of photocrosslinkable, biodegradable poly(β-amino ester)s (PBAEs) has been developed as a class of materials for a range of biomedical applications. This library was screened to identify a polymer with osteoconductive properties. Libraries of soluble factors were also screened using high throughput technology to identify potential osteoinductive properties. The development of these material synthesis and screening techniques is crucial in rapidly detecting useful formulations for applications in tissue engineering.

Hypothesis: The governing hypothesis of this proposal is that high throughput screening (HTS) techniques can be used to more rapidly identify potential materials and soluble cues for tissue engineering applications, specifically mineralized tissue regeneration. Specific hypotheses are: (1) a combinatorial library of photopolymerizable poly(β-amino ester)s can be synthesized with tunable degradation, mechanical, and cellular interaction properties, (2) screening techniques can identify materials that have osteoconductive properties, and (3) HTS techniques can be utilized to discover new osteoinductive soluble cues.

To test these hypotheses, the following specific aims were proposed and accomplished:

Specific Aim 1. Synthesize and characterize a combinatorial library of poly(β-amino ester)s. A library of easily synthesized, photopolymerizable, and biodegradable materials was synthesized through the addition reaction of commercially available diacrylates and amines. The mechanical properties, degradation, and cellular interactions of these materials were investigated with changes in monomer chemistry, macromer molecular weight, and the addition of trifunctional monomers to induce branching.

Specific Aim 2. Screen libraries of materials to optimize osteoconductive properties. Human mesenchymal stem cells (hMSCs) and osteoblast-like sarcoma cells (SaOS-2) were investigated in 2D in vitro cultures to screen for optimal osteoconductive macromers. Highly porous scaffolds were synthesized from the optimized material, loaded with recombinant human bone morphogenetic protein-2 (rhBMP-2), and

implanted in intramuscular, cranial, and femoral defects to confirm osteoconductive properties in vivo.

Specific Aim 3. Use HTS techniques to identify new osteoinductive factors. HTS of the National Institute of Neurological Diseases and Stroke (NINDS) library of small molecules was used to identify potential osteogenic promoters of hMSC differentiation. The most potent promoters were characterized with materials identified in Aim 2 in vitro.

2.2 Research Summary

The motivation for the development of materials to support mineralized tissue formation has already been discussed in Chapter 1. For critical-sized defects, current techniques are limited in their ability to form new native bone to replace the implant or grafted materials. Chapter 3 reviews previous reports in the use of combinatorial libraries to expand the availability of materials that can be used for tissue engineering, techniques for screening and processing these materials, and the use of HTS techniques to identify molecules or cytokines that can be used to drive stem cell differentiation.

The introduction of PBAEs as a photopolymerizable, biodegradable material will be discussed in Chapter 4. The wide range of mechanical properties and degradation rates available with the library demonstrates the versatile potential that this library affords. These characteristics can be further tuned by controlling the macromer molecular weight as explored in Chapter 5 or by the introduction of branching in Chapter 6. These changes add additional functionality and diversity to the polymers and provide basic material investigation of structure-function relationships. These chapters will also

explore the ability of these materials to support cell attachment and growth, as well as techniques to produce porous scaffolds.

The screening of the PBAE library for an osteoconductive material will be discussed in Chapter 7. This includes using design criteria for initially reducing the library of 120 materials to 10 materials for further testing. These candidates were put through *in vitro* testing to find the material that was the best in terms of cell viability and osteoconductive capabilities of attached MSCs. The best material identified as A6, a combination of diethylene glycol diacrylate and isobutylamine, was then implanted as 3D scaffolds into different rat models to determine biocompatibility and the ability to support mineralized tissue formation into the scaffolds with and without the addition of an osteoinductive growth factor.

The animal models in Chapter 7 investigated mineralization in scaffolds that were unloaded, which typically leads to intramembranous ossification. In Chapter 8, a femur window defect was created and filled with the same scaffold. The window defect should allow for straining of the scaffold, which is linked to endochondral ossification. The mineralization was evaluated not only through microCT and histology, but the mechanics were measured to evaluate the functionality of the new bone produced.

HTS techniques were used to evaluate a library of small molecules on mesenchymal stem cells (MSCs) and is covered in Chapter 9. These molecules were tested for their promotion and inhibition of osteogenesis on MSCs, and the 'hits' for osteogenesis were then evaluated in typical 2D culture either alone or in combination with biodegradable polymers.

Finally, in Chapter 10, overall conclusions and future directions for this work are discussed. This includes utilizations of the PBAE library for different tissues or applications and the limitations of the methods and models used. The results and implications of the HTS of small molecules are further discussed, as well as possible studies for how these molecules could be used in treatment of FOP patients, a clinical scenario where mineralization is not desired.

CHAPTER 3: Review of High-Throughput and Combinatorial Technologies used in Tissue Engineering

(Adapted from: A Peter, DM Brey, JA Burdick. High-throughput and combinatorial technologies for tissue engineering applications. Tissue Eng Part B Rev. 2009. 15(3):225-39.)

3.1 Introduction

Over the past few decades, scientists and engineers have sought to develop combinations of cells, scaffolds, and signaling molecules as the ideal microenvironments for application in tissue engineering [1-3]. The important environmental factors vary with the tissue of interest, as well as the type of cells recruited or delivered in the approach. Through this research, numerous scaffolds have been developed from a wide range of materials and incorporating numerous molecules (e.g., growth factors) to enhance matrix production and accumulation [2]. This has advanced our understanding of the importance of many cues towards optimal tissue engineering approaches, yet the field of tissue engineering has proceeded in a relatively iterative fashion with the use of tedious low-throughput studies. Due to the nature of the field, the input parameters to a tissue engineering approach are nearly endless and include the material selected, material properties, cell choice, culture environments, and soluble cues.

With this in mind, the complexity of cell signaling with the environment due to the multitude of factors involved may have slowed down tissue engineering development,

due to the difficulty in isolating effects to one parameter. For example, it is necessary to examine not only the bulk material properties such as mechanics and degradation, but also how scaffolds interact with cells through toxicity studies, as well as their ability to regulate cellular behavior such as adhesion, proliferation, or even stem cell differentiation [3, 4]. Adding to the complexity, proliferation and differentiation are largely controlled by cell-cell and cell-extracellular matrix (ECM) interactions, soluble factor stimuli, and the physical structure of the microenvironment itself [3, 4]. Additionally, intrinsic cellular factors such as small molecules and RNA also play an important role in cell signaling and differentiation [3].

Traditional methods of assessing these various factors have involved iterative approaches that require a tremendous amount of time and effort. Recently, the development and use of high-throughput and combinatorial techniques in tissue engineering have significantly enhanced this process through its efficient and productive platforms. For example, polymers may be synthesized through combinatorial processes, which accelerates the often tedious synthesis and purification schemes that may be necessary for development of non-toxic and biodegradable polymers [5]. Upon synthesis, the identification of optimal properties from large numbers of materials may also be performed through newly developed rapid assessment techniques [5]. This continues with the assessment of optimal cell/material interactions in a rapid fashion, often through the development of microdevices or use of printing technology [6]. For example, radically polymerized polymers with various functionalities can be synthesized in nanoliter volumes and plated in combinations onto a microarray to analyze the influence of the biomaterial on cell growth and differentiation [1]. These techniques also

include platforms such as microfluidics, which can analyze combinations of biomaterial gradient streams in a dynamic and temporally changing 3-dimensional microenvironment, and high-throughput screens to characterize the role of small molecules and RNAs in cellular behavior through the screening of large libraries of soluble factors [2, 3]. Notably, all of these areas may lead to the more rapid identification of optimal tissue engineering components and their unique combinations.

While these techniques also have applications in gene therapy and drug candidacy analysis, this chapter will focus specifically on applications in tissue engineering for injury and degenerative disease treatments [4]. Regenerative medicine techniques are being developed for a wide range of treatments for conditions such as cardiac ischemia, liver disease, and spinal cord injury and combinatorial and high-throughput approaches are accelerating the process for many tissue types [6]. As this field progresses, existing and new high-throughput techniques will be crucial in efficiently and rapidly developing ideal synergies between microenvironments and signaling factors for engineered tissues to be successful in clinical applications. This chapter will present the current landscape of high-throughput and combinatorial techniques as they apply to tissue engineering applications, the experimental and clinical benefits of these techniques, and the future directions of this rapidly growing field. Specifically, the focus will be on (1) combinatorial polymer synthesis, (2) tools for the rapid assessment of material properties, (3) high-throughput assessment of cell/material interactions, (4) microfluidic devices for the rapid development of engineered environments, and (5) high-throughput screening for identification of small molecules that influence cellular behavior.

3.2 Combinatorial Polymer Synthesis

In the pharmaceutical industry, researchers have used high-throughput, combinatorial techniques including automation, miniaturization, and parallel synthesis to transform their approach to developing new small molecules and discovering drug candidates [7]. These approaches are now being utilized in biomaterial development and in the field of tissue engineering due to the numerous advantages to accelerating material design and development. This includes the synthesis of polymers with a wide range of chemical components and bulk properties. Typically, polymer development has involved the use of tedious synthetic and purification steps, along with iterative design for material development since it is often difficult to predict the resulting polymer properties based on the polymer chemistry and structure. With advanced approaches where syntheses are performed more rapidly, many polymers can be developed quickly and then screened for the desired properties.

For over two decades, the pharmaceutical industry has developed and utilized methods in combinatorial synthesis and high-throughput analysis in its drug discovery efforts (originally reviewed by Gordon *et al.*[8] in 1994). The goal was to create large, diverse combinatorial libraries and characterize their pharmaceutical effects through a range of techniques. The synthesis and screening of combinatorial libraries primarily used either tagged methods (e.g., phage technology, peptides-on-plasmids, and encoded combinatorial libraries) or untagged synthesis/analysis techniques (e.g., "mixture synthesis" and "portioning-mixing") [9]. These initial approaches have been expanded and there has been extensive research and development in combinatorial synthesis and characterization in identifying lead compounds and therapeutically-relevant combinations

for pharmaceutical applications [10, 11]. Beyond drug development, similar techniques have been applied to gene therapy efforts over the years to identify unique polymers that would be most effective in non-viral gene therapy approaches on a range of length scales [12-15]. One approach has been the combinatorial synthesis of degradable cationic polymers (e.g., poly(β-amino ester)s (PBAEs)) and the analysis of structure/function relationships, something that would not be possible on this scale without combinatorial synthesis procedures [12-14]. While there are numerous applications that would benefit from this technology, this section will focus on polymer development applicable to the field of tissue engineering.

Some of the early combinatorial polymer libraries were created for subsequent high-throughput analysis of material properties specific to an application of interest (e.g., engineered bone and artificial medical implants). One such library, developed by Kohn and coworkers [16], combined tyrosine-derived diphenols and diacids in permutationally-designed monomer systems to produce alternating A-B type copolymers (A- contains reactive group for pendent chain attachments; B- allows for systematic variations in polymer backbone structure). Combining these copolymers, the system allowed for the production and analysis of a library of 112 polyarylates with small structural differences and some similar properties, but also with slight differences in polymer free volume, bulkiness, flexibility, hydrophobicity, and cellular response that affected their potential utility in medical implant applications [16]. Another study investigated more traditional polymer combinations of poly(D,L-lactide) and poly(ε-caprolactone) and their resulting influence on osteoblast activity [17]. This study employed composition spread and temperature gradients (and specifically heat-induced phase separation) to synthesize and

screen hundreds of combinatorial polymers with varying characteristics and thereby demonstrated differences in osteoblast response.

Since these early models, researchers have developed many additional methods of parallel, automated, and combinatorial polymer synthesis including polycondensation, radical polymerization (free-radical polymerization, controlled radical polymerization), ring-opening polymerization, polyolefins (mostly for applications in the chemical industry), and supramolecular polymerization [5]. For example, Gravert *et al.* [18] utilized free-radical polymerizations to construct block copolymers, which were subsequently twice split and used as macroinitiators to polymerize other sets of monomers. The final polymers displayed variable solubility profiles and functionality and demonstrated that this process may be used for a variety of high-throughput applications. Numerous other synthesis methods in controlled radical polymerization and ring-opening polymerization have been effective as well [5, 19-21]. Additionally, the development of synthesis methods for supramolecular polymers, which include both covalent and non-covalent bonds (as opposed to only covalent bonds), has introduced another variety of polymers with potential biomedical applications [5]. This research included the first method for fully automated production of supramolecular coordination polymers developed by Schmatloch *et al.* [22], which helped realize the potential for developing many new supramolecular polymers [5].

In 2006, we developed the first combinatorial library of degradable photocrosslinked biomaterials building on a previously developed library of potential gene carriers [13]. Specifically, a combinatorial approach was used to synthesize a library of 120 acrylate-terminated PBAE macromers that could be formed into networks

using a photoinitiated polymerization. The synthesis did not involve any purification steps and used commercially available reagents, which accelerated the synthesis process. This rapid process produced polymers that varied greatly in their property characteristics including degradation behavior (e.g. mass loss) and mechanical properties (e.g. elastic modulus) [23]. The general synthesis procedure and an example of the diverse mass loss between polymers are shown in Figure 3.1. We also found that properties such as molecular weight and macromer branching significantly influence the resulting PBAE network and bulk properties [24, 25]. With the appropriate screening process, photocrosslinked polymer scaffolds could be selected to meet design criteria including optimal degradation profiles and mechanical properties for specific engineered tissue functions.

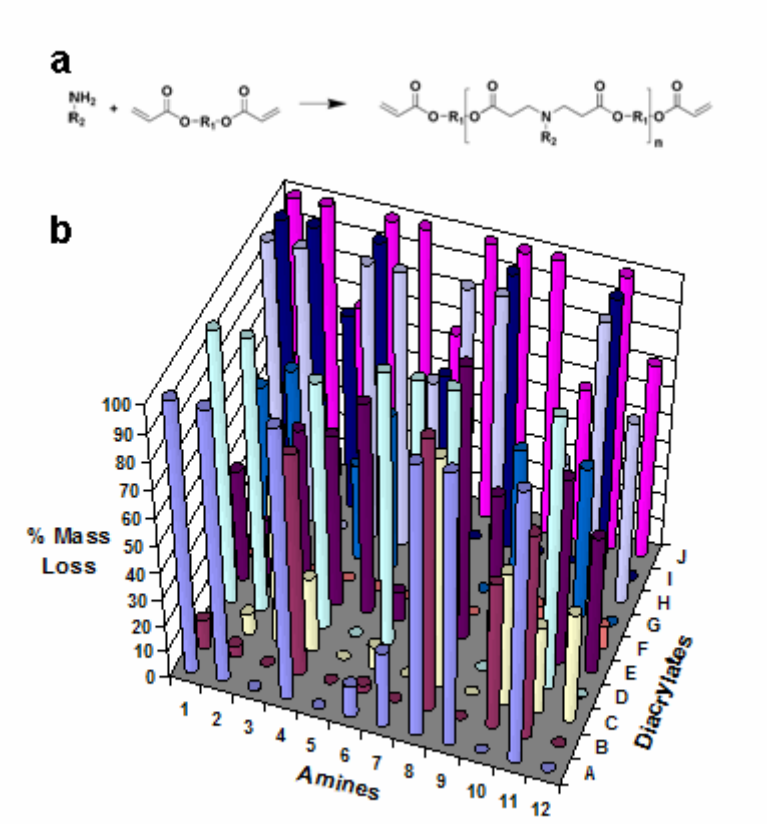

Figure 3.1 Combinatorial polymer synthesis. (a) Schematic of synthesis scheme for fabrication of poly(β-amino ester)s (PBAEs) from primary amines and diacrylates, where the versatility is found in the selection of reagents for synthesis (i.e., R1 and R2). (b) Representative mass loss for polymers formed from a group of 120 PBAE macromers after 32 days. The PBAE library exhibits a range of degradation and mechanical properties for diverse applicability in tissue engineering applications.

Combinatorial syntheses can also be performed on the nanoliter-scale by mixing reactive macromers and spotting onto a surface [1, 26, 27]. This was performed with 24 polymers in various combinations and ratios to produce 3456 individual spots on a single

array with the goal of analyzing cell-biomaterial interactions [27]. This platform relied on the use of a photoinitiated radical polymerization compatible with the technology. A robotic handling system was modified to handle the unique challenges of polymerizing diverse monomers including the viscous nature of some acrylate monomers and the inhibition of radical polymerization by oxygen [1, 27]. Therefore, array synthesis was performed in an atmosphere of humid argon with oxygen present at <0.1% and used a long-wave UV lamp to quickly polymerize the monomers [1, 27]. One of the benefits of this technology is that it is relatively universal to radically polymerized materials, a group of materials that is gaining interest in tissue engineering [28]. For example, natural polymers such as hyaluronic acid (HA) can be modified to be photopolymerizable and utilized in tissue engineering applications [28-33]. Schmidt and coworkers [32] constructed a variety of photopolymerized, crosslinked glycidyl methacrylate-HA (GMHA) hydrogels with a corresponding range of degradation rates, swelling, mesh size, and other properties and demonstrated their potential use in wound healing applications by implanting them subcutaneously in rats. Subsequently, in 2005, Burdick *et al.* [34] analyzed the use of photopolymerizable HA as a scaffold for both 3T3-fibroblasts and auricular swine chrondrocytes for macromers with a range of molecular weights and formed into gels at different concentrations. With the range of polymers available, these nano-scale approaches may help in identification of unique materials as well as their combinations (i.e., copolymers) that would be tedious to characterize individually. Overall, the development of a large variety of advanced polymer libraries, both synthetic and natural, has laid the framework for the identification of highly effective microenvironments for tissue engineering applications.

These synthetic techniques can also be used with a variety of preparation techniques to further their combinatorial possibilities. These preparation methods include flow-coating devices that produce thin films with gradients in thickness and temperature-gradient thin film platforms that provide composition/thickness, composition/temperature, or thickness/temperature two-dimensional libraries, and methods using photopolymerization to create a gradient polymer film [5, 35-37]. A more recent setup employed the use of a microextruder with two feeder heads designed by Potyrailo *et al.* [38] that was capable of producing polymers with a variety of step or gradient polymer combinations for subsequent analysis. Gradients provide the ultimate combinatorial synthesis method since polymer development extends beyond discrete formulations, providing even more compositions, as long as characterization techniques are available for assessment. All of these synthesis and preparation methods have contributed to the development of combinatorial polymer libraries with unique properties and functionalities, which can then be analyzed in high-throughput to identify ideal polymeric combinations for applications such as tissue engineering. Polymer synthesis in 3-dimensional environments is also of interest for tissue engineering applications. For example, scaffolds were constructed from varying compositions of two biodegradable tyrosine-derived polycarbonates, resulting in 3-dimensional combinatorial libraries on 96-well plates [39]. This 3-dimensional design should provide a variety of microenvironments that are more similar to *in vivo* conditions and should thereby enhance the development of ideal polymer scaffolds for tissue engineering applications.

As identified by Kohn [40] in 2004 and further described by Kohn *et al.* [41] in 2007, one important issue to consider as combinatorial molecule synthesis moves from

drug discovery applications to material science and tissue engineering applications is the need for reproducibility in polymer synthesis (e.g., molecular weight and polydispersities). With small molecule development, the chemical structure is the essential driving factor; however, there are a variety of factors that are significant when considering polymer design, including the polymer molecular weight, the molecular weight distribution of polymers within the sample, the presence of trace impurities, and the mechanism of fabrication, which all play a role in resulting material properties [40, 41]. One solution to this issue is the use of parallel synthesis of polymers (i.e., using individual reaction vessels to synthesize many individual polymers simultaneously and separately) [40, 41]. The next step requires the characterization of the synthesized polymers with respect to their formed properties including surface protein adsorption, rate of degradation, cytotoxicity, level of biocompatibility *in vivo* and cellular response [40, 41].

3.3 Tools for the Rapid Assessment of Material Properties

The previous section indicates that the synthesis of a large number of polymers rapidly is possible; however, without ample techniques to characterize the properties of these materials, their rapid development may not be advantageous. One of the earliest methods of rapidly assessing material properties was demonstrated by Kohn and colleagues [42] in 1998. This was aimed at assessing the combinatorial polymer library consisting of 112 polyarylates that was described in the previous section. In addition to creating many distinct polymers, this work enabled the researchers to determine relationships between polymer structure and glass transition temperature (T*g*),

hydrophobicity, and mechanical properties. These properties were determined by systematic analysis using gel-permeation chromatography (for molecular weight), differential scanning calorimetry (for T_g), thermogravimetric analysis (for decomposition temperature), and goniometry and sessile drop method (for air-water contact angle). Some of their conclusions included that oxygen substitution in the backbone is effective in increasing polymer T_g and in decreasing hydrophobicity (for substitution in the backbone and/or pendent chain) and that additional methylene groups in the backbone and/or pendent chain can significantly diminish polymer strength and stiffness. Thus, these approaches can also be used to develop polymer structure/property correlations for future material development.

In early 2004, Meier *et al.* [43] provided a comprehensive overview of the current development in high-throughput screening and assessment of material properties, which built on a previous review published in 2003 [5]. For the high-speed characterization of standard polymer molecular weights, recent high-throughput techniques have focused on using methods such as gel permeation chromatography in combination with high-speed columns, parallelization, and/or flow-injection analysis (FIA) [43, 44]. Parallelization utilizes more machines to run test samples, but is obviously limited by lab space and costs. New, higher speed columns allow for rapid size exclusion separations to occur in 2-6 minutes rather than 30 minutes to 3 hours [44]. Additionally, researchers have utilized matrix assisted laser desorption ionization time-of-flight mass spectrometry (MALDI-TOF MS) techniques for absolute determinations of molecular weight, molecular-weight distribution, and end group analysis of macromolecules (which can be optimized using multiple-layer spotting sample preparation techniques, online monitoring

of reactions, and/or ink-jet printing) [45-47]. Next, optical screening methods have been increasingly improved for high-throughput property and chemical composition assessment purposes [43]. These methods have been enhanced by combining them with imaging and commercial reader technologies for absorbance, fluorescence, and infrared (and near infrared) spectroscopy [43].

Infrared and near infrared spectroscopy-based techniques, including attenuated total reflection Fourier-transform infrared spectroscopy (ATR-FT-IR), are effective tools for measuring monomer/polymer compositions and polymerizations [48-50], while fluorescence spectroscopy approaches have been used to determine properties such as molecular weight, amount of branching, and catalyst selectivity [51]. Lastly, numerous methods have been developed to address the area of screening for morphology and physical properties, particularly for polymer film analysis [52-57]. These methods include using relationships between various physical properties and the preceding optical data, as well as the evaluation of thin films to determine adhesion, crystallization, or dewetting property characteristics [52, 53, 55-57]. Fast differential scanning calorimetry (DSC) analyses have been considerably accelerated with automated large sample array DSC. This field is still developing and should continue to improve the speed of property characterization while maintaining equal or even better accuracy of data compared to traditional methods [43].

In combination with the above mentioned synthetic nanoliter-spotting techniques, Tweedie *et al.* [26] synthesized a library of over 1700 photopolymerizable acrylate-based biomaterials using automated array synthesis and characterized the resulting mechanical properties with nanoindentation. Nanoindentation is a method of measuring nanometer-

scale displacement with respect to load while depressing the material's surface with a rigid indenter. These methods were found to be quick and accurate in determining numerous mechanical response characteristics and could potentially be applied to other sets of combinatorial/crosslinked polymers [26]. This example presents a situation where a technology was modified to accelerate material property characterization with a new rapid synthesis process. An additional method for measuring mechanical properties of thin films was strain induced elastomer buckling instability for mechanical measurements [58]. This method utilizes the light scattering produced by the buckling of two mismatched polymers, the glassy thin film of interest and a softer silicone sheet.

The rapid characterization of polymer properties and cellular responses will be vital for the continuing development of tissue engineering research. As Kohn *et al.* [41] described, the chemical composition of polymeric scaffolds significantly affects its mechanical/cell interaction properties and therefore, will often determine the applicability of a potential engineered tissue scaffold. Kohn *et al.* [41] cite recent studies that demonstrate how slight differences in polymer composition and structure (poly(L-lactic acid) vs. poly(DTE carbonate) and poly(DTE carbonate) vs. poly(DTB carbonate), respectively) can significantly affect cell response and long-term tissue growth including differences in bone resorption, inflammatory response, tissue degradation, tissue in-growth, and foreign body response [59]. The considerable effects of minor polymeric differences support the need to develop and utilize high-throughput methods that rapidly and systemically characterize the many polymer compositions. In the future, this may increasingly depend on computational programming as we will discuss in the subsequent section on assessing cell/material interactions [41]. Additionally, x,y spatially-resolved

libraries, in which polymer composition varies across the x and y coordinates, respectively, have also been utilized to assess a wide range of polymer mixtures using some of the analytical methods previously described (i.e., optical microscopy) [36, 41, 60]. This type of method should also play an important role in the future development of rapid material characterization.

The availability and quality of high-throughput assays for material characterization is commercially relatively limited, leading to inefficient iterative approaches for analysis. Recently, there has been significant progress in characterizing various biomaterial assays and developing reliable and advanced high-throughput assay systems. Additionally, the use of computational systems to artificially determine cell-biomaterial interactions based on known properties has gained traction, but remains limited due to the complexity of these interactions [40]. These algorithmic systems have the potential to exponentially increase efficiency in developing and analyzing combinatorial virtual libraries by bypassing the actual, physical production of thousands of polymeric combinations. It is clear that there is still room for the development of new techniques to rapidly characterize material properties from large libraries of polymers. Beyond bulk properties and towards tissue engineering applications, it is also necessary to rapidly characterize how cells interact with a range of materials.

3.4 High-throughput Assessment of Cell/Material Interactions

Using the vast array of combinatorial polymer libraries and many of the tools for material property analysis, the next step in developing the ideal microenvironment for engineered tissue is the high-throughput assessment of cell/material interactions. This

ideal microenvironment will often seek to mimic the natural environment of particular cell types or even improve on this environment by cultivating growth and proliferation [4]. Particularly in the field of tissue engineering, the extracellular environment, including surface properties such as roughness and hydrophobicity and specific cell-surface interaction, maintains a large influence on cellular attachment, spreading, overall growth, and differentiation in the case of stem cells [1]. The use of high-throughput systems to improve the speed and breadth of characterizing and understanding these effects on cellular responses would significantly accelerate the process of developing effective engineered tissue constructs that could be utilized in medical applications.

The development of systems for analyzing cell/material interactions in bulk began in the late 1990s, shortly after the production of the first large combinatorial polymer libraries. In addition to developing a combinatorial polymer library and demonstrating rapid polymer property characterization, Kohn and coworkers [42] also performed one of the earliest high-throughput analyses of cell/material interactions in 1998. This analysis studied the interaction between 42 polyarylate polymers (a subset of the 112 polymer library) and fibroblast cells, focusing on proliferation using an MTS (3-(4,5-dimethylthiazol-2-yl)-5-(3-carboxymethoxyphenyl)-2-(4-sulfophenyl)-2H-tetrazolium) assay. In general, these investigators found a linear correlation between decreased proliferation and increased surface hydrophobicity of materials derived from non-oxygen-containing diacids. The analysis also showed that all polymers derived from oxygen-containing diacids acted as good substrates for fibroblast proliferation. Along with these findings and others, this study illustrated the ability to determine important material interactions with only small amounts of polymer material.

Since these early pioneering analyses, high-throughput assessment has seen significant growth in the volume of analyses, the breadth of cells and polymers studied, and the variety of cell responses that have been characterized. In one study, over 1700 combinatorial nanoliter-scale polymer spots of various (meth)acrylates were introduced to a single slide, thereby providing a high-throughput platform for analyzing cell attachment, cell spreading, and cell-type specific growth [1, 7]. This work examined the effects of these polymers on human embryonic stem (hES) cells and C2C12 cells (a mouse myoblast stem cell line), including cell growth, adhesion, and proliferation [1]. Additionally, positive matches for cell attachment and spreading were also tested for differentiation into cytokeratin-positive cells. A representative polymer array with cells attached is shown in Figure 3.2. The process of successfully identifying cell/material interactions and the ease of producing and characterizing cytokeratin-positive cells in particular could be utilized in developing engineered epithelia tissue. C2C12 cells showed similar attachment and growth to hES cells, but with success on almost all material combinations. This differentiation between the two cell types could also be effectively used in advanced scaffolding for engineered tissue applications. Lastly, it was found that cell growth and proliferation is dependent on the presence of retinoic acid for some specific polymer combinations, which could potentially be employed to control cell behavior in tissue engineering. This study relied on fluorescent techniques that could be quantified with image analyses. The importance of this work is that it assessed many formulations, including material/soluble factor combinations, rapidly and that it went beyond identifying correlations and focused on the identification of random combinations by utilizing the benefits of high-throughput studies.

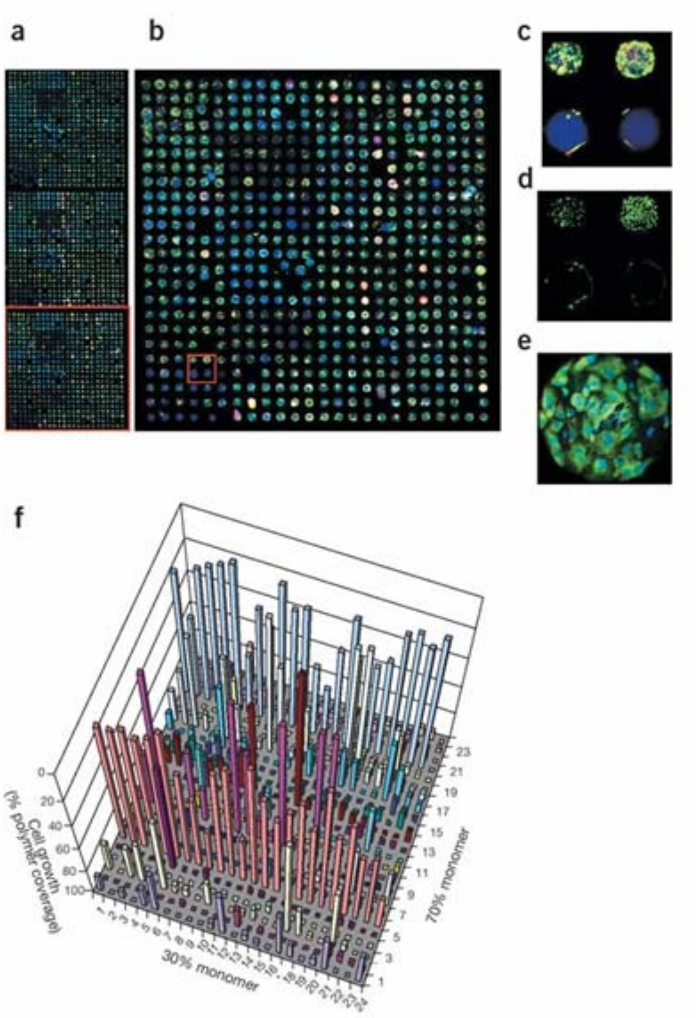

Figure 3.2 Polymer arrays to assess cell/material interactions. (a−c) Examples of fluorescent images of human embryonic stem cells cultured on polymer arrays in the presence of retinoic acid for 6 days and then stained for cytokeratin 7 (green) and vimentin (red) (a-c, e) or nuclei (green) in (d). (f) Quantification of cell coverage as a function of polymer composition after 6 days. These techniques are useful to identify unexpected relationships between material chemistry/properties and cellular interactions, including stem cell differentiation [1].

This technology was further expanded to encompass arrays consisting of 3456 individual combinations of biodegradable polymers and the interactions of human mesenchymal stem cells (hMSCs) was assessed with regards to properties such as attachment and spreading [27]. This platform maintained the added benefit on being able to synthesize and characterize polymeric materials using conventional methods instead of producing nanoliter-scale materials on the array. Many of the combinations were found to foster attachment and growth including PLGA combined with L-lactide. These characterizations display the potential of designing effective biomaterials to enhance stem cell development including neural stem cell growth and perhaps differentiation through engineered, combinatorial microenvironments. Looking forward, Anderson *et al.* [27] identified the screening of biomaterial interactions with other microenvironment components such as proteins as a potential application for this specific high-throughput microarray platform.

As researchers have continued to study cell/biomaterial interactions, these analyses have become increasingly complex and multifunctional. For instance, Neuss *et al.* [61] developed a grid-based system for the screening of various combinations of 7 different stem cell lines (including pluripotent embryonic and multipotent adult stem cells) and 19 polymeric materials. Through this research, five factors (morphology, vitality, cytotoxicity, apoptosis, and proliferation) were characterized using multiplex assays for each of 140 combinations. From this standardized, parallel analysis, they were able to identify combinations of stem cells and polymer scaffolds including human dental pulp stem cells on poly-DL-lactic acid and human preadipocytes on texin that support cell adhesion and proliferation and prevent apoptosis and necrosis. This type of diverse

combinatorial assessment of numerous cell/material parameters should be extremely useful in quickly characterizing cell and scaffolding combinations for specific tissue engineering functions.

As the field has progressed, high-throughput methods have increasingly taken advantage of fluorescence-based analysis of cellular responses. For instance, investigators have recently developed a high-throughput method for testing the growth, adhesion, and morphology responses of mouse connective tissue fibroblast cells (L929) on a set of 214 polyurethane-based polymers [62]. In this study, a probe composed of nonfluorescent 5-chloromethylfluorescein diacetate was utilized to enter the cell and then display fluorescence when it was cleaved by intracellular esterases. Combining image capture and screening analysis with the appearance of fluorescence enabled the team to rapidly quantify the growth, adhesion, and morphology of the fibroblasts. In addition to identifying clear trends relating cellular adhesion and polymer structure, the researchers also emphasized that this methodology could be scaled up to 1024 individual experiments per slide, allowing very high-volume and quick analyses with only small quantities of materials [62]. Numerous other studies have also utilized fluorescence-based analyses of cell behavior [27, 63-65] or protein/material interactions [66] as these techniques are easily applied and effective. Modern transfection techniques have allowed researchers to transfect cell lines with genes for fluorescent proteins that are activated when the reporters of genes of interest are activated [3, 67]. This allows for passive observation of genetic activation of cell differentiation along desired lines.

Another trend is the progression towards complete microenvironment analyses, including both the extracellular matrix components and the soluble growth factors and

molecules. This holistic approach should better represent the actual *in vivo* conditions and enhance the assessment of cellular response to these conditions. Flaim *et al.* [67] developed one of the first models for this type of analysis, which consisted of a platform for 1200 simultaneous experiments studying the effects of 240 different microenvironments on stem cell behavior. These microenvironments were composed of mixtures of both extracellular matrix (fibronectin, laminin, collagen I, collagen III, collagen IV) and soluble factors (wnt3a, activin A, bone morphogenetic protein-4, and fibroblast growth factor-4). Flaim *et al.* [67] employed an overall microarray design but also utilized a multiwell platform, in which each well contained several spots where a single extracellular matrix arrangement was maintained and soluble factor composition was varied. Growth levels were recorded by measuring the amount of nuclear DNA while differentiation was again measured using a fluorescence-based reporter gene. This approach could potentially be utilized with any set of environmental factors and cell lines, thereby creating a more 'natural' environment for engineered tissue development.

As mentioned previously, one of the recent advances in engineered tissue development was the design and production of the first large-pore polymer biomaterials that could be analyzed in 3-dimensional, high-throughput environments for their effects on cell behavior (developed by Yang *et al.* [39]). Previous studies, including one performed by Levenberg *et al.* [68], had completed similar work including the analysis of hES cell growth and differentiation in a 3-dimensional 50% PLGA / 50% PLLA environment with growth factors. While successful growth and differentiation was found with different growth factors in specific pore environments (250-500 μm), this study did not vary the polymer composition or analyze polymer variations in high-throughput [68].

In their advanced, high-throughput analysis, Yang *et al.* [39] found a relationship between increasing poly(desaminotyrosyl-tyrosine ethyl ester carbonate) content and increasing osteoblast adhesion. It was also determined that protein adsorption affects cell responses including osteoblast adhesion for these polymeric scaffolds. Overall, this analysis demonstrates a tremendous improvement over 2-dimensional films or surfaces that have traditionally been used in studying cell/material interactions. This is due largely to the similarity of 3-dimensional environments to *in vivo* conditions, as well as the varying cell response to the environment structure and material topography. Even so, in this case, Yang *et al.* [39] found that the cell adhesion trends in 3-dimensional scaffolds fit with the trends previously determined in 2-dimensional screening, which indicates that 2-dimensional screening may be used to effectively predict cell response in 3-dimensional environments. In the end, the capacity to use 3-dimensional screening for cell/material interactions should enhance the development of applicable polymeric scaffolding and engineered tissues.

Beyond experimental assessment, computational system analysis of combinatorial polymer virtual libraries has been identified as an area of great potential in analyzing material properties for tissue engineering applications. One recent development in computational methods was designed by Kohn and coworkers [69] to successfully predict the cell growth response to a biomaterial based on its chemical composition and physical properties such as glass transition temperature (T_g) and contact angle (θ). The model, called the Logical Analysis of Data (LAD), was developed using 62 known polymers and was then able to distinguish between high and low growth polymers for 50 uncharacterized materials and even correctly characterize several materials that cultivated

especially high cell growth. This particular model was used to predict the response of rat lung fibroblasts and foreskin fibroblasts to the set of polymers, but could potentially be applied to other cell types and other biomaterials. While this study demonstrates the potential of computational systems to enhance efficiency in combinatorial analysis by bypassing the physical construction of polymer libraries, this type of modeling software still requires further development, including the addition of more input parameters and output measurements, to become widely applicable across various analyses [69].

Quantitative structure activity relationship (QSAR) analyses have been previously used in the pharmaceutical industry, but are recently being applied to the study of cell/biomaterial interactions [70]. Recent models have utilized this quantitative analysis to predict cellular response and protein adsorption to biodegradable polymeric biomaterials [70, 71]. The model predicted the biological activity for 6 polyarylates with an average percent error of only 15.8% compared to the measured values using a quantitative system based on 5 parameters including the number of tertiary carbons, the number of branches in the pendent chain, the molar refractivity, the polar surface area, and the logarithm of the octanol-water partition coefficient [70]. A subsequent model again utilized 5 input parameters chosen through QSAR analyses and put into an Artificial Neural Network (ANN) platform to predict the protein adsorption and biological response for 77% and 71% of the polymeric test materials, respectively [71]. Kohn and his colleagues [72] also utilized an ANN model to predict fibrinogen absorption and cell growth for the previously presented 112 polyarylate library.

More recently, larger scale attempts at computationally predicting cell/material interactions have been pursued. A study performed by Kholodovych *et al.* [73] analyzed

the cellular response to a combinatorial library of 2000 polymethacrylates using a Polynomial Neural Network (PNN) as opposed to the traditionally used ANN algorithms. The benefits of the PNN tool include its ability to assemble the architecture (i.e., the precise number of neurons in the input, output, and hidden layers, etc.) in response to the characteristics of the data and to handle very small or very large data sets [73]. These qualities will likely make PNN algorithms, in conjunction with QSPR analyses, extremely useful in the future for computationally screening many diverse cell/biomaterial interactions. Even so, despite this progress, the computational prediction field still needs further development to become fully applicable across the wide range of polymeric materials and the complex variety of cell lines. However, it could help to rapidly assess and identify optimal material formulations, beyond traditional experimental techniques.

Overall, the field of high-throughput assessment of cell/material interactions has experienced a tremendous amount of progress as a variety of platforms and analysis techniques have been designed to better identify successful microenvironments. Even so, this field is still considered to be in its early stage [4]. In moving forward, researchers will need to continue to develop platforms and microenvironments that emulate actual *in vivo* conditions (i.e., scaffolding combined with soluble factors and fluidic environments), as well as move from the micro-scale to the macro-scale in order to fully approach tissue engineering applications [4].

3.5 Microfluidic Devices for the Rapid Development of Engineered Environments

One effective method to assess cell/material interactions is the use of microfluidic systems. Microfluidic systems can be used for a variety of applications and simulations, but for tissue engineering, these devices are primarily used for high-throughput screening, characterization of cell/material interactions, and the optimization of the conditions that precisely regulate cell behavior and fate [2], [74]. Like many other microscale techniques, microfluidics are inexpensive and able to operate with fewer cells and reagents [2]. In addition to these advantages, microfluidic devices provide a fluid, dynamic environment that is much more similar to *in vivo* conditions compared to traditional static platforms, such as those described in the previous section.

One microfluidic platform that has gained use involves the generation of gradients of soluble or bound factors to assess the factor's influence on interacting cells [75]. For instance, in 2005, Chung *et al.* [76] produced a microfluidic system that delivered a gradient of growth factors including epidermal growth factor (EGF), fibroblast growth factor 2 (FGF2), and platelet-derived growth factor (PDGF) to human neural stem cells (NSCs). In response, these cells proliferated and differentiated into astrocytes proportionally to the concentration of growth factors. Proliferation was directly proportional to growth factor concentration and conversely, differentiation occurred in an inversely proportional relationship with growth factor concentration. For this experiment, the actual microfluidic device was produced using the techniques of rapid prototyping and soft lithography. The gradient flow of multiple factors allows for the rapid optimization of culture conditions while using low concentrations of relatively expensive growth factors and cells [76]. These benefits of gradient-generating

microfluidic platforms should considerably enhance the process of optimizing culture and scaffolding conditions for a variety of tissue engineering applications. Also, microfluidics allow precise control over the timing of multiple soluble factors.

Microfluidics have also helped identify ideal cell microenvironments through the development of control over soluble chemical distribution within a scaffold. This strategy was explored in contrast to previous research, which has largely focused on adjusting the chemical and mechanical characteristics of the scaffold [77]. In 2007, Choi *et al.* [77] described a method for managing this distribution by using microfluidic channels constructed within the cell/biomaterial combination to complete convective mass transfer of the solutes. The solute exchange is completed in two steps involving interfacial convective mass transfer between the flowing solutions and the walls of the microchannels and molecular diffusion between these walls and the bulk of the scaffold [77]. This model included a calcium alginate hydrogel and chondrocyte cell lines and utilized lithography to develop the microfluidic structure. This precise control of soluble chemical distribution could help prevent necrosis from developing at the center of thick engineered tissues as well as guide cell growth towards regions within engineered tissue [77].

Khademhosseini and coworkers [78] have also developed microfluidic channels in cell-seeded agarose hydrogels using soft lithographic techniques. This work showed that cell viability in large engineered tissue constructs can depend largely on the distribution of nutrients and oxygen through vasculature-like channels and proved that microfluidics can help overcome the difficulty in transport and exchange of materials, namely nutrients, that typically causes cell necrosis in large 3-dimensional engineered

tissues. While further development is necessary, this method will certainly enhance the progress towards engineered 3-dimensional scaffolds with artificial vasculature that allow for the exchange of nutrients, waste, and signaling molecules. The technology could also be used for assessment and screening of multiple environments in single constructs. This work has been expanded to produce 3-dimensional cardiac organoids on a patterned hyaluronic acid (HA) platform [79]. In this model, seeded cardiomyocytes grew parallel to the pattern direction and subsequently detached from the scaffold to develop into contractile cardiac organoids. For confirmation, contractile properties were assessed and quantified using imaging technology. This method displays the double advantage of both growing and aligning the myocytes on a biocompatible scaffold and allowing for natural detachment of the contractile cells without requiring enzymes. In addition to a variety of other studies, these methods, namely the microfluidic patterning, could potentially be used in biodegradable scaffolds to organize cell growth for the purposes of tissue engineering and full tissue replacement [79].

Other researchers have also used soft lithography techniques to develop hydrogel-based microfluidic platforms. For instance, in 2007, Figallo *et al.* [80] used soft lithography methods to design a micro-bioreactor array (MBA), which consists of layers of poly(dimethylsiloxane) (PDMS) and glass and maintains microfluidic channels throughout the system. The microfluidic channels are able to supply the perfusion of a controlled medium and enhance the growth of cells in high density through advantages including the purging of residual non-polymerized reactants. A schematic of the device, as well as representative cellular outcomes are shown in Figure 3.3. The miniaturization of the bioreactor allows for better use of expensive media factors while still maintaining

this advantage of a fluid, dynamic system. In different perfusion setups, the MBA system of twelve micro-bioreactors was utilized to compare the expression of smooth muscle actin and cell density (for various cells including human embryonic stem cells (hESCs)). Additionally, the group was able to analyze cell differentiation by quantifying the expression of cell differentiation markers using an *in situ* and automated image analysis system. As noted by Figallo *et al.* [80], this complete system should prove to be quite useful for the study of cell behavior, especially the complex development of hESCs, in fluidic environments.

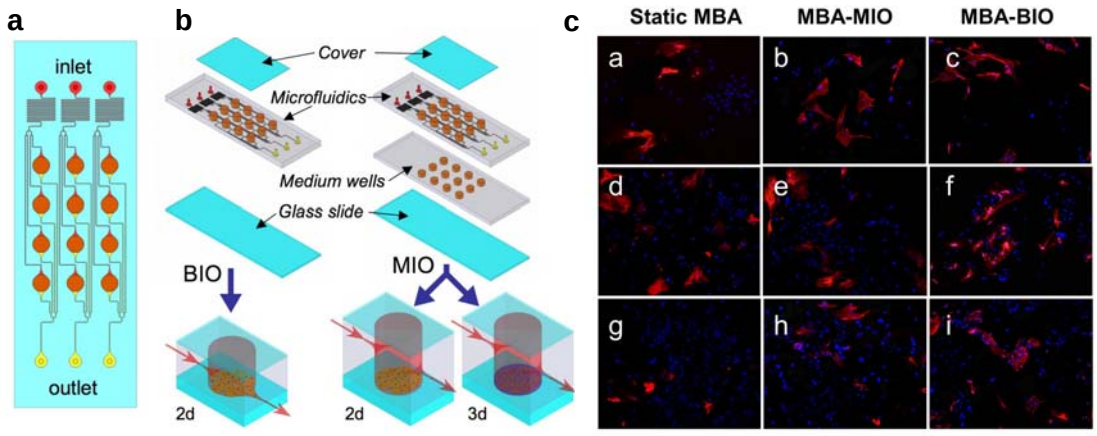

Figure 3.3 Micro bioreactor arrays for identification of ideal cellular environments. Micro bioreactor arrays for identification of ideal cellular environments. Microfluidic device (a) and well schematics (b) for configurations that include a bottom inlet/outlet (BIO) where the flow is directly over the cells and a middle inlet/outlet (MIO) configuration where the cells are in a well with fluid flow over top. Human embryonic stem cells were cultured and stained for smooth muscle actin (red) and DAPI (Blue) in three different flow configurations (c): static (left column: a, d, g), perfused BIO (middle column: b, e, h) and perfused MIO (right column: c, f, i) at three different cell densities: 60 ± 6 (top row: a, b, c), 160 ± 4 (middle row: d, e, f) and 314 ± 15 (bottom row: g, h, i). This technology is useful to assess microenvironments for tissue engineering, particularly under a range of flow conditions [80].

Other microfludic platforms have been developed for the purposes of complex cell culture and experimentation in conditions very similar to an *in vivo* environment. In 2007, Lee *et al.* [81] developed such a model consisting of a cell culture niche, an

artificial, microfluidic endothelial (perfusion) layer, and a nutrient transport vessel. This system utilized microfluidics to direct mass transport on the microscale and to help localize cells for increased density and viability in certain areas of the microenvironment. More recently, chip-based microfluidic devices have been developed and utilized to produce microscale scaffolds. For instance, Lee and colleagues [82] have constructed tissue engineering scaffolds by integrating poly(lactic-*co*-glycolic acid) (PLGA) microfibers into a microfluidic chip. In this preparation, the microfibers were generated by precipitating streams of PLGA in dimethyl sulfoxide (DMSO) out of a water/glycerol mixture and varying the flow rate of PLGA to produce fibers of different widths [82]. Neural progenitor cells were then grown on the 3D scaffolds to determine its potential for use in neural tissue engineering [82].

It is clear that complex environments are crucial to truly assess the potential of approaches in recapitulating the complex microenvironments found *in vivo*. This includes systems that utilize fluid flow, 3-dimensional structures, and both bound and soluble cues. Thus, microfluidics provide platform technology for rapidly assessing these environments, whether it is with gradients of cues or through the interface of fluid flow and arrays of polymers. However, much of this previous work has focused on the assessment of known soluble cues (i.e., growth factors) for tissue engineering applications.

3.6 Screening Molecules for Stem Cell Differentiation

The identification of molecules that control cellular behavior is essential to expand the breadth of cues that may be incorporated into tissue engineering approaches. One emerging field is the use of high-throughput screening (HTS) of molecule libraries for the control of stem cell differentiation. Extensive studies have assessed potential drugs and growth factors looking for soluble cues to direct the fate of stem cells towards a desired phenotype. These attempts have been limited to smaller studies of a limited number of factors due to the techniques in culture and cost of reagents and proteins. Additionally, efforts to recapitulate growth factor cocktails and precise timing of their delivery, as seen during development, have been similarly limited in scope and complexity. With the advent of HTS techniques, smaller numbers of cells can be used to screen a wider range of potential drugs and cytokine delivery schemes in order to optimize stem cell differentiation. Although many cell types could be investigated, this section will focus specifically on the use of HTS technology towards stem cell differentiation.

To date, few studies have specifically investigated the use of HTS of small molecules for stem cell differentiation. One of the earliest examples involved a study from the Schultz lab that screened a heterocycle combinatorial library [83]. This library was built using the template of known kinase inhibitor scaffolds, such as purine and pyrimidines, to include nearly 50,000 different small molecules of unknown potential. Originally, this library was thought to be a possible source for new ligands to further investigate the function of new proteins by inhibiting or stimulating their signaling; however, they soon began to investigate their differentiation potential on stem cells. For

example, the library was screened with mouse embryonic mesoderm fibroblasts C3H10T1/2 cells for osteogenic differentiation [84]. The initial screen used increased alkaline phophastase (ALP) expression, which is important to bone mineralization, as a marker for differentiation. 15 compounds were identified that stimulated ALP activity, but the molecule they named purmorphamine was the most potent of these. This compound was shown to be more potent than BMP-4 with optimized concentrations, and the combined effect of BMP-4 and purmorphamine were synergistic and not surrogate. The osteogenic nature of purmorphamine was confirmed with increases in the induction of the transcription factor Cbfa1 and histological staining for ALP on several other murine mesenchymal cell lines. Further investigation [85] found that purmorphamine stimulated osteogenic differentiation along the hedgehog signaling pathway.

Similarly, HTS was used to identify molecules from this library that drove neuronal [86] and cardiomyogenic [87] differentiation of murine embryonic stem cells. Hits were initially screened using transfection of reporter gene activated luciferase plasmids. The use of the library to drive dedifferentiation [88] also led to the discovery of 'reversine' which allowed murine myoblasts to dedifferentiate into stem-like cells and then redifferentiate along osteogenic or adipogenic cell lines. This could be important in discovering new autologous sources for cell therapies. These discoveries were largely used to investigate the processes and signaling used during differentiation, not for actual therapy.

More recent studies have screened libraries for suppressors of differentiation rather than looking for new promoters [85, 89]. These can be useful for treating certain disease progressions where it would be therapeutically advantageous to prevent

differentiation or in understanding the nature of diseases where normal function is inhibited but the causes are not understood. The study by Yui *et al.* [85] screened over 7500 commercially available compounds by investigating their effects on the normal embryonic development of the dorsal structures in zebrafish. This required the observation and measurement of several individual embryos manually, so it lost some of the rapidity of the soluble factor assays previously discussed, but includes the complexity of the *in vivo* system that 2D culture lacks. This method was able to identify dorsomorphin as a BMP Type I receptor inhibitor, which prevents osteogenic differentiation.

A high throughput siRNA library was used to screen hMSCs for osteogenic suppressors by Zhao and Ding [89]. MSCs were transfected by a library of 10,000 unique sequences, 2 per gene, and the ALP activity was then imaged. An increase in ALP activity indicated that the inhibited gene was normally an osteogenic suppressor. This initial screen identified 55 'hits' for osteogenic prevention, which included genes for a wide variety of kinases, extracellular matrix proteins, protein receptors, ion channels, amongst others. From this initial screen, 12 were picked to investigate further for prevention of osteogenic differentiation. Interestingly, the different suppressors fell in two types the authors designated 'fate specific' or 'fate nonspecific.' The fate specific genes were suppressors of osteogenic differentiation because they preferred an adipogenic lineage. The fate nonspecific type prevented differentiation along any line. These would be important in maintaining the multipotency and proliferation of stem cells, and may be useful for understanding and prolonging a stem cell line *in vitro* or possibly in the dedifferentiation of committed cell lines.

One recent study by Mauck and coworkers [90] used HTS of hMSC pellets to find molecules that stimulate or suppress chondrogenesis. Since MSCs typically undergo chondrogenesis in pellets, it was necessary to scale down pellet cultures for rapid assessment and culture in round bottom 384-well plates. Chondrogenesis was assayed by measuring the glycosaminoglycan (GAG) content of the pellets after a week in culture. The setup was first run to evaluate the combinatorial effects of four different growth factors at different concentrations. This allowed for the confirmation of BMP-2 and TGF-β as being very synergistic in chondrogenic differentiation, but also demonstrated how FGF-2 increased cell proliferation and chondrogenic potential of hMSCs. The small volumes of the 384 well plates allow for extensive screening of different growth factor cocktails that are often limited in large scale experiments by the cost of cytokines. Secondly, the National Institute of Neurological Disorders and Stroke (NINDS) library was screened for both chondrogenic inducers and inhibitors. The chondrogenic inhibitors eliminated compounds that led to a 40% reduction in DNA content to eliminate compounds that reduced GAG content due to their cytoxicity. This method identified 24 potential inhibitors, including many antimitotics, antibiotics, and antineoplastics among others. Outcomes, which include hits for molecules that either induce or inhibit stem cell chondrogenesis are shown in Figure 3.4. Dose response investigation may be useful in these cases to determine if changes in the dose would lead to further cell death or increased effectiveness.

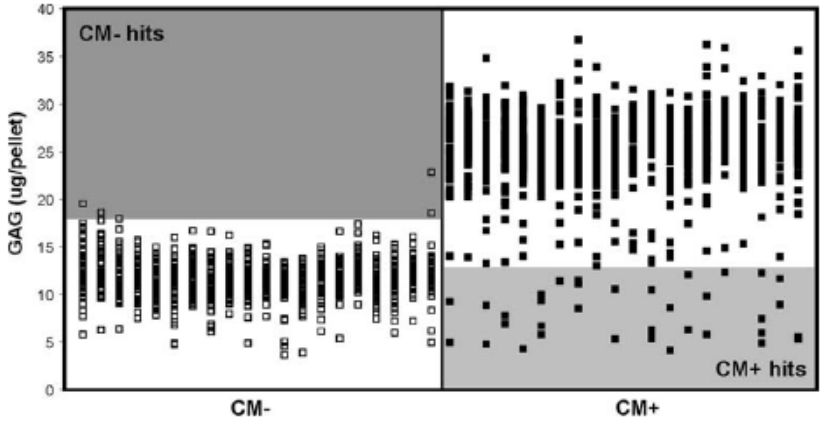

Figure 3.4 High-throughput screening of small molecules that influence stem cell differentiation. Screening of a small molecule library (NINDS) to identify inducers (CM- hits, grey area) and inhibitors (CM+ hits, grey area) of mesenchymal stem cell chondrogenesis, measured by glycosaminoglycan (GAG) levels. This technology is applicable to a range of cell types useful in tissue engineering applications [90].

HTS techniques are beneficial due to their ability to quickly screen large libraries of small molecules for desired outcomes. Often, though, the hits are just the beginning, whereby the mechanisms of their action must be investigated and the optimization of the dosage must be further investigated. Thankfully, the same HTS setups can aid in the optimization of dosage or the synergies of multiple factors. As always, *in vitro* culture is often limited in capturing effects in an artificial environment that may not translate *in vivo*. The zebrafish experiments [85] are interesting in their ability to add a level of complexity, but made it difficult to isolate the effects on specific cells.

Rubin [91] lamented that often more information could be gleaned from these experiments if the researchers had more diverse sets of compounds and the expertise in

chemistry and drug design to further develop initial hits. As such, often researchers are limited by smaller more established sets, such as the NINDS library, that is already characterized for other applications and may already be in use for other therapeutics. This has the benefit of a possibly faster implementation of these therapies if they are discovered, but that the larger research misses out on the true promise of these screens to investigate more diverse and uncharted libraries.

From a tissue engineering standpoint, these small molecule discoveries can be useful in the design of materials, the differentiation of implanted cells, or to discover new cell sources. Scaffolds can incorporate the release of newly discovered small molecules into the environment around these implants to either drive specific differentiation of incorporated cell therapies or to recruit native local stem cells and drive their differentiation for desired outcomes. The molecules, as shown previously [88], can be used to dedifferentiate autologous cells towards a stem cell line that can then be expanded to increase cells numbers to therapeutic levels. Then the cells can be differentiated along the desired lineage *in vitro* before implantation.

3.7 Summary and Future Directions

Through this chapter, we have discussed many of the stages involved in research and development for tissue engineering applications and have specifically focused on high-throughput and combinatorial techniques in polymer synthesis, material characterization, cell/material interactions including microfluidic platforms, and small molecule screening to direct cell behavior. While combinatorial synthesis methods have been studied for years and for various applications, these techniques are still developing

as a crucial tool in rapidly producing a wide variety of polymeric materials as potential scaffolds. In the future, miniaturization of polymer libraries to the nano-scale level, the design of 3-dimensional combinatorial libraries, and parallel synthesis methods should continue to influence the ease and utility of using libraries to develop polymer scaffolds. In assessing the characteristics of these large libraries, a variety of techniques, from parallelization to fluorescence spectroscopy, have been developed and employed, yet there is still room from improvement in the commercialization and standardization of these methods. Moving forward, computational systems should play an increasingly important role in determining polymer properties and cell/material interactions as they become applicable to a wider variety of cell and/or material combinations.

The high-throughput analysis of cell/material interactions is perhaps the most important step in developing a successful engineered tissue. This field has also seen significant progress as researchers have produced more complex and high-throughput screening platforms as well as designing 3-dimensional screening environments and including additional factors such as soluble growth factors. Microfluidic systems have also proved to be quite useful in replicating an *in vivo* environment and should be further utilized in studying a range of polymer arrays and soluble factors in high-throughput and under fluid conditions. Ideally, microfluidic platforms will provide structural support; a 3-dimensional, dynamic environment for analysis of cell behavior; and pathways to control solute and factor distribution/flow. New imaging techniques will be developed that will help accelerate the identification of optimal environments during screening. Finally, although it is a young field, the application of high-throughput techniques to the screening of molecules for stem cell response has increased the speed of characterizing

large libraries of small molecules. These techniques can help a number of engineered tissue factors, but should be most useful in controlling cell differentiation. To this end, future research should maintain a partial focus on the standardization of techniques for measuring differentiation (e.g., the previously discussed fluorescence and transfection tools). Additionally, the further development of analysis methods for the tremendous amount of data produced by these high-throughput systems will be necessary for the field to progress appropriately in the coming years. Overall, all of these platforms and analyses will continue to contribute to the development of the ideal microenvironment for engineered tissue including the optimal synergy between cells, scaffolding, and extracellular factors. In pursuing this goal, the use of high-throughput and combinatorial techniques should continue to enhance our progress towards *in vivo* testing and clinical tissue engineering applications

References:

[1] Anderson DG, Levenberg S, Langer R. Nanoliter-scale synthesis of arrayed biomaterials and application to human embryonic stem cells. Nature Biotechnology 2004;22(7):863-866.

[2] Khademhosseini A, Langer R, Borenstein J, Vacanti JP. Microscale technologies for tissue engineering and biology. Proceedings of the National Academy of Sciences of the United States of America 2006;103(8):2480-2487.

[3] Underhill GH, Bhatia SN. High-throughput analysis of signals regulating stem cell fate and function. Current Opinion in Chemical Biology 2007;11(4):357-366.

[4] Yliperttula M, Chung BG, Navaladi A, Manbachi A, Urtti A. High-throughput screening of cell responses to biomaterials. European Journal of Pharmaceutical Sciences 2008;35(3):151-160.

[5] Hoogenboom R, Meier MAR, Schubert US. Combinatorial methods, automated synthesis and high-throughput screening in polymer research: Past and present. Macromolecular Rapid Communications 2003;24(1):16-32.

[6] Park H, Cannizzaro C, Vunjak-Novakovic G, Langer R, Vacanti CA, Farokhzad OC. Nanofabrication and microfabrication of functional materials for tissue engineering. Tissue Engineering 2007;13(8):1867-1877.

[7] Goldberg M, Mahon K, Anderson D. Combinatorial and rational approaches to polymer synthesis for medicine. Advanced Drug Delivery Reviews 2008;60(9):971-978.

[8] Gordon EM, Barrett RW, Dower WJ, Fodor SPA, Gallop MA. Applications of Combinatorial Technologies to Drug Discovery .2. Combinatorial Organic-

Synthesis, Library Screening Strategies, and Future-Directions. Journal of Medicinal Chemistry 1994;37(10):1385-1401.

[9] Janda KD. Tagged Versus Untagged Libraries - Methods for the Generation and Screening of Combinatorial Chemical Libraries. Proceedings of the National Academy of Sciences of the United States of America 1994;91(23):10779-10785.

[10] Houghten RA, Pinilla C, Appel JR, Blondelle SE, Dooley CT, Eichler J, et al. Mixture-based synthetic combinatorial libraries. Journal of Medicinal Chemistry 1999;42(19):3743-3778.

[11] Sanchez-Martin RM, Mittoo S, Bradley M. The impact of combinatorial methodologies on medicinal chemistry. Current Topics in Medicinal Chemistry 2004;4(7):653-669.

[12] Akinc A, Lynn DM, Anderson DG, Langer R. Parallel synthesis and biophysical characterization of a degradable polymer library for gene delivery. Journal of the American Chemical Society 2003;125(18):5316-5323.

[13] Anderson DG, Lynn DM, Langer R. Semi-automated synthesis and screening of a large library of degradable cationic polymers for gene delivery. Angewandte Chemie-International Edition 2003;42(27):3153-3158.

[14] Lynn DM, Anderson DG, Putnam D, Langer R. Accelerated discovery of synthetic transfection vectors: Parallel synthesis and screening of degradable polymer library. Journal of the American Chemical Society 2001;123(33):8155-8156.

[15] Putnam D. Polymers for gene delivery across length scales. Nature Materials 2006;5(6):439-451.

[16] Brocchini S, James K, Tangpasuthadol V, Kohn J. A combinatorial approach for polymer design. Journal of the American Chemical Society 1997;119(19):4553-4554.

[17] Meredith JC, Sormana JL, Keselowsky BG, Garcia AJ, Tona A, Karim A, et al. Combinatorial characterization of cell interactions with polymer surfaces. Journal of Biomedical Materials Research Part A 2003;66A(3):483-490.

[18] Gravert DJ, Datta A, Wentworth P, Janda KD. Soluble supports tailored for organic synthesis: Parallel polymer synthesis via sequential normal/living free radical processes. Journal of the American Chemical Society 1998;120(37):9481-9495.

[19] Charmot D, Mansky P, Kolosov O, Benoit D, Klaerner G, Petro M, et al. High throughput synthesis and screening in specialty polymers applications. Abstracts of Papers of the American Chemical Society 2001;222:340-POLY.

[20] Hawker CJ, Bosman AW, Frechet JMJ, Harth E, Heumann A, Ranger M, et al. High-throughput synthesis of nanoscale materials. Abstracts of Papers of the American Chemical Society 2001;222:447-POLY.

[21] Zhang HQ, Hoogenboom R, Fijten MWM, Schubert US. Screening and application of ATRP catalysts utilizing an automated synthesizer. Abstracts of Papers of the American Chemical Society 2002;224:260-POLY.

[22] Schmatloch S, Braendli C, Nguyen-Ngoc HH, Schubert US. Combinatorial material research: A supramolecular approach to novel polymers. Abstracts of Papers of the American Chemical Society 2002;224:165-PMSE.

[23] Anderson DG, Tweedie CA, Hossain N, Navarro SM, Brey DM, Van Vliet KJ, et al. A combinatorial library of photocrosslinkable and degradable materials. Advanced Materials 2006;18(19):2614-+.

[24] Brey DM, Erickson I, Burdick JA. Influence of macromer molecular weight and chemistry on poly(beta-amino ester) network properties and initial cell interactions. Journal of Biomedical Materials Research Part A 2008;85A(3):731-741.

[25] Brey DM, Ifkovits JL, Mozia RI, Katz JS, Burdick JA. Controlling poly(beta-amino ester) network properties through macromer branching. Acta Biomaterialia 2008;4(2):207-217.

[26] Tweedie CA, Anderson DG, Langer R, Van Vliet KJ. Combinatorial material mechanics: High-throughput polymer synthesis and nanomechanical screening. Advanced Materials 2005;17(21):2599-+.

[27] Anderson DG, Putnam D, Lavik EB, Mahmood TA, Langer R. Biomaterial microarrays: rapid, microscale screening of polymer-cell interaction. Biomaterials 2005;26(23):4892-4897.

[28] Ifkovits JL, Burdick JA. Review: Photopolymerizable and degradable biomaterials for tissue engineering applications. Tissue Engineering 2007;13(10):2369-2385.

[29] Hansen JK, Thibeault SL, Walsh JF, Shu XZ, Prestwich GD. In vivo engineering of the vocal fold extracellular matrix with injectable hyaluronic acid hydrogels: Early effects on tissue repair and biomechanics in a rabbit model. Annals of Otology Rhinology and Laryngology 2005;114(9):662-670.

[30] Ji Y, Ghosh K, Shu XZ, Li BQ, Sokolov JC, Prestwich GD, et al. Electrospun three-dimensional hyaluronic acid nanofibrous scaffolds. Biomaterials 2006;27(20):3782-3792.

[31] Khademhosseini A, Eng G, Yeh J, Fukuda J, Blumling J, Langer R, et al. Micromolding of photocrosslinkable hyaluronic acid for cell encapsulation and entrapment. Journal of Biomedical Materials Research Part A 2006;79A(3):522-532.

[32] Leach JB, Bivens KA, Patrick CW, Schmidt CE. Photocrosslinked hyaluronic acid hydrogels: Natural, biodegradable tissue engineering scaffolds. Biotechnology and Bioengineering 2003;82(5):578-589.

[33] Smeds KA, Grinstaff MW. Photocrosslinkable polysaccharides for in situ hydrogel formation. Journal of Biomedical Materials Research 2001;54(1):115-121.

[34] Burdick JA, Chung C, Jia XQ, Randolph MA, Langer R. Controlled degradation and mechanical behavior of photopolymerized hyaluronic acid networks. Biomacromolecules 2005;6(1):386-391.

[35] Meredith JC, Karim A, Amis EJ. High-throughput measurement of polymer blend phase behavior. Macromolecules 2000;33(16):5760-5762.

[36] Meredith JC, Smith AP, Karim A, Amis EJ. Combinatorial materials science for polymer thin-film dewetting. Macromolecules 2000;33(26):9747-9756.

[37] Smith AP, Douglas JF, Meredith JC, Amis EJ, Karim A. High-throughput characterization of pattern formation in symmetric diblock copolymer films. Journal of Polymer Science Part B-Polymer Physics 2001;39(18):2141-2158.

[38] Potyrailo RA, Wroczynski RJ, Pickett JE, Rubinsztajn M. High-throughput fabrication, performance testing, and characterization of one-dimensional libraries of polymeric compositions. Macromolecular Rapid Communications 2003;24(1):124-130.

[39] Yang Y, Bolikal D, Becker ML, Kohn J, Zeiger DN, Simon CG. Combinatorial polymer scaffold libraries for screening cell-biomaterial interactions in 3D. Advanced Materials 2008;20(11):2037-+.

[40] Kohn J. New approaches to biomaterials design. Nature Materials 2004;3(11):745-747.

[41] Kohn J, Welsh WJ, Knight D. A new approach to the rationale discovery of polymeric biomaterials. Biomaterials 2007;28(29):4171-4177.

[42] Brocchini S, James K, Tangpasuthadol V, Kohn J. Structure-property correlations in a combinatorial library of degradable biomaterials. Journal of Biomedical Materials Research 1998;42(1):66-75.

[43] Meier MAR, Hoogenboom R, Schubert US. Combinatorial methods, automated synthesis and high-throughput screening in polymer research: The evolution continues. Macromolecular Rapid Communications 2004;25(1):21-33.

[44] Pasch H, Kilz P. Fast liquid chromatography for high-throughput screening of polymers. Macromolecular Rapid Communications 2003;24(1):104-108.

[45] Meier MAR, de Gans BJ, van den Berg AMJ, Schubert US. Automated multiple-layer spotting for matrix-assisted laser desorption/ionization time-of-flight mass spectrometry of synthetic polymers utilizing ink-jet printing technology. Rapid Communications in Mass Spectrometry 2003;17(20):2349-2353.

[46] Meier MAR, Hoogenboom R, Fijten MWM, Schneider M, Schubert US. Automated MALDI-TOF-MS sample preparation in combinatorial polymer research. Journal of Combinatorial Chemistry 2003;5(4):369-374.

[47] Meier MAR, Schubert US. Evaluation of a new multiple-layer spotting technique for matrix-assisted laser desorption/ionization time-of-flight mass spectrometry of synthetic polymers. Rapid Communications in Mass Spectrometry 2003;17(7):713-716.

[48] Lanzendorfer M, Schmalz H, Abetz V, Muller AHE. Application of FT-NIR spectroscopy for monitoring the kinetics of living polymerizations. Abstracts of Papers of the American Chemical Society 2001;221:198-POLY.

[49] Tuchbreiter A, Kappler B, Stockmann R, Mulhaupt R, Honerkamp J. Near infrared reflection spectroscopy: A versatile tool for rapid characterization of olefin copolymers and high-throughput experiments. Macromolecular Materials and Engineering 2003;288(1):29-34.

[50] Tuchbreiter A, Marquardt J, Zimmermann J, Walter P, Mulhaupt R. High-throughput evaluation of olefin copolymer composition by means of attenuated total reflection Fourier tranform infrared spectroscopy. Journal of Combinatorial Chemistry 2001;3(6):598-603.

[51] Potyrailo RA, Lemmon JP, Leib TK. High-throughput screening of selectivity of melt polymerization catalysts using fluorescence spectroscopy and two-wavelength fluorescence imaging. Analytical Chemistry 2003;75(17):4676-4681.

[52] Potyrailo RA, Ezbiansky K, Chisholm BJ, Morris WG, Cawse JN, Hassib L, et al. Development of combinatorial chemistry methods for coatings: High-throughput

weathering evaluation and scale-up of combinatorial leads. Journal of Combinatorial Chemistry 2005;7(2):190-196.

[53] Ashley KM, Meredith JC, Amis E, Raghavan D, Karim A. Combinatorial investigation of dewetting: polystyrene thin films on gradient hydrophilic surfaces. Polymer 2003;44(3):769-772.

[54] Potyrailo RA, Pickett JE. High-throughput multilevel performance screening of advanced materials. Angewandte Chemie-International Edition 2002;41(22):4230-4233.

[55] Beers KL, Douglas JF, Amis EJ, Karim A. Combinatorial measurements of crystallization growth rate and morphology in thin films of isotactic polystyrene. Langmuir 2003;19(9):3935-3940.

[56] Potyrailo RA, Chisholm BJ, Morris WG, Cawse JN, Flanagan WP, Hassib L, et al. Development of combinatorial chemistry methods for coatings: High-throughput adhesion evaluation and scale-up of combinatorial leads. Journal of Combinatorial Chemistry 2003;5(4):472-478.

[57] Stafford CM, Forster AM, Harrison C, Davis CH, Amis EJ, Karim A. High-throughput measurements of polymer adhesion and mechanical properties. Abstracts of Papers of the American Chemical Society 2003;226:134-PMSE.

[58] Davis CH, Beers KL, Forster AM, Stafford CM, Smith AP, Harrison C, et al. Polymer Science at the NIST Combinatorial Methods Center. Polymeric Materials: Science and Engineering 2003;88:386.

[59] James K, Levene H, Parsons JR, Kohn J. Small changes in polymer chemistry have a large effect on the bone-implant interface: evaluation of a series of

degradable tyrosine-derived polycarbonates in bone defects. Biomaterials 1999;20(23-24):2203-2212.

[60] Smith AP, Douglas JF, Meredith JC, Amis EJ, Karim A. Combinatorial study of surface pattern formation in thin block copolymer films. Phys Rev Lett 2001;87(1).

[61] Neuss S, Apel C, Buttler P, Denecke B, Dhanasingh A, Ding XL, et al. Assessment of stem cell/biomaterial combinations for stem cell-based tissue engineering. Biomaterials 2008;29(3):302-313.

[62] Pernagallo S, Unciti-Broceta A, Diaz-Mochon JJ, Bradley M. Deciphering cellular morphology and biocompatibility using polymer microarrays. Biomedical Materials 2008;3(3).

[63] Chang KH, Zandstra PW. Quantitative screening of embryonic stem cell differentiation: Endoderm formation as a model. Biotechnology and Bioengineering 2004;88(3):287-298.

[64] Treiser MD, Liu E, Dubin RA, Sung HJ, Kohn J, Moghe PV. Profiling cell-biomaterial interactions via cell-based fluororeporter imaging. Biotechniques 2007;43(3):361-+.

[65] Yan YN, Wang XH, Pan YQ, Liu HX, Cheng J, Xiong Z, et al. Fabrication of viable tissue-engineered constructs with 3D cell-assembly technique. Biomaterials 2005;26(29):5864-5871.

[66] Weber N, Bolikal D, Bourke SL, Kohn J. Small changes in the polymer structure influence the adsorption behavior of fibrinogen on polymer surfaces: Validation

of a new rapid screening technique. Journal of Biomedical Materials Research Part A 2004;68A(3):496-503.

[67] Flaim CJ, Teng D, Chien S, Bhatia SN. Combinatorial signaling microenvironments for studying stem cell fate. Stem Cells and Development 2008;17(1):29-39.

[68] Levenberg S, Huang NF, Lavik E, Rogers AB, Itskovitz-Eldor J, Langer R. Differentiation of human embryonic stem cells on three-dimensional polymer scaffolds. Proceedings of the National Academy of Sciences of the United States of America 2003;100(22):12741-12746.

[69] Abramson SD, Alexe G, Hammer PL, Kohn J. A computational approach to predicting cell growth on polymeric biomaterials. Journal of Biomedical Materials Research Part A 2005;73A(1):116-124.

[70] Kholodovych V, Smith JR, Knight D, Abramson S, Kohn J, Welsh WJ. Accurate predictions of cellular response using QSPR: a feasibility test of rational design of polymeric biomaterials. Polymer 2004;45(22):7367-7379.

[71] Smith JR, Kholodovych V, Knight D, Welsh WJ, Kohn J. QSAR models for the analysis of bioresponse data from combinatorial libraries of biomaterials. Qsar & Combinatorial Science 2005;24(1):99-113.

[72] Smith JR, Seyda A, Weber N, Knight D, Abramson S, Kohn J. Integration of combinatorial synthesis, rapid screening, and computational modeling in biomaterials development. Macromolecular Rapid Communications 2004;25(1):127-140.

[73] Kholodovych V, Gubskaya AV, Bohrer M, Harris N, Knight D, Kohn J, et al. Prediction of biological response for large combinatorial libraries of biodegradable polymers: Polymethacrylates as a test case. Polymer 2008;49(10):2435-2439.

[74] Whitesides GM, Ostuni E, Takayama S, Jiang XY, Ingber DE. Soft lithography in biology and biochemistry. Annual Review of Biomedical Engineering 2001;3:335-373.

[75] Burdick JA, Khademhosseini A, Langer R. Fabrication of gradient hydrogels using a microfluidics/photopolymerization process. Langmuir 2004;20(13):5153-5156.

[76] Chung BG, Flanagan LA, Rhee SW, Schwartz PH, Lee AP, Monuki ES, et al. Human neural stem cell growth and differentiation in a gradient-generating microfluidic device. Lab on a Chip 2005;5(4):401-406.

[77] Choi NW, Cabodi M, Held B, Gleghorn JP, Bonassar LJ, Stroock AD. Microfluidic scaffolds for tissue engineering. Nature Materials 2007;6(11):908-915.

[78] Ling Y, Rubin J, Deng Y, Huang C, Demirci U, Karp JM, et al. A cell-laden microfluidic hydrogel. Lab on a Chip 2007;7(6):756-762.

[79] Khademhosseini A, Eng G, Yeh J, Kucharczyk PA, Langer R, Vunjak-Novakovic G, et al. Microfluidic patterning for fabrication of contractile cardiac organoids. Biomedical Microdevices 2007;9(2):149-157.

[80] Figallo E, Cannizzaro C, Gerecht S, Burdick JA, Langer R, Elvassore N, et al. Micro-bioreactor array for controlling cellular microenvironments. Lab on a Chip 2007;7(6):710-719.

[81] Lee PJ, Gaige TA, Ghorashian N, Hung PJ. Microfluidic tissue model for live cell screening. Biotechnology Progress 2007;23(4):946-951.

[82] Hwang CM, Khademhosseini A, Park Y, Sun K, Lee SH. Microfluidic chip-based fabrication of PLGA microfiber scaffolds for tissue engineering. Langmuir 2008;24(13):6845-6851.

[83] Ding S, Gray NS, Wu X, Ding Q, Schultz PG. A combinatorial scaffold approach toward kinase-directed heterocycle libraries. Journal of the American Chemical Society 2002;124(8):1594-1596.

[84] Wu X, Ding S, Ding Q, Gray NS, Schultz PG. A small molecule with osteogenesis-inducing activity in multipotent mesenchymal progenitor cells. Journal of the American Chemical Society 2002;124(49):14520-14521.

[85] Yui PB, Hong CC, Sachidanandan C, Babitt JL, Deng DY, Hoyng SA, et al. Dorsomorphin inhibits BMP signals required for embryogenesis and iron metabolism. Nature Chemical Biology 2008;4(1):33-41.

[86] Ding S, Wu TYH, Brinker A, Peters EC, Hur W, Gray NS, et al. Synthetic small molecules that control stem cell fate. Proceedings of the National Academy of Sciences of the United States of America 2003;100(13):7632-7637.

[87] Wu X, Ding S, Ding G, Gray NS, Schultz PG. Small molecules that induce cardiomyogenesis in embryonic stem cells. Journal of the American Chemical Society 2004;126(6):1590-1591.

[88] Chen SB, Zhang QS, Wu X, Schultz PG, Ding S. Dedifferentiation of lineage-committed cells by a small molecule. Journal of the American Chemical Society 2004;126(2):410-411.

[89] Zhao YX, Ding S. A high-throughput siRNA library screen identifies osteogenic suppressors in human mesenchyrnal stem cells. Proceedings of the National Academy of Sciences of the United States of America 2007;104(23):9673-9678.

[90] Huang AH, Motlekar NA, Stein A, Diamond SL, Shore EM, Mauck RL. High-throughput screening for modulators of mesenchymal stem cell chondrogenesis. Annals of Biomedical Engineering 2008;36(11):1909-1921.

[91] Rubin LL. Stem cells and drug discovery: The beginning of a new era? Cell 2008;132(4):549-552.

CHAPTER 4*: A Combinatorial Library of Photocrosslinkable and Degradable Material*

(Adapted from: DG Anderson, CA Tweedie, N Hossain, SM Navarro, DM Brey, KJ Van Vliet, R Langer, JA Burdick. A combinatorial library of photocrosslinkable and degradable materials. Adv Mat 2006. 18(19): 2614-8.)

4.1 Introduction

Photocrosslinkable and degradable polymers are finding a broad range of applications as drug delivery vehicles, tissue engineering scaffolds, and in the fabrication of microdevices [1-3]. However, the synthesis of multifunctional macromers that form these degradable networks commonly involves multiple functionalization and purification steps, which makes the development of large numbers of polymers with diverse properties difficult. Here, we develop the first combinatorial library of degradable photocrosslinked materials. A library of acrylate terminated poly(β-amino ester)s was synthesized in parallel, via a condensation reaction that combines primary or secondary amines with diacrylates. This library of macromers was then photopolymerized to form degradable networks, with a wide range of degradation times (< 1 day to minimal mass loss after 3 months), mass loss profiles, and mechanical properties (~ 4 to 350 MPa). We believe this library approach will allow for the rapid screening and design of degradable polymers for a variety of applications.

The spatial and temporal control afforded during photoinitiated polymerizations has motivated their wide application in the general field of biomaterials [1, 3]. For example, photocrosslinkable hydrogels are used for the delivery of cells to injured tissues [4-8], for the encapsulation and controlled delivery of biological molecules [9-11], and for controlled fluid flow and cell confinement in microfluidics [12, 13]. Additionally, highly crosslinked photopolymers are currently used in dentistry [14] and are being developed as bone-replacement materials [15, 16] and for the fabrication of micro devices [17]. Many of these applications are only possible due to the controlled nature of this type of polymerization. For example, photoinitiated control of polymerization allows for their application as injectable biomaterials [18, 19] with a non-cytotoxic polymerization process [20]. Additionally, through use of masks and lasers, the spatial control of the polymerization process allows for unique patterning and construction of complex materials [21].

Numerous photopolymerizable and degradable materials have been developed, including polyanhydrides, poly(propylene fumarates), poly(ethylene glycol), and polysaccharides [8, 15, 16, 18], all utilizing multiple reaction and purification steps for synthesis of the photopolymerizable precursors. Despite this work, it has proven challenging to predict specific desirable properties (e.g., degradation and mechanics) from known chemical and structural details of the network precursors. These properties are essential in the design of degradable polymers. For instance, it may be desirable to synthesize a very hard material for some applications (e.g., orthopaedics), whereas a soft material is advantageous for other applications (e.g., tissue adhesive) [22, 23]. One potential solution to the inability to predict physical behavior is the generation of a higher

throughput approach to rapidly synthesize and screen photopolymerizable libraries of biomaterials. Combinatorial polymer synthesis has been previously performed by numerous investigators [24-27] and has led to the identification of polymers with unique properties. However, this has not been previously performed for the synthesis of photoreactive macromers that formed crosslinked and degradable polymers.

To this end, we have synthesized degradable photocrosslinkable macromers through the conjugate addition of primary or bis(secondary) amines to diacrylates (Figure 4.1) to form functionalized poly(β-amino ester)s. Polymerization of the macromer occurs by a step-growth mechanism and the resulting linear macromers contain both esters and tertiary amines in their backbones [28]. Side chain functionalized polymers can be synthesized by incorporation of functionalized amines or diacrylates (e.g., R_2 or R_3 in Figure 4.1). By altering the ratio of the diacrylate to amine, poly(β-amino ester)s with a wide range of molecular weights and end groups can be synthesized. To form crosslinked networks, acrylate terminated poly(β-amino ester)s were readily obtained by performing synthesis with an excess of diacrylate (amine molar ratio of 1.2). After photocrosslinking, the poly(β-amino ester) networks degrade under physiological conditions via hydrolysis of their backbone esters to yield small molecule bis(β-amino acid)s, diol products, and poly(acrylic acid) kinetic chains. In addition to the simplicity of synthesis, the benefits of this system are that: i) amine and diacrylate monomer reagents are inexpensive and commercially available, ii) polymerization can be accomplished without the need for additional protection/deprotection schemes because amines participate directly in the bond-forming processes in these reactions, iii) no byproducts are generated during synthesis which eliminates the need for purification

steps, and iv) the conjugate addition reaction is generally tolerant of additional functionality such as alcohols, ethers, and tertiary amines, which further expands the available amines and diacrylates available for the library.

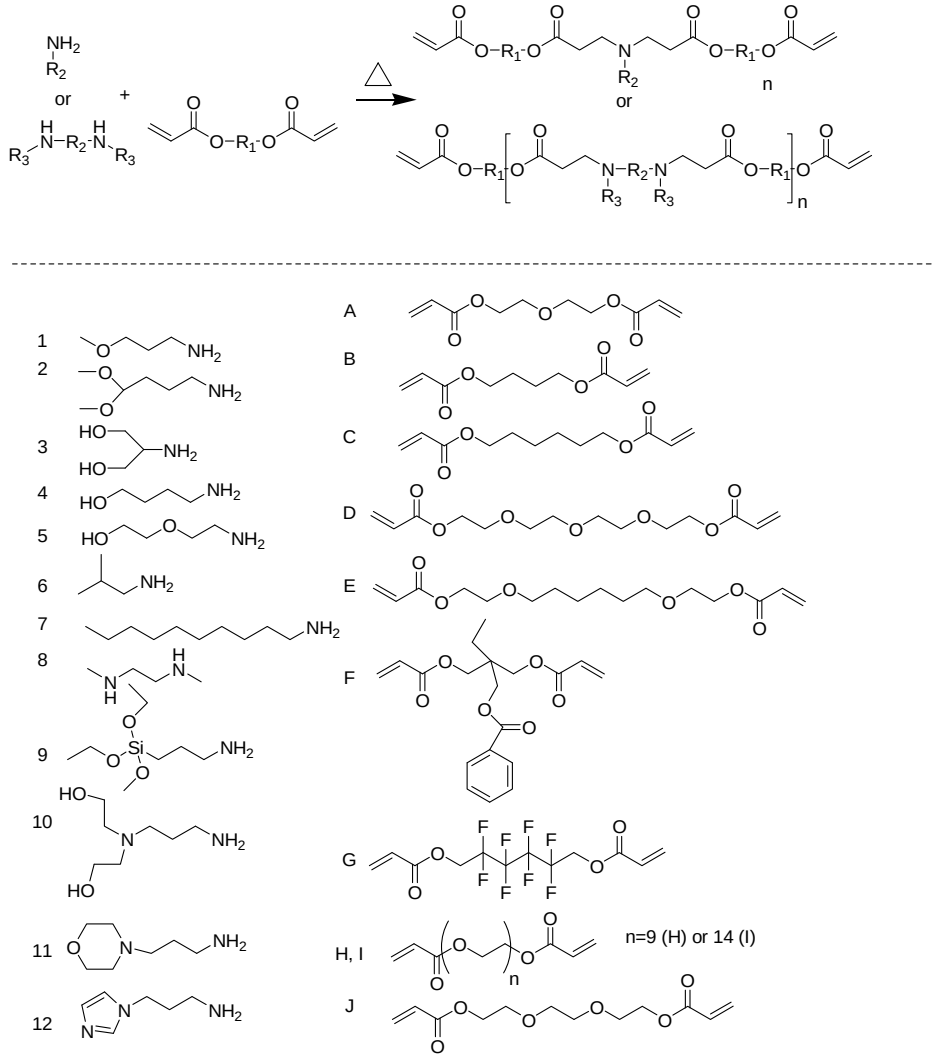

Figure 4.1 General polymerization scheme and chemical structures. Diacrylated macromers were synthesized by the condensation polymerization of an amine with a diacrylate (top). The various monomers used included 12 amines and 10 diacrylates (bottom) to produce a library of 120 photopolymerizable macromers. The macromers were crosslinked into polymers with exposure to ~10 mW/cm^2 ultraviolet light (365 nm) for 5 minutes.

4.2 Materials and Methods

4.2.1 Macromer synthesis and characterization

Macromers were synthesized in parallel by the mixture of the amine and diacrylate in a 10 ml scintillation vial. The vial was reacted while stirring at 90ºC overnight. Samples were stored at 4ºC prior to analysis. The chemical structures and molecular weights of several polymer systems were verified with gel permeation chromatography and ^{1}H-NMR.

GPC was performed using a Hewlett-Packard 1100 Series isocratic pump, a Rheodyne Model 7125 injector with a 100-μL injection loop, and a Phenogel MXL column (5 μm mixed, 300 × 7.5 mm, Phenomenex, Torrance, CA). 70% THF/30% DMSO (v/v) + 0.1 M piperidine was used as the eluent at a flow rate of 1.0 mL/min. Data were collected using an Optilab DSP interferometric refractometer (Wyatt Technology, Santa Barbara, CA) and processed using the TriSEC GPC software package (Viscotek Corporation, Houston, TX). The molecular weights and polydispersities of the polymers were determined relative to monodisperse polystyrene standards.

The macromer chemical structures were analyzed with proton nuclear magnetic resonance (^{1}H-NMR, 360 MHz, DMX360, Bruker, Madison, WI). The ^{1}H-NMR spectra were taken for the initial diacrylates and amines and compared to the spectra for the synthesized macromers in each of the diacrylate to amine ratios. The MMW was calculated using ratios of the areas of acrylate peaks (ppms) to the peaks in the macromer backbone.

4.2.2 Polymerization and degradation

The macromers were mixed with the photoinitiator 1,1-dimethoxy-1-phenyl acetophenone (DMPA, Sigma, dissolved 10 wt% in methylene chloride) and placed in a vacuum desiccator overnight for solvent removal. The macromer/initiator mixture was placed between two glass slides separated with a 1mm spacer and polymerized with exposure to ~10 mW/cm^2 ultraviolet light (Blak-Ray® UV lamp, 365 nm) for 5 minutes. Polymer slabs (~0.8 cm×1.2 cm, 3 per macromer) were cut from the samples, weighed, and placed in tissue culture cassettes. The cassettes were submerged in 150 mM phosphate buffered saline (PBS) and placed on an orbital shaker in a 37ºC incubator for degradation. At each time point, samples were removed, dried and weighed to determine the mass loss. A3, A5, A10, A12, B3, B9, B12, C5, C7, C9, D3, D5, D9, D10, D12, E10, F3, F5, F8, F9, G3, G8, G10, G12, I3, I9, J5, J7, J9, J10, J12 crosslinked during the polymerization process and were not evaluated in the degradation study.

4.2.3 Mechanical properties characterization

Macromers were dissolved at 1:2 v:v ratio in tetrahydrofuran containing 2 wt% DMPA and a spot volume of 10 µl was pipetted onto the surface of an epoxy monolayer-coated glass slide (Xenopore XENOSLIDE E, Hawthorne, NJ) (~18 spots per slide). The THF was allowed to evaporate for 30 - 60 minutes at room temperature. The deposited macromer was then polymerized by exposure to long-wave UV (Blak-Ray®) for 10 minutes in the presence of argon. They were again vacuum desiccated for at least 7 days prior to analysis. Polymer spot thickness was analyzed via contact profilometry (Tencor P10 Surface Profilometer, San Jose, CA) and was >200 µm for all spots. Nanoindentation

was conducted on a pendulum-based nanoindenter (force resolution: 1.5 μN, displacement resolution: 0.1 nm, force maxima: 30 mN, displacement maxima: 4 μm) equipped with a scanning stage (NanoTest600 NT1 and NT0, Micro Materials, Wrexham, UK) and fitted with a spherical indenter of radius R = 500 μm. For this contact-based approach, it was necessary that polymers adhered well to the underlying slide substrate; polymers not meeting this criterion upon photocrosslinking were excluded from this analysis. Indentations were conducted in load control at a rate of 5 μN/s to a maximum depth of 600 nm, resulting in maximum loads ranging from 20 μN to 800 μN and contact strains < 1%. This method was previously described in detail [29]. Load-depth responses were analyzed for E via the method of Field and Swain [30]. Each of the 79 polymers was synthesized and analyzed in triplicate, with three indentations conducted per spot or a total of nine indentations per polymer.

4.3 Results and Discussion

The library of 120 diacrylate terminated poly(β-amino ester) macromers (12 amines and 10 diacrylates reacted at a diacrylate to amine molar ratio of 1.2) was synthesized using the reagents shown in Figure 4.1. These reagents were chosen to provide chemical diversity, including variations in hydrophobicity [31]. The synthesis of representative macromers was verified by nuclear magnetic resonance (NMR, Figure 4.2) and gel permeation chromatography (GPC, Figure 4.3). The NMR results illustrate the disappearance of the amine protons during macromer synthesis and the prevalence of acrylate components in the final macromer. The GPC results indicate that macromer molecular weights are ~2-3 kDa with polydispersities of ~1.5. These results were

completed with the Langer lab at the Massachusetts Institute of Technology and were not able to be repeated through on the equipment in our lab.

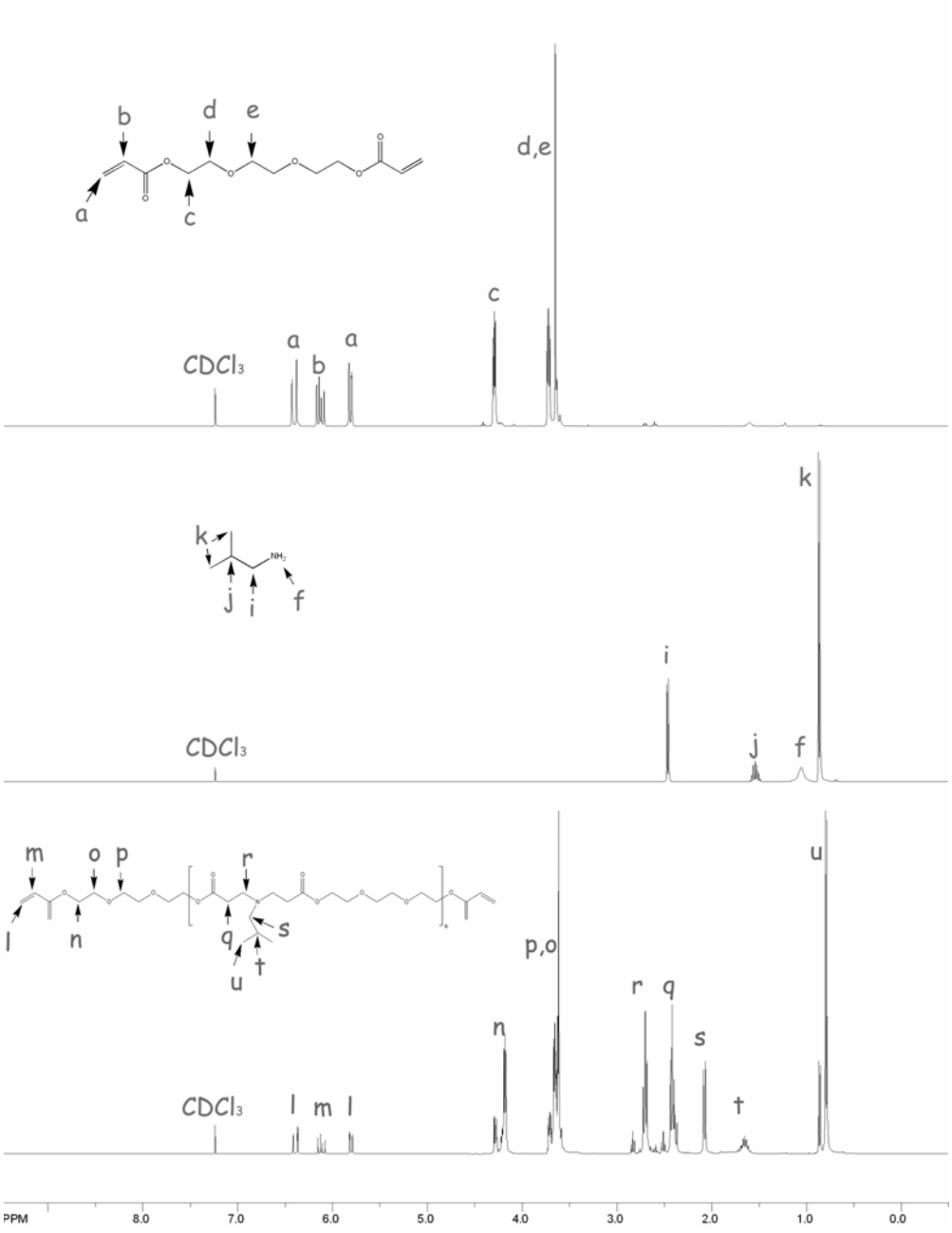

Figure 4.2 NMR results for a diacrylate (J, top) and an amine (6, middle) used for the synthesis of a photopolymerizable macromer (J6, bottom). Note the acrylate peaks and disappearance of amine protons in the synthesized macromer.

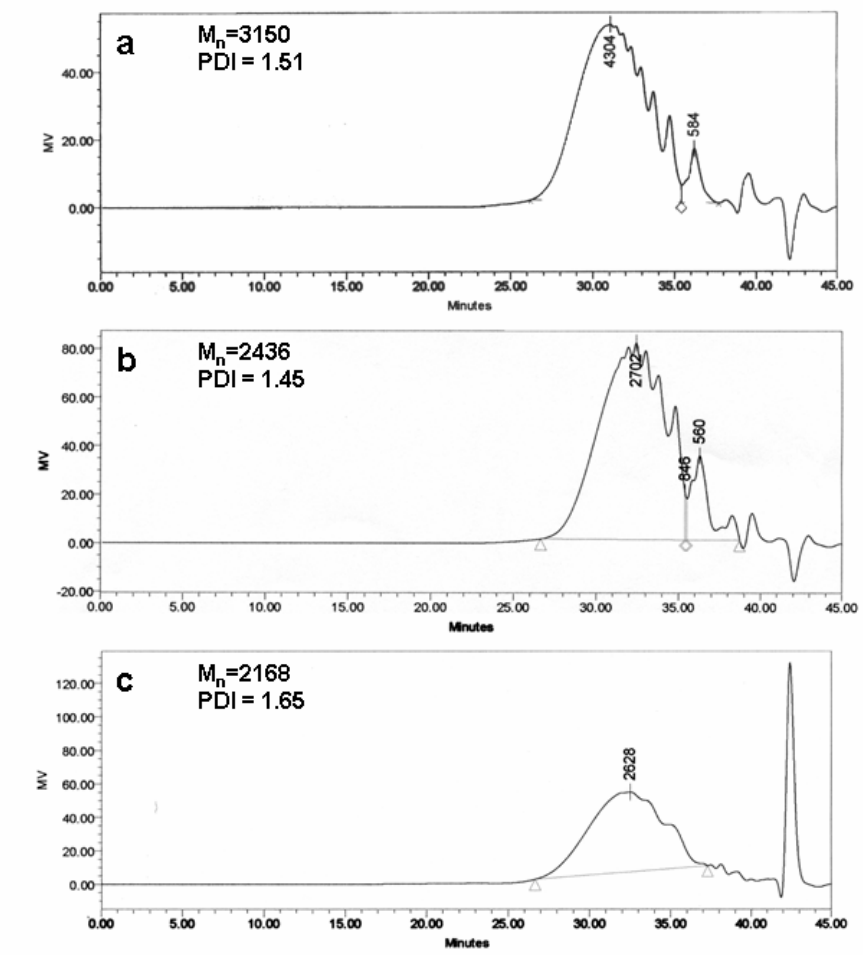

Figure 4.3 Representative GPC results, including number average molecular weight (Mn, g/mol) and polydispersity (PDI), for synthesiszed macromers (a. A1, b. B1, c. D8).

Eighty-nine liquid macromers from this library were polymerized into crosslinked and degradable networks of approximately 200 mg. This polymerization was characterized using FTIR to monitor the acrylate double bond conversion (Figure 4.4). With UV exposure, the double bonds were consumed with time indicating macromer

conversion into a network. The degradation behavior was monitored over several months in triplicate. (Several macromers crosslinked during synthesis and were not investigated further; see methods section for more details.) We characterize degradation as the ability to cleave ester linkages in the polymer networks, which releases network components (i.e., crosslinks, kinetic chains) when immersed in 150 mM phosphate buffered saline while rotating at 37ºC.

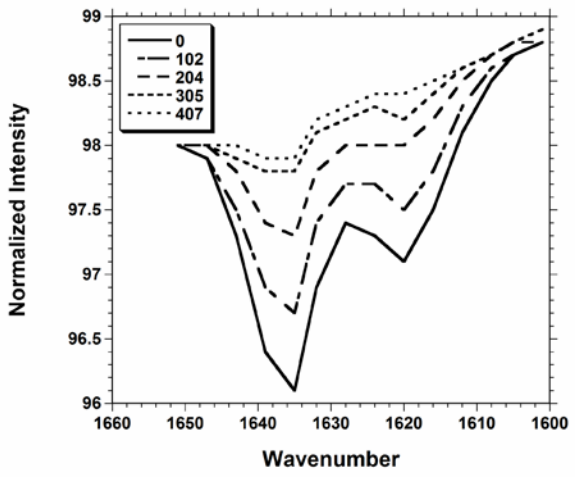

Figure 4.4 Representative FTIR plot of double bond conversion with UV exposure. The FTIR intensity of the acrylate peak normalized to the carbonyl peak is consumed with increased UV exposure (0-407 seconds).

The distributions of polymer mass loss at two time points (24 hours and 57 days) are shown in Figure 4.5. The polymers exhibited a wide range of degradation behavior with mass loss of 100% within 24 hours for some networks, while others lost little mass even after 57 days of immersion. As seen in Figure 4.5a (data included as Table 4.1), many of the polymers that had degraded within 24 hours (such as D, H, I, and J) were

synthesized from diacrylates containing hydrophilic ethylene glycol units. Mass loss was much slower when a more hydrophobic amine (e.g., 7, which contains a long aliphatic chain) was incorporated into the macromer. After 57 days (shown in Figure 4.5b), a number of other polymers completely degraded, while others lost only a small amount of their initial mass. These results show a wide distribution of mass loss at these two time points and that chemical versatility, through unique combinations of amines and diacrylates, plays a role in polymer degradation behavior. Since variations in polymer degradation behavior are desired depending on the application, these results indicate that the polymer library could be useful for applications where polymers completely degrade very quickly to applications where little mass loss is desirable for extended periods.

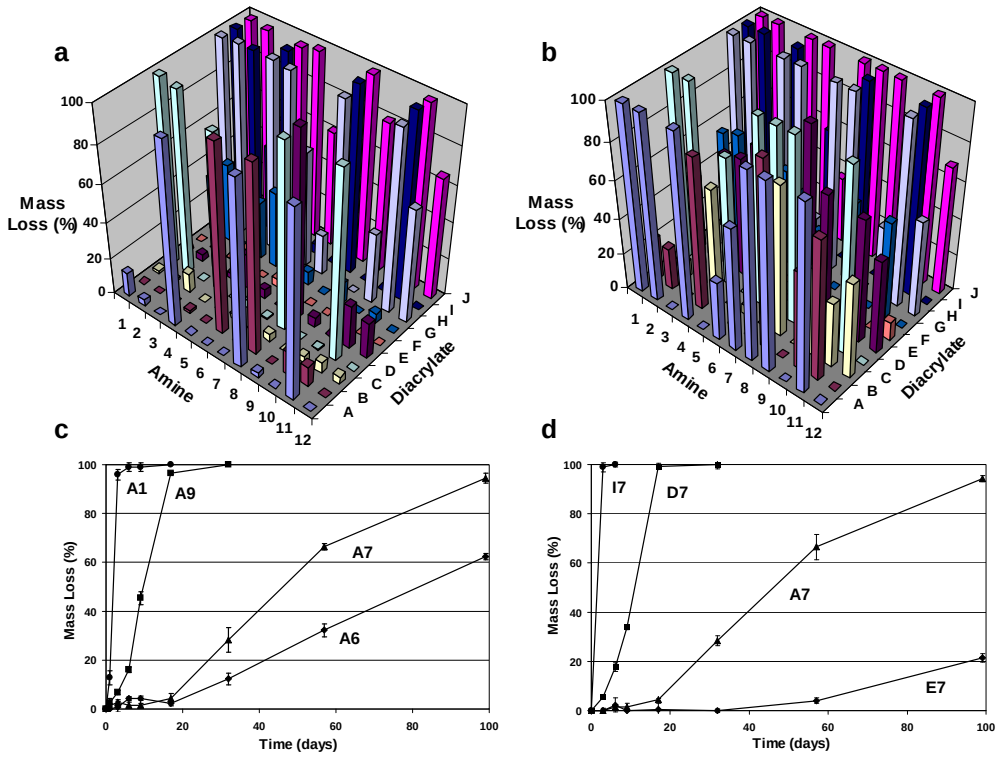

Figure 4.5 Degradation behavior of polymers fabricated from the macromer library. The mass loss after 1 (a) and 57 days (b) for the polymers formed from the macromer array synthesized with 12 amines (1-12) and 10 diacrylates (A-J). Additionally, the mass loss profiles are reported for macromers synthesized with one diacrylate (A) and 4 amines (1, 6, 7, and 9) (c) and one amine (7) and 4 diacrylates (A, D, I, E). Degradation was performed by immersing the samples in PBS on an orbital shaker at 37ºC. These results illustrate the breadth of degradation profiles that are obtained using the macromer library.

Table 4.1 Data (expressed as mean +/- standard deviation) for the degradation studies reported in Figure 4.5

Macromer	Polymer Mass Loss (1 day)	Polymer Mass Loss (57 Days)
A1	14.5 ± 0.2	100.0
A2	3.1 ± 2.2	100.0
A3	-	-
A4	97.6 ± 2.1	100.0
A5	-	-
A6	0.1 ± 2.1	32.2 ± 2.7
A7	1.2 ± 1.0	66.5 ± 1.2
A8	98.3 ± 1.5	100.0
A9	2.6 ± 1.6	100.0
A10	-	-
A11	99.5 ± 3.0	100.0
A12	-	-
B1	0.2 ± 1.7	23.9 ±2.9
B2	0.2 ± 1.3	23.0 ±2.9
B3	-	-
B4	1.3 ±3.4	82.1 ±5.2
B5	-	-
B6	1.0 ±2.6	1.1 ± 3.4
B7	0.7 ± 0.7	1.5 ± 1.3
B8	99.5 ± 4.8	100.0
B9	-	-
B10	12.6 ± 3.3	53.4 ± 2.4
B11	11.2 ± 1.3	76.0 ± 2.2
B12	-	-
C1	1.7 ± 2.4	4.4 ± 2.8
C2	1.4 ± 1.7	8.8 ± 6.3
C3	10.5 ± 2.8	60.3 ± 2.2
C4	1.9 ± 2.1	60.0 ± 1.8
C5	-	-
C6	3.0 ± 1.9	5.3 ± 1.0
C7	-	-
C8	3.9 ± 2.7	81.7 ± 4.7
C9	-	-
C10	3.2 ± 1.8	48.5 ± 2.0
C11	5.8 ± 1.9	35.7 ± 2.7
C12	4.2 ± 2.0	52.3 ± 3.1
D1	99.1 ± 3.0	100.0
D2	97.1 ± 1.6	100.0
D3	-	-
D4	85.0 ± 0.5	87.2 ±2.6
D5	-	-
D6	4.3 ± 2.2	100.0
D7	0.5 ± 0.5	100.0
D8	98.9 ± 1.7	100.0
D9	-	-
D10	-	-
D11	100.0	100.0
D12	-	-
E1	2.3 ± 0.3	50.6 ± 0.3
E2	3.4 ± 1.6	36.8 ± 1.1
E3	24.7 ± 2.5	62.0 ± 2.5
E4	2.7 ± 3.1	64.8 ± 2.5
E5	18.9 ± 2.4	75.3 ± 1.4
E6	4.7 ± 1.4	8.3 ± 1.4
E7	0.2 ± 0.8	4.1 ± 1.8
E8	99.5 ± 2.4	100.0
E9	5.2 ± 3.9	70.1 ± 6.4
E10	-	-
E11	23.7 ± 2.5	67.0 ± 1.9
E12	20.0 ± 0.5	50.7 ± 15.4

Macromer	Polymer Mass Loss (1 day)	Polymer Mass Loss (57 Days)
F1	1.3 ± 2.2	16.7 ± 2.8
F2	0.2 ± 0.3	10.3 ± 2.2
F3	-	-
F4	10.5 ± 5.7	100.0
F5	-	-
F6	4.5 ± 0.1	24.7 ± 5.0
F7	1.1 ± 0.9	4.3 ± 1.9
F8	-	-
F9	-	-
F10	0.5 ± 2.6	5.9 ± 3.8
F11	3.9 ± 0.6	26.8 ± 4.8
F12	6.1 ± 2.5	10.1 ± 4.8
G1	30.8 ± 1.4	54.3 ± 3.8
G2	42.7 ± 2.1	57.4 ± 5.7
G3	-	-
G4	31.3 ± 1.7	42.8 ± 5.5
G5	41.3 ±1.3	51.5 ± 1.5
G6	5.7 ± 1.2	43.4 ± 0.8
G7	7.3 ± 1.1	27.8 ± 5.5
G8	-	-
G9	11.8 ± 1.7	53.6 ± 3.0
G10	-	-
G11	5.6 ± 0.6	53.4 ± 8.6
G12	-	-
H1	99.3 ± 2.1	100.0
H2	100.0	100.0
H3	-	-
H4	100.0	100.0
H5	98.9 ± 2.5	100.0
H6	62.5 ± 1.1	38.3 ± 22.6
H7	22.0 ± 1.9	100.0
H8	97.5 ± 2.2	100.0
H9	-	-
H10	38.0 ± 3.4	39.0 ± 11.7
H11	97.3 ± 1.4	100.0
H12	61.2 ± 1.5	52.6 ± 26.6
I1	99.1 ± 0.5	100.0
I2	92.4 ± 5.7	100.0
I3	45.4 ± 3.5	49.7 ± 30.6
I4	99.6 ± 4.2	100.0
I5	-	-
I6	5.3 ± 0.5	66.5 ± 1.5
I7	-	-
I8	99.7 ± 1.5	100.0
I9	-	-
I10	-	-
I11	100.0	100.0
I12	-	-
J1	99.0 ± 0.3	100.0
J2	97.7 ± 0.6	100.0
J3	55.3 ± 3.4	13.1± 31.7
J4	96.9 ± 0.8	100.0
J5	98.8 ± 1.9	100.0
J6	62.2 ± 1.2	55.4 ± 17.6
J7	18.2 ± 15.7	100.0
J8	99.4 ± 2.8	100.0
J9	80.2 ± 15.4	100.0
J10	47.8 ± 2.2	38.9 ± 22.4
J11	98.4 ± 1.1	100.0
J12	65.7 ± 3.3	69.6 ± 1.6

The degradation behavior for one specific diacrylate (A) polymerized with several amines and photocrosslinked is shown in Figure 4.5c. Here, one chemical component was held constant and the other was altered to control the degradation profiles. In this example, polymers degraded in ~1 week (A1), ~ 3 weeks (A9), ~3 months (A7), and > 3 months (A6). This trend cannot be inferred easily from the chemical structure of the amines indicated in Fig. 4.1, underscoring the advantage of a combinatorial approach for this application. Additionally, one amine (7) was polymerized with several diacrylates and photocrosslinked. The degradation behavior is shown in Figure 4.5d and illustrates polymers that degrade in ~1 week (I7), ~ 2 weeks (D7), ~3 months (A7), and > 3 months (E7). This result follows the general trend that polymers formed from the more hydrophilic macromers (e.g., I and D) degraded faster than polymers A (fewer ethylene glycol repeat units) and E (longer aliphatic chain). The overall degradation profiles range from relatively linear mass loss to systems where mass loss is slow at early times and accelerates as network degradation proceeds. These variations, achieved through simple chemical modifications, illustrate the versatility of this polymer library in tuning or choosing polymers with specific degradation properties. This may prove useful in the identification of degradable polymers for tissue engineering and drug delivery. For example, polymer matrices for tissue engineering ideally degrade slowly enough for sufficient tissue formation on the 3-dimensional scaffold, yet rapidly enough so that tissue development is not physically impeded. The release rate of encapsulated drugs from delivery systems is commonly controlled by affecting the degradation rate of encapsulating polymers. We expect this diversity in polymer degradation times could

prove useful in tuning encapsulated drug release kinetics to a target profile, an important factor in optimizing tissue regeneration [32].

As the mechanical properties of biomaterials are typically important for medical applications, the library was mechanically characterized. The elastic modulus (E) was determined for ~80 members of the polymer library using a rapid nanoindentation technique [29], as shown in Figure 4.6. Within this library subset, E varied from ~4 to ~350 MPa with an average modulus of 21.2 MPa (standard deviation of 5.3% among experiments on an individual polymer). Approximately 95% of the polymers exhibited E within the range of 4 to 25 MPa, which is on the order of moduli for elastomers and non-biodegradable polyurethanes. However, several polymers (e.g., F4, G9, H9) exhibited significantly greater E, on the order of moduli for nylon and high-density polyethylene [33, 34]. Although it would have been difficult to predict a priori that these specific polymers would exhibit superior elastic stiffness, especially since polymers with similar chemistry had moduli that were much lower, this property may be desirable for certain load-bearing or stress-matching applications. Importantly, mechanical stiffness does not correspond directly with degradation rate, demonstrating the potential to derive materials from this library with optimal stiffness and degradation behavior independently.

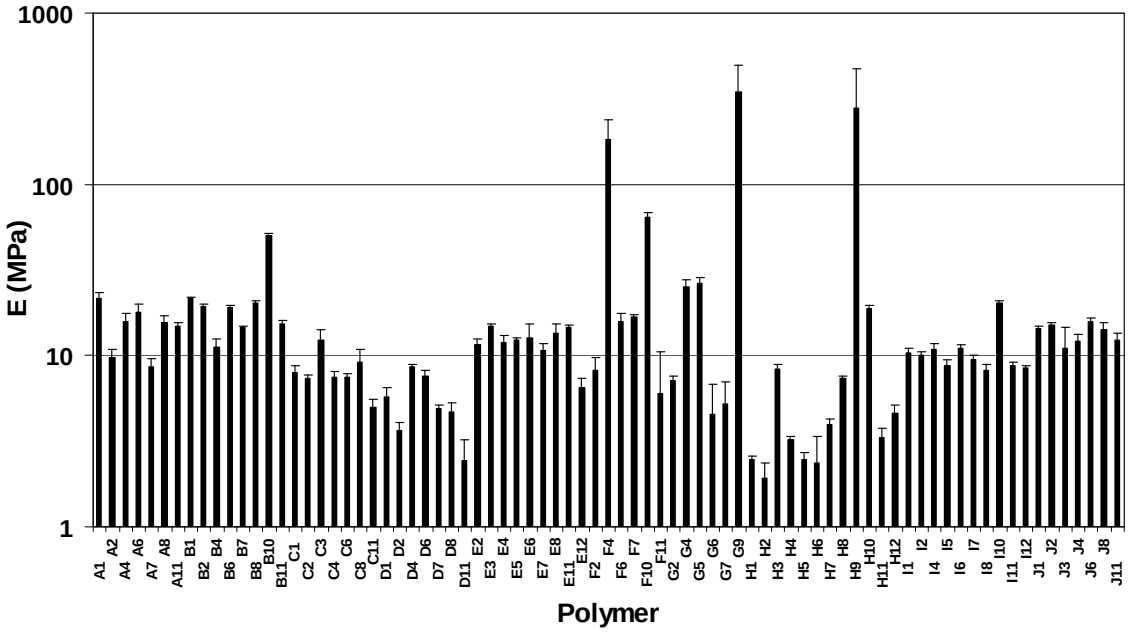

Figure 4.6 Mechanical behavior of polymers fabricated from the macromer library. The elastic modulus (*E*), determined with a nanoindentation method, is reported for 79 of the candidate polymers from the macromer library. These polymers exhibit a range of E ranging from ~4 to ~350 MPa (note the log scale on the y-axis).

At this point, diversity in polymer mechanics and degradation kinetics has been investigated based on the amines and diacrylates chosen for the macromer library. The available degradation and mechanical properties of the library could be further expanded by adjusting the ratio of diacrylate to amine during macromer synthesis. In this work, the ratio was held at 1.2 for the diacrylate to amine, leading to acrylate terminated macromers. By decreasing the amount of diacrylate, the macromer molecular weight will increase, since the polymerizing chains will not terminate as quickly with more reactive

amines present. Additional flexibility could also be attained by copolymerizing various macromers within the polymer library.

4.4 Conclusions

In summary, we have synthesized and characterized the first library of degradable photocrosslinked materials. The large diversity in degradation profiles and elastic moduli demonstrates the potential of this approach in the rapid optimization of material properties. Since crosslinking is radically initiated, these materials may also find non-medical uses as degradable plastics. The chemical diversity presented by these materials could offer other advantages, including potential for specific cellular interactions [35], modification of toxicity, and the facilitation of drug delivery [36, 37]. We believe this combinatorial approach will provide a new method for identification and optimization of degradable and photopolymerized materials.

References:

[1] Anseth KS, Burdick JA. New directions in photopolymerizable biomaterials. Mrs Bulletin 2002;27(2):130-136.

[2] Beebe DJ, Moore JS, Yu Q, Liu RH, Kraft ML, Jo BH, et al. Microfluidic tectonics: A comprehensive construction platform for microfluidic systems. Proceedings of the National Academy of Sciences of the United States of America 2000;97(25):13488-13493.

[3] Fisher JP, Dean D, Engel PS, Mikos AG. Photoinitiated polymerization of biomaterials. Annual Review of Materials Research 2001;31:171-181.

[4] Burdick JA, Anseth KS. Photoencapsulation of osteoblasts in injectable RGD-modified PEG hydrogels for bone tissue engineering. Biomaterials 2002;23(22):4315-4323.

[5] Leach JB, Bivens KA, Patrick CW, Schmidt CE. Photocrosslinked hyaluronic acid hydrogels: Natural, biodegradable tissue engineering scaffolds. Biotechnology and Bioengineering 2003;82(5):578-589.

[6] Mann BK, Gobin AS, Tsai AT, Schmedlen RH, West JL. Smooth muscle cell growth in photopolymerized hydrogels with cell adhesive and proteolytically degradable domains: synthetic ECM analogs for tissue engineering. Biomaterials 2001;22(22):3045-3051.

[7] Nguyen KT, West JL. Photopolymerizable hydrogels for tissue engineering applications. Biomaterials 2002;23(22):4307-4314.

[8] Smeds KA, Grinstaff MW. Photocrosslinkable polysaccharides for in situ hydrogel formation. Journal of Biomedical Materials Research 2001;54(1):115-121.

[9] Anseth KS, Metters AT, Bryant SJ, Martens PJ, Elisseeff JH, Bowman CN. In situ forming degradable networks and their application in tissue engineering and drug delivery. Journal of Controlled Release 2002;78(1-3):199-209.

[10] Burdick JA, Ward M, Liang E, Young MJ, Langer R. Stimulation of neurite outgrowth by neurotrophins delivered from degradable hydrogels. Biomaterials 2006;27(3):452-459.

[11] West JL, Hubbell JA. Photopolymerized Hydrogel Materials for Drug-Delivery Applications. Reactive Polymers 1995;25(2-3):139-147.

[12] Eddington DT, Beebe DJ. Flow control with hydrogels. Advanced Drug Delivery Reviews 2004;56(2):199-210.

[13] Khademhosseini A, Yeh J, Jon S, Eng G, Suh KY, Burdick JA, et al. Molded polyethylene glycol microstructures for capturing cells within microfluidic channels. Lab on a Chip 2004;4(5):425-430.

[14] Anseth KS, Newman SM, Bowman CN. Polymeric dental composites: Properties and reaction behavior of multimethacrylate dental restorations. Biopolymers II:Advances in Polymer Science, 1995. p. 177-217.

[15] Anseth KS, Shastri VR, Langer R. Photopolymerizable degradable polyanhydrides with osteocompatibility. Nature Biotechnology 1999;17(2):156-159.

[16] Fisher JP, Holland TA, Dean D, Engel PS, Mikos AG. Synthesis and properties of photocross-linked poly(propylene fumarate) scaffolds. Journal of Biomaterials Science-Polymer Edition 2001;12(6):673-687.

[17] Hutchison JB, Haraldsson KT, Good BT, Sebra RP, Luo N, Anseth KS, et al. Robust polymer microfluidic device fabrication via contact liquid photolithographic polymerization (CLiPP). Lab on a Chip 2004;4(6):658-662.

[18] Elisseeff J, Anseth K, Sims D, McIntosh W, Randolph M, Langer R. Transdermal photopolymerization for minimally invasive implantation. Proceedings of the National Academy of Sciences of the United States of America 1999;96(6):3104-3107.

[19] Luman NR, Smeds KA, Grinstaff MW. The convergent synthesis of poly(glycerol-succinic acid) dendritic macromolecules. Chemistry-a European Journal 2003;9(22):5618-5626.

[20] Bryant SJ, Nuttelman CR, Anseth KS. Cytocompatibility of UV and visible light photoinitiating systems on cultured NIH/3T3 fibroblasts in vitro. Journal of Biomaterials Science-Polymer Edition 2000;11(5):439-457.

[21] Liu VA, Bhatia SN. Three-dimensional photopatterning of hydrogels containing living cells. Biomedical Microdevices 2002;4(4):257-266.

[22] El-Ghannam A. Bone reconstruction: from bioceramics to tissue engineering. Expert Review of Medical Devices 2005;2(1):87-101.

[23] Ji BH, Gao HJ. Mechanical properties of nanostructure of biological materials. Journal of the Mechanics and Physics of Solids 2004;52(9):1963-1990.

[24] Brocchini S, James K, Tangpasuthadol V, Kohn J. Structure-property correlations in a combinatorial library of degradable biomaterials. Journal of Biomedical Materials Research 1998;42(1):66-75.

[25] Moss JA, Stokols S, Hixon MS, Ashley FT, Chang JY, Janda KD. Solid-phase synthesis and kinetic characterization of fluorogenic enzyme-degradable hydrogel cross-linkers. Biomacromolecules 2006;7(4):1011-1016.

[26] Smith JR, Seyda A, Weber N, Knight D, Abramson S, Kohn J. Integration of combinatorial synthesis, rapid screening, and computational modeling in biomaterials development. Macromolecular Rapid Communications 2004;25(1):127-140.

[27] Vogel BM, Cabral JT, Eidelman N, Narasimhan B, Mallapragada SK. Parallel synthesis and high throughput dissolution testing of biodegradable polyanhydride copolymers. Journal of Combinatorial Chemistry 2005;7(6):921-928.

[28] Lynn DM, Langer R. Degradable poly(beta-amino esters): Synthesis, characterization, and self-assembly with plasmid DNA. Journal of the American Chemical Society 2000;122(44):10761-10768.

[29] Tweedie CA, Anderson DG, Langer R, Van Vliet KJ. Combinatorial material mechanics: High-throughput polymer synthesis and nanomechanical screening. Advanced Materials 2005;17(21):2599-+.

[30] Field JS, Swain MV. A Simple Predictive Model for Spherical Indentation. Journal of Materials Research 1993;8(2):297-306.

[31] Anderson DG, Lynn DM, Langer R. Semi-automated synthesis and screening of a large library of degradable cationic polymers for gene delivery. Angewandte Chemie-International Edition 2003;42(27):3153-3158.

[32] Huang YC, Riddle K, Rice KG, Mooney DJ. Long-term in vivo gene expression via delivery of PEI-DNA condensates from porous polymer scaffolds. Human Gene Therapy 2005;16(5):609-617.

[33] Unal H, Mimaroglu A. Influence of filler addition on the mechanical properties of nylon-6 polymer. Journal of Reinforced Plastics and Composites 2004;23(5):461-469.

[34] Wang Q, Gao J, Wang R, Hua Z. Mechanical and rheological properties of HDPE/graphite composite with enhanced thermal conductivity. Polymer Composites 2001;22(1):97-103.

[35] Anderson DG, Levenberg S, Langer R. Nanoliter-scale synthesis of arrayed biomaterials and application to human embryonic stem cells. Nature Biotechnology 2004;22(7):863-866.

[36] Anderson DG, Peng WD, Akinc A, Hossain N, Kohn A, Padera R, et al. A polymer library approach to suicide gene therapy for cancer. Proceedings of the National Academy of Sciences of the United States of America 2004;101(45):16028-16033.

[37] Leach JK, Mooney DJ. Bone engineering by controlled delivery of osteoinductive molecules and cells. Expert Opinion on Biological Therapy 2004;4(7):1015-1027.

CHAPTER 5*: Controlling Poly(β-amino ester) Network Properties via Macromer Molecular Weight*

(Adapted from: DM. Brey, IE Erickson, and JA Burdick, "Influence of Macromer Molecular Weight and Chemistry on Poly(β-amino ester) Network Properties and Initial Cell Interactions," J Biomed Mater Res A, 2008, 85(3): 731-41)

5.1 Introduction

Injectable biomaterials have been used for many years for applications such as bone cements and for filling dental caries [1]. In recent years, injectable materials and specifically, photocrosslinkable polymers, have been developed for a variety of clinical applications; including adhesion prevention [2], tissue engineering [3-10], and drug and gene delivery [11]. Photopolymerization can be advantageous over other polymerization techniques for many of these applications because they occur rapidly at physiological temperature (37°C) and in biological environments without the use of solvents, which permits network formation *in vivo* [3]. Additionally, the polymerization is temporally and spatially controlled, which is not afforded by thermal initiation and allows for better control over the polymerization reaction (e.g., for minimizing exotherms) [1, 12] and for the fabrication of materials with complex structures (e.g., for tissue engineering scaffolds and microfluidic devices) [13-15].

For many of these intended applications, the overall mechanical properties of the biomaterial and the ability of the material to degrade (either enzymatically or

hydrolytically) in a controlled fashion are extremely important. For instance, degradation is important in tissue engineering scaffolds to prevent the necessity of a secondary surgery for implant removal and may aid in healing if the degradation rate is matched to cell penetration and tissue formation. In drug delivery, the controlled release of the payload is typically controlled by properties such as degradation and diffusion. Mechanics are an important design criteria for many applications if the material is to bear the load of the tissue [16], to control the interaction of cells with the material [17-19], and may be correlated to properties like swelling which subsequently controls encapsulated cell viability [20].

Numerous photopolymerizable and degradable biomaterials have been developed to date. These include materials like poly(propylene fumarate)s (PPF) [21], photocrosslinkable polyanhydrides [22], poly(ethylene glycol)s [18, 23-25], and crosslinkable polysaccharides [4, 8, 10]. Typically, the syntheses of these polymers involve several reaction and purification steps. These lengthy and often tedious synthesis procedures limit the potential variations in polymer chemistry and structure that can be developed and rapidly tested for various applications. This is particularly important since the degradation, mechanical, and cellular interaction properties of these degradable polymer systems have proven difficult to predict based on chemistry alone; leading to long iterative processes for material development.

To expedite the development of novel photocrosslinkable polymers, conjugate addition polymerizations have been used to create large libraries of poly(β-amino ester) (PBAE) macromers by combining commercially available primary and secondary amines with diacrylates [26, 27]. This procedure is relatively simple and does not require

protection/deprotection schemes, does not generate byproducts that must be removed through further purification steps, and is tolerant of most functional groups. Similarly, through precise control over reagent concentration and selection of appropriate precursor molecules, a large library of PBAE macromers with acrylate end groups (ratio of acrylate to amine > 1) was synthesized that form degradable networks using photoinitiated polymerizations [28]. This macromer library was produced with only a diacrylate to amine ratio of 1.2, so variations in molecular weight were not investigated. Networks formed from this macromer library were screened for degradation and initial mechanical properties and showed that a wide range of degradation behavior and mechanical properties are possible from the library. Now, application-specific design criteria can be used to identify candidate polymers from this library that can be further developed for a variety of applications (e.g., tissue engineering, drug delivery, microfluidics).

The overall aim of this study is to utilize the advantages of this synthesis process to further expand the library by investigating the control over macromer molecular weight (MMW) during synthesis and examine how this influences network reaction behavior, bulk properties, and degradation. Specifically, three macromers from the original library were selected and utilized for this fundamental study of macromer structure/function relationships. Additionally, for the first time, the interaction of cells with these novel materials was investigated. This work represents another step towards the development of advanced polymers for a variety of biological applications, and specifically as scaffolding for tissue engineering.

5.2 Materials and Methods

5.2.1 Macromer synthesis and characterization

Acrylate terminated PBAEs were synthesized in parallel by the step-growth polymerization of commercially available primary amines and diacrylates [28]. The diacrylates and amines (Figure 5.1) included triethylene glycol diacrylate (J) and 1,6-hexanediol diacrylate (C) (Scientific Polymer Products, Ontario, NY); 1,6-hexanediol ethoxylate diacrylate (E), 1-amino-2-methylpropane (6), and 1-(3-aminopropyl)imidazole (12) (Sigma, St Louis, MO); and 3-methoxypropylamine (1) (TCI America, Portland, OR). These liquid reagents were mixed at molar ratios of 1:1, 1.05:1, 1.1:1, 1.2:1, and 1.4:1 of diacrylate to amine (J6, C12 or E1) in glass scintillation vials at 90°C overnight while stirring (700 rpm, Telesystem HP15/RM, Variomag USA, Daytona Beach, FL). The sample notation is consistent with our previous report on the development of the initial photocrosslinkable macromer library [28]. The viscous liquid macromers were immediately used for testing, polymerized into networks, or stored at 4°C until use.

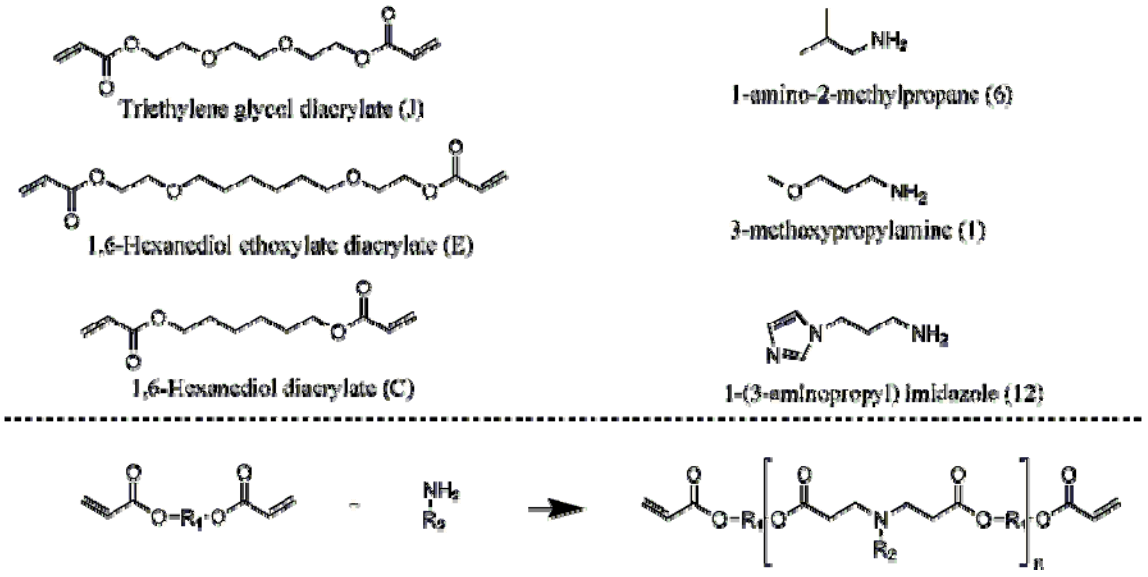

Figure 5.1 Chemical structures of diacrylates (J, E, C) and amines (6, 1, 12) used in the synthesis of acrylate terminated poly(β-amino ester)s. These macromers can be crosslinked into degradable networks using a free-radical photoinitiated polymerization.

The macromer chemical structures were analyzed with proton nuclear magnetic resonance (^{1}H-NMR, 360 MHz, DMX360, Bruker, Madison, WI) and Fourier transform infrared (FTIR, Nicolet 6700, Thermo Electron, Waltham, MA) spectroscopy. The ^{1}H-NMR spectra were taken for the initial diacrylates and amines and compared to the spectra for the synthesized macromers in each of the diacrylate to amine ratios. The MMW was calculated using ratios of the areas of acrylate peaks (ppms) to the peaks in the macromer backbone. For FTIR analysis, a drop of the liquid macromer was placed on a zinc selenium crystal and spectra were obtained in attenuated total reflectance (ATR) FTIR mode. The ATR-FTIR spectra were then analyzed to monitor variations in

the areas of the acrylate peaks (~1630 cm^{-1}) normalized to the carbonyl peak (~1730cm^{-1}) as the ratio of diacrylate:amine was altered.

5.2.2 Photopolymerization and network characterization

The photoinitiator 2,2-dimethoxy-2-phenyl acetophenone (DMPA, Sigma) was added to the liquid macromers at a final concentration of 0.5% (w/w) by addition of a 10% (w/v) solution of DMPA in methylene chloride and solvent was removed in a vacuum desiccator overnight. The polymerization behavior was monitored using an ATR-FTIR system with a zinc selenium crystal. A drop of the macromer/initiator solution was placed directly on the horizontal crystal, covered with a glass cover slip, and exposed from above to ultraviolet light (~1.3 W/cm^2 at tip of light guide, distance of 24 cm, 365 nm, Omnicure Series 1000, Exfo, Quebec, Canada). The change in area of the double bond peak (~1630 cm^{-1}) was used to monitor double-bond conversion in real-time. Values were normalized to the area of the carbonyl peak (~1730 cm^{-1}) and converted to double bond conversion using the initial peak areas.

For mechanical testing, the macromer/initatior solution was placed between glass slides with either a 1 mm (tensile and degradation samples) or 2 mm (compression samples) spacer and polymerized with exposure to ~10 mW/cm^2 ultraviolet light (365nm, Blak-Ray B-100 AP, Ultraviolet Products, Upland, CA) for 5 minutes. The polymers were then cut into 25 mm x 5 mm slabs for tensile testing and 5 mm disks were punched for compression testing. Tensile testing was performed on a materials testing machine (Microtester 5848, Instron, Norwood, MA) with a constant strain rate of 0.1% per second until macroscopic failure. The elastic modulus was then calculated as the slope of the

linear portion of the stress versus strain plot. Unconfined compression testing was completed on a custom made mechanical testing device designed as described in Soltz et al.[29] Samples were creep tested under a 2 gram load until equilibrium and then stressed to 10% strain at 1μm/sec and allowed to relax. The compressive moduli were calculated as the slope of the stress versus strain plots between 5 and 10% strain.

The soluble (sol) fraction of the various networks was determined by placing polymer discs in methylene chloride overnight. This allowed unreacted macromer to swell from the network. After drying, the sol fraction was calculated as the percent of initial mass lost during overnight swelling (only one cycle). Negligible mass loss was observed with subsequent swelling and drying cycles indicating that the sol fraction was removed during the first cycle.

5.2.3 Polymer degradation

Samples were polymerized as described above and 5 mm x 5 mm squares were cut from the 1 mm thick slabs and weighed (initial mass). Samples were placed in histology cassettes and degraded in phosphate buffered saline (PBS) at 37°C (pH 7.4) on an orbital shaker. Samples were removed after 1, 2, 4, 7, 10, 13, and 17 weeks of degradation, dried in an oven, and weighed (final mass). The overall mass loss was calculated from the recorded initial and final mass values. Mechanical properties with degradation were determined through tensile and compressive analysis of samples as described above after 2 and 4 weeks of degradation.

5.2.4 Cell interaction studies

To prepare films for cell interaction studies, the macromer/initiator solutions were dissolved in ethanol at a 1:2 (w/v) ratio and pipetted (30 μl) into 24-well plates. The ethanol was allowed to evaporate off overnight to leave a thin film of the macromer and initiator. The plates were placed in a transparent chamber being purged with nitrogen and polymerized for 10 minutes with ultraviolet light (Blak Ray). To sterilize the films, the plates were placed under a germicidal lamp in a laminar flow hood for 30 minutes. Wells were filled with PBS and left in an incubator overnight. After washing with PBS, the wells were filled with growth media for 30 minutes prior to cell seeding.

Human sarcoma osteoblast-like cells (SaOS-2, ATCC, Manassas, VA) were grown in media comprised of Modified McCoy's Medium (ATCC) with 10% fetal bovine serum (FBS, Hyclone, Logan, UT) and 1% penicillin/streptomycin (Invitrogen, Carlsbad, CA). SaOS-2 cells were seeded on the polymer films at 50,000 cells per well. The cells were cultured for 24 hours and fixed in 2.5% glutaraldehyde (Polysciences, Warrington, PA) for 15 minutes. Phase contrast photomicrographs were taken using an inverted microscope (Axiovert, Zeiss, Oberkochen, Germany) and a digital camera (Axiovision, Zeiss). The total cell number was determined by counting adhered cells in at least 5 random fields on 3 individual films for each composition at each time point. Cell area was measured using NIH ImageJ software (3 samples per polymer/ratio, 5 pictures per well, 20 cells per picture, at least 300 cells per composition).

5.2.5 Statistical analysis

Statistical analysis was performed using ANOVA with Tukey's post-hoc among the groups with significance defined as a confidence level of 0.05. All values are reported as the mean and the standard deviation of the mean.

5.3 Results and Discussion

5.3.1 Macromer synthesis and characterization

Three macromers (E1, C12, and J6) were selected from our previously reported library of acrylate terminated PBAE macromers [28] and synthesized as shown in Figure 5.1. These specific macromers were chosen because they illustrated potential as scaffolding for tissue engineering due to their gradual mass loss and overall degradation times (~4 months). For certain tissues, such as bone, this would allow for sufficient cell and tissue infiltration prior to complete degradation, yet would not inhibit tissue growth [30]. The initial macromer library incorporated a large range of chemical reagents (amines and diacrylates) and the influence of chemical alterations on polymer mechanics and degradation was investigated, however only one diacrylate to amine molar ratio was examined (i.e., 1.2). This ratio controls the extent of polymerization that occurs before the amines are consumed and all macromer ends are terminated with acrylate groups (with a ratio > 1). It is anticipated that simple alterations in the ratio can lead to changes in the MMW. In this study, the diacrylate to amine ratio was varied at 1:1, 1.05:1, 1.1:1, 1.2:1, and 1.4:1 in order to change the MMW of the macromer and investigate the influence of MMW on polymer properties and cell interactions. It should be noted that the objective of this study is not to illustrate that one of these macromers is ideal for

tissue engineering, but to investigate the influence of chemical and structural alterations of the macromer on the final properties. This information can then aid in development of biodegradable PBAEs for a specific application.

The resulting macromers were characterized with ^{1}H-NMR and representative spectra are shown in Figure 5.2. These spectra demonstrate the chemical diversity of the different macromers, illustrate the complete consumption of amine protons during synthesis, and show the maintenance of peaks for acrylate reactive moieties. Protons from the amine group are represented by a broad peak found around ~1.1 ppm and are found in the spectra of the initial amine reagents but are not present in any of the synthesized macromer spectra. The area of acrylate peaks (labeled in Figure 5.2 as a and b at ~6.4, 6.0, and 5.7 ppm for one ratio) changed with variations in the diacrylate to amine ratios (i.e., smaller peaks for lower ratios) indicating variations in the MMWs (see Figure 4.4).

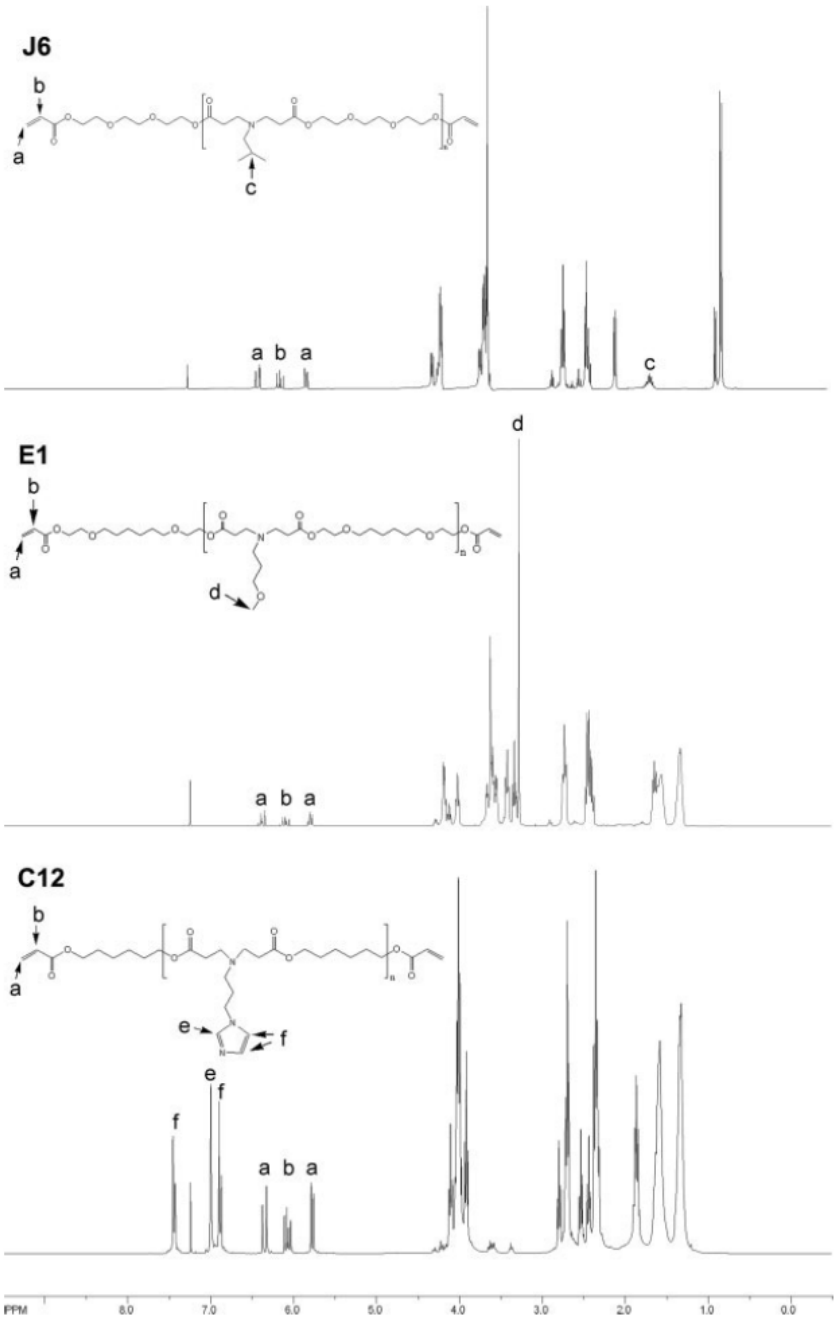

Figure 5.2 NMR spectra of macromers J6, E1, and C12 synthesized at a diacrylate to amine ratio of 1.2:1. Of interest is the maintenance of acrylate proton peaks (~6.4, 6.0, 5.7 ppm) and the disappearance of the amine proton peaks (~1.1 ppm).

The MMW was calculated with ^{1}H-NMR, via end group analysis (comparison of acrylate protons to backbone protons), and the results are shown in Table 5.1. The area of the acrylate peaks (representing 6 hydrogen atoms, 3 per macromer end group) was divided by the area of a peak corresponding to distinct protons in the backbone (labeled c, d, e, and f). This gives the average number of repeat units, and this value can be used to calculate the number average molecular weight (Table 5.1). For all cases, the MMW increases as the diacrylate to amine ratio decreases, as expected since the reaction can proceed further prior to termination when a more equivalent molar ratio is used. The calculated number average molecular weight is anticipated to be an overestimation of the MMW, since this analysis assumes that all end groups are diacrylates. However, impurities in the original diacrylate reagents (which were 85-90% pure) can lead to end-groups that are not acrylates, but hydroxyl groups.

Table 5.1 Number of repeat units (n) and number average molecular weight (MMW) determined with end group analysis using ^{1}H-NMR, as well as the sol fraction of the photopolymerized networks polymerized from the various macromers and MMWs.

Macromer	Ratio	n	MMW	Sol Fraction (%)
J6	1:1	17.5	6070	47.5 ± 1.1
	1.05:1	12.2	4317	36.9 ± 1.0
	1.1:1	11.4	4049	24.5 ± 0.3
	1.2:1	5.8	2182	12.8 ± 1.9
	1.4:1	3.5	1406	2.2 ± 0.3
C12	1:1	13.8	5080	47.2 ± 0.4
	1.05:1	10.6	3945	44.9 ± 3.8
	1.1:1	8.3	3159	33.8 ± 0.9
	1.2:1	5.7	2230	17.4 ± 0.6
	1.4:1	3.6	1486	10.9 ± 0.4
E1	1:1	9.1	3982	48.9 ± 0.6
	1.05:1	8.0	3531	33.9 ± 0.4
	1.1:1	6.9	3111	23.2 ± 0.2
	1.2:1	5.7	2596	12.0 ± 0.7
	1.4:1	3.6	1768	4.3 ± 0.9

Additionally, the ATR-FTIR spectra of the various macromers at the different ratios were obtained to assess variations in the acrylate peak (~1630 cm^{-1}) and are shown in Figure 5.3 for macromer E1. The acrylate region (Figure 5.3A) is suppressed as the ratio decreases, indicating once again that the MMW is increasing. Figure 5.3B shows the area of the acrylate peak normalized to the area of the carbonyl peak (~1730 cm^{-1}). Again, these values illustrate an increase in acrylate concentration with an increase in the diacrylate:amine ratio during synthesis.

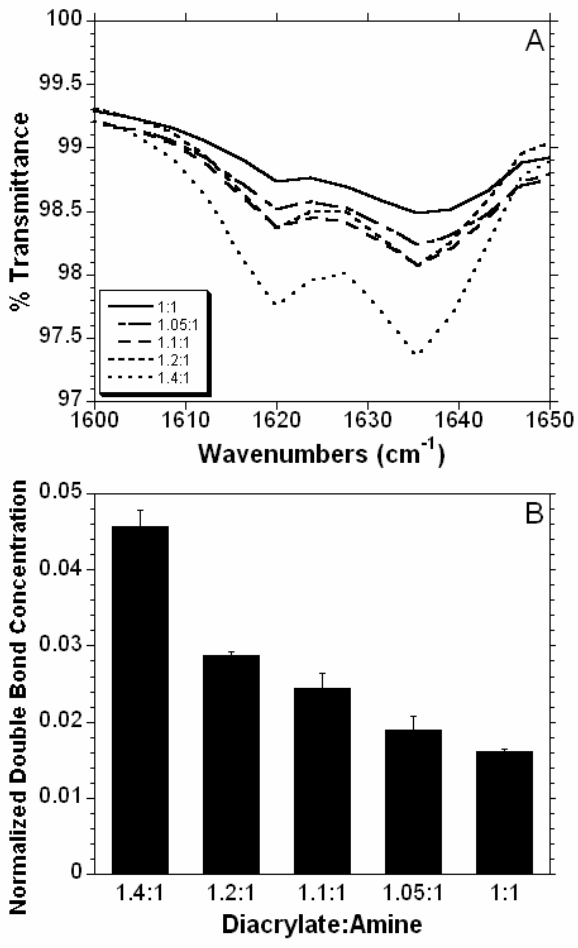

Figure 5.3 Macromer characterization with ATR-FTIR. Initial ATR-FTIR spectra for the acrylate double bond (~1630 cm^{-1}) with varying ratios of diacrylate to amine (A) and the normalized double bond concentration calculated as the ratio of the acrylate to carbonyl (~1730 cm^{-1}) peak areas.

5.3.2 Photopolymerization and network characterization

Free radical polymerizations of the synthesized macromers were initiated by ultraviolet light exposure of the macromer with 0.5% DMPA as the initiator. Although a solvent was used to add the initiator to the macromer, the solvent was evaporated prior to

polymerization. This reaction was monitored in real time using ATR-FTIR to determine the real-time conversion of the acrylate double bonds that form network kinetic chains and ultimately lead to a crosslinked polymer. The conversion profiles (Figure 5.4A) of macromer E1 for all MMWs indicate that lower MMWs react much faster and to higher double bond conversions (Figure 5.4B) after 10 minutes than the higher MMWs. This is likely due to the increase in the concentration of reactive groups for the lower MMWs and an increase in initial diffusion limitations for the higher MMWs. The overall reaction behavior and ultimate double bond conversion is important because it is correlated to network mechanical properties and unreacted macromer that may leach from the network and be toxic. The sol fraction, listed in Table 5.1, is also an indicator of the lack of the complete acrylate conversion with the high MMW. The sol fraction for the 1:1 ratio is over 47% for all three macromer chemistries. The high concentration of soluble factors is likely due to these unreacted double bonds found during monitoring of the reaction with ATR-FTIR. These molecules are never reacted into the 3-dimensional network and are released when the network is swollen in methylene chloride. Also, impurities in the original diacrylate reagents produce macromers with one or both ends without acrylate moieties, which increases the sol content.

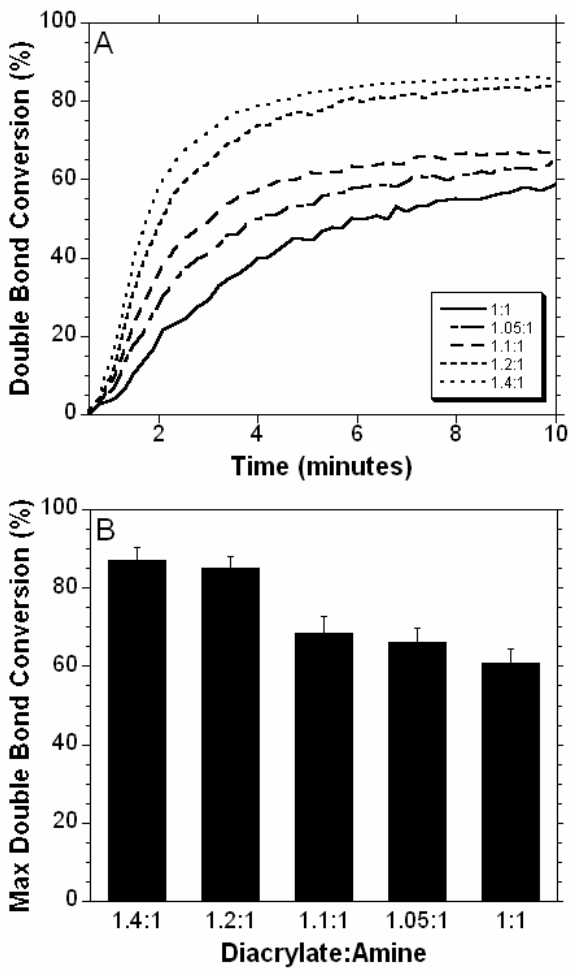

Figure 5.4 ATR-FTIR of the double conversion with UV exposure. Real-time double bond conversion of macromer E1 synthesized at various MMWs and polymerized on a zinc selenium crystal with exposure to ultraviolet light measured with ATR-FTIR (A) and the double bond conversion after 10 minutes (B) of ultraviolet light exposure.

The mechanical properties of polymers J6, C12, and E1 formed from all MMWs were measured in both tension and compression. The tensile moduli for J6, C12, and E1 for the different MMWs are shown in Figure 5.5A. For all of the polymers, a general trend is seen between the tensile modulus and the MMW (i.e. the moduli increases with

increasing diacrylate:amine ratio). For instance, J6 at the 1:1 ratio had a modulus of 0.22 ± 0.012 MPa and a modulus of 4.50 ± 1.08 MPa for the 1.4:1 ratio, which represents a 20 fold increase in modulus. The mean moduli were statistically different between ratios of the same polymer for all cases except 1:1 and 1.05:1 for C12 and J6, 1:1 and 1.1:1 for J6, and 1.05:1 and 1.1:1 for all polymers. Lower MMWs (greater diacrylate:amine ratio) led to networks with a higher crosslinking density, which corresponds to a greater modulus. Variations in the chemistry also contributed to the tensile properties, as the moduli for the C12 polymers were significant greater than the corresponding ratios of all E1 polymers and the 1:1, 1.05:1, and 1.4:1 ratios of J6. This is attributed to the polymer chemistry and not the actual MMW since the MW for the C12 polymer fell between the J6 and E1 polymer at all ratios (see Table 5.1). The J6 polymers are significantly larger that the E1 for the 1.2:1, 1.1:1, and 1:1 ratios.

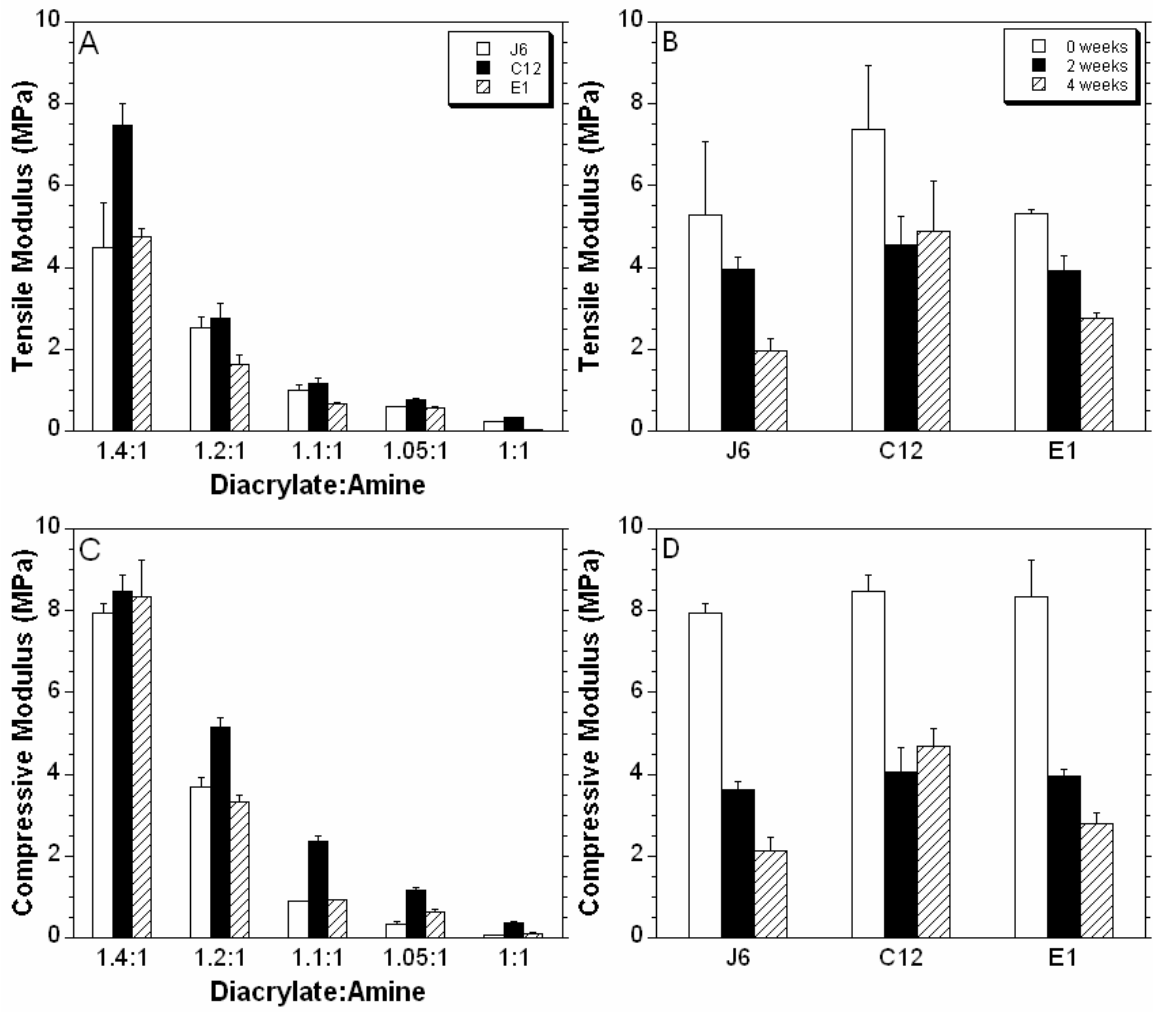

Figure 5.5 Mechanical property changes with respect to chemistry, MMW, and degradation. Moduli calculated in tension (A) and compression (C) for polymers formed from the J6, C12, and E1 macromers at various MMWs. The tensile (B) and compressive (D) moduli measured after 2 and 4 weeks of degradation in PBS at 37°C for the 1.4:1 ratio of all three polymers.

The compressive moduli (Figure 5.5C), shows a similar trend as the tensile moduli with respect to MMW. For example, the compressive moduli for the J6 1.4:1 and

1:1 were found to be 7.93 ± 0.23 and 0.075 ± 0.003 MPa, respectively. At the highest ratio, there was no significant difference between the three chemistries, but for the other ratios, the C12 polymers were significantly stiffer. For the 1.05:1 ratio, the modulus for J6 was significantly larger than E1. The lower MMWs correspond to higher reactive group concentrations and subsequently, higher crosslinking densities. The reaction behavior indicates that this also leads to greater double bond conversions. These properties correspond to alterations and control over the bulk mechanics of the polymer. The macromer chemistry can also play a role and the C12 macromers have a large imidazole ring in each repeat unit, which intuitively may alter polymer mechanics.

The ability to change mechanical properties by altering the MMW could be useful for fine tuning these properties in order to properly adapt to a desired application. This is useful in tissue engineering applications as different cell types prefer different extracellular environments. Cells have been shown to exert forces on their environment in order to sense the stiffness of their environment [17] and subsequently respond to it. Thus, material properties can play a role in cellular interaction behavior. Recently Engler and coworkers [31] reported that matrix elasticity directs mesenchymal stem cells (MSC) differentiation. When MSCs were grown on polyacrylamide gels of different stiffnesses, but in the same media, the cells grown on the soft gels expressed neurogenic markers, stiffer gels were myogenic, and the stiffest gels displayed osteogenic markers. Therefore, the ability to control matrix stiffness can be used to alter MSC differentiation without soluble factors.

5.3.3 Polymer degradation

The degradation of the various polymers was monitored over 17 weeks and the mass loss profiles are shown in Figure 5.6. Typically, degradation began with a period of rapid mass loss, likely due to unreacted macromer release as indicated by the sol fraction from Table 5.1. The rate of degradation increased with a decrease in the diacrylate:amine ratios. For example, for the C12 polymer 88.2% of the mass is lost after 17 weeks for the 1.05:1 ratio, whereas only 58.5% is lost for the 1.4:1 ratio. As the MMW increases, there are more hydrolytically susceptible bonds between the crosslinks. Therefore, there is a greater probability that multiple bonds are hydrolyzed in the crosslink and a polymer fragment (i.e., degradation product) can be released into solution. With this control, the degradation rate can be tuned to a particular application.

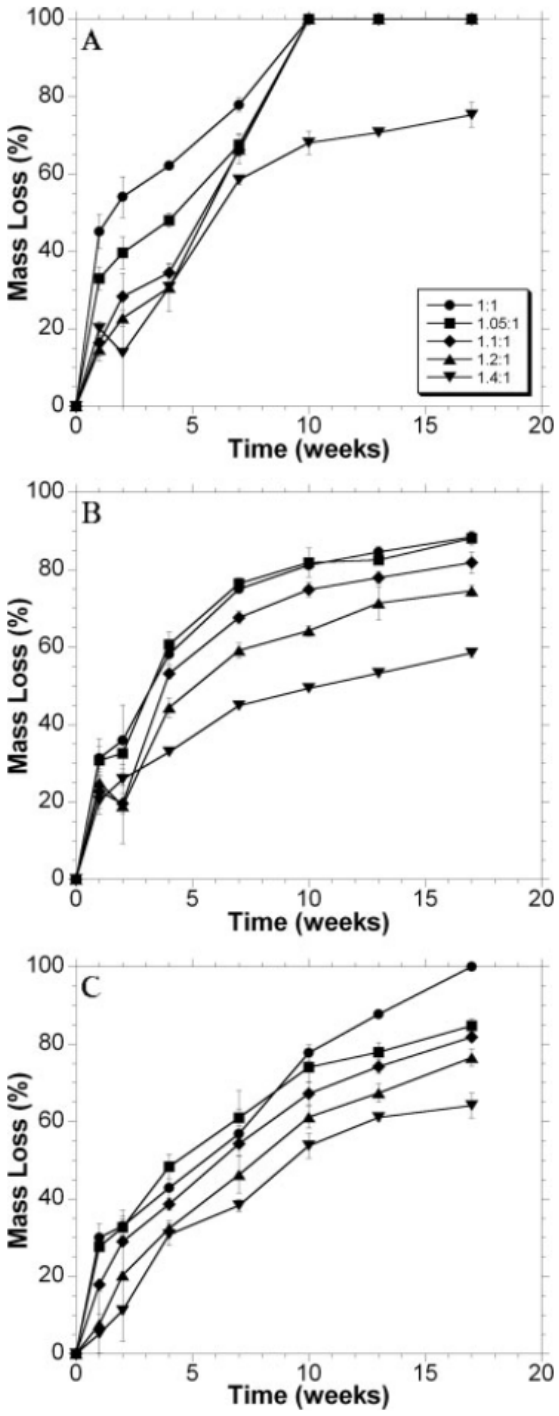

Figure 5.6 Degradation with varying MMW. Network mass loss with degradation in PBS at 37°C for the various MMWs of J6 (A), C12 (B), and E1 (C).

The influence of polymer chemistry on degradation is apparent in the mass loss profiles. In Figure 5.6, the degradation of the J6 polymers occurs much faster than the C12 or E1 polymers. After 9 weeks, all of the ratios, except the 1:1.4 ratio, have degraded completely for the J6 polymer. The C12 polymer (Figure 5.6B) has distinct separation between the ratios as degradation proceeds, but the mass loss appears to plateau, which may indicate that there are non-degradable crosslinks incorporated in the network. E1 polymer degradation for all MMWs is fairly linear. The influence of macromer chemistry on degradation was reported previously during the initial development of the PBAE macromer library, but now more control over the degradation behavior is afforded by alterations in MMW.

In general, mass loss correlates with a decrease in both the compressive and tensile moduli as shown in Figure 5.5B and D. J6 and E1 polymers were consistently weaker with degradation, for the ratios (1.4:1 shown in Figure 5.5) studied. The C12 polymer showed an initial decrease in mechanics after 2 weeks, but no change was observed between 2 and 4 weeks. This may be due to a portion of non-degradable crosslinks in the network as mentioned previously. The decrease in polymer moduli with time is typical of a bulk-degrading polymer, which may be useful for tissue engineering applications since the surface is not shed with degradation and could potentially support cellular adhesion and growth.

The ability to control degradation can be utilized in a number of medical applications. Since molecule release is typically controlled by both diffusion and degradation, degradation can be used to alter and optimize the release of therapeutic molecules from degradable polymers. The local and controlled release of drugs and

growth factors can be used to treat diseased or damaged tissues without the side effects associated with larger, systemic treatments [32, 33]. For example, this has been demonstrated in slow release of chemotherapeutics in neuronal implants, drug eluding stents, and microsphere treatments for prostate cancer [33]. In tissue engineering, control over degradation can be used to optimize extracellular matrix production and distribution [34]. The desired degradation rate is likely specific to tissue type, as some tissues exhibit regenerative capabilities like skin and bone, while others have limited regenerative potential, such as cartilage [35]. Thus, the ideal degradation can be adjusted by varying the MMW of these polymers or others from our initial PBAE library.

5.3.4 Cell interaction studies

SaOS-2 cells, a human osteoblast-like cell, were seeded onto polymer films to see how well anchor dependent cells attached and spread on the polymers with changes in the polymer chemistry and structure (i.e., MMW). This experiment gives some indication of the toxicity of the polymers and how substrate properties influence cellular interactions. As a control, cells were also cultured under typical conditions on tissue culture polystyrene (TCPS).

Figure 5.7 shows photomicrographs of cells grown on the surface of the J6 polymer at each ratio (Figure 5.7B-F) as well as a control on standard tissue culture polystyrene (TCPS) (Figure 5.7A) after 24 hours in culture. While cells adhered to all surfaces, cells were in a more rounded morphology on the lower ratios (i.e., higher MMWs) and showed no spreading on the lowest ratio, unlike the controls. As the ratio increased, the cells appeared to spread out more. A similar trend was seen on the E1

polymers. However, cell viability was low on the C12 polymers, potentially due to changes in the pH as indicated by color changes in the phenol-red containing media. This limits the use of this polymer for tissue engineering applications, but fortunately there are other potentially viable candidates from the polymer library. Quantification of cell adhesion is shown in Figure 5.8A. There was no statistical difference in the numbers of cells adhered to the films with variation in the MMW. The areas of cell spreading on films of polymer J6 are plotted as a histogram in Figure 5.8B. For higher MMWs the cells, while similar in number in Figure 5.8A, are dominated by cells with spread areas less than 300 μm^2. As the ratio increases, the cells are more distributed with larger areas. The higher ratios have more of the most spread cells (>1000 μm^2), but still not as many as the TCPS cells. While these are just short term measurements (24 hr), they indicate that chemistry can play a role in cell adhesion, as the cells appear to adhere to the E1 polymers more readily than the J6 polymers. The MMW (i.e., diacrylate to amine ratio) influenced the spreading of cells on the polymer films to morphologies similar to that of the TCPS controls. This could be due to a few differences caused by changing the MMW. First, many anchorage dependent cells have more organized cytoskeletons and more stable adhesions to stiffer environments [17] (hence why attachment to the stiff TCPS is so high) and therefore spread better on the stiffer matrices of the more highly crosslinked networks. Also, polymers from higher MMWs had a higher sol fraction, which may release more potentially toxic components into the media.

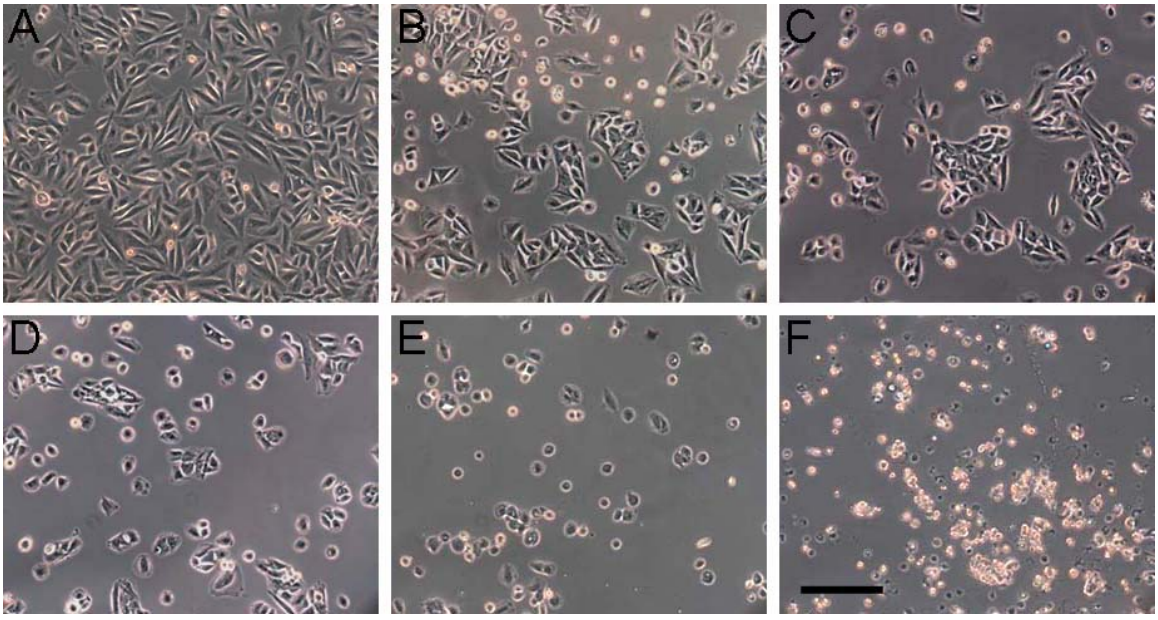

Figure 5.7 Cell Seeding on J6 thin films. Photomicrographs of SaOS-2 cells 24 hours after seeding on TCPS (A), and films of polymers from the J6 macromers synthesized at diacrylate:amine ratios of 1.4:1 (B), 1.2:1 (C), 1.1:1 (D) , 1.05:1 (E), and 1:1 (F). The scale bar represents 200 μm.

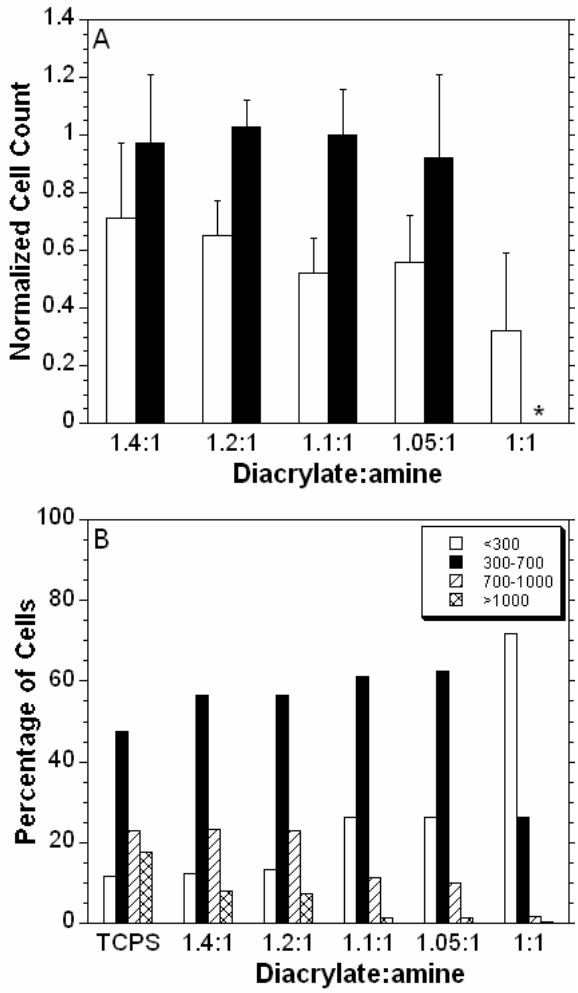

Figure 5.8 Cell adherence and spread on J6 and E1. Number of cells adhered to J6 (white) and E1 (black) normalized to the number of cells adhered to the TCPS control (A). The C12 films created an acidic environment and there were no cells adhered to the polymer after 24 hours. Histogram of the percentage of cells in ranges of spreading area for polymer J6 (B). * denotes that the polymer was not transparent at that composition and could not be analyzed.

5.4 Conclusions

We have shown that by varying the ratio of diacrylates to amines in forming three different PBAE macromers, we can adjust the MMW. By increasing the diacrylate to amine ratio (i.e., decreasing the MMW), the photopolymerization is faster and more complete. This leads to increased mechanical stiffness and decreased rates of mass loss. For given ratios, the chemical structure of the networks can also affect the mechanical properties and degradation. The mechanical properties decreased with degradation, which is indicative of bulk degradation. Two of the polymers were found to support attachment and spreading of human SaOS-2 cells, and spreading was heavily dependent on MMW, with greater cell spreading on polymers formed from lower MMWs. Although no claims can be made regarding the suitability of these specific compositions for tissue regeneration applications, particularly due to high sol fractions, this work is beneficial in better understanding fundamental structure-function relationships and can be used for better designing photocrosslinkable biomaterials.

References:

[1] Anseth KS, Goodner MD, Reill MA, Kannurpatti AR, Newman SM, Bowman CN. The influence of comonomer composition on dimethacrylate resin properties for dental composites. Journal of Dental Research 1996;75(8):1607-1612.

[2] Hillwest JL, Chowdhury SM, Sawhney AS, Pathak CP, Dunn RC, Hubbell JA. Prevention of Postoperative Adhesions in the Rat by in-Situ Photopolymerization of Bioresorbable Hydrogel Barriers. Obstetrics and Gynecology 1994;83(1):59-64.

[3] Anseth KS, Burdick JA. New directions in photopolymerizable biomaterials. Mrs Bulletin 2002;27(2):130-136.

[4] Chung C, Mesa J, Miller GJ, Randolph MA, Gill TJ, Burdick JA. Effects of auricular chondrocyte expansion on neocartilage formation in photocrosslinked hyaluronic acid networks. Tissue Engineering 2006;12(9):2665-2673.

[5] Chung C, Mesa J, Randolph MA, Yaremchuk M, Burdick JA. Influence of gel properties on neocartilage formation by auricular chondrocytes photoencapsulated in hyaluronic acid networks. Journal of Biomedical Materials Research Part A 2006;77A(3):518-525.

[6] Elisseeff J, McIntosh W, Anseth K, Riley S, Ragan P, Langer R. Photoencapsulation of chondrocytes in poly(ethylene oxide)-based semi-interpenetrating networks. Journal of Biomedical Materials Research 2000;51(2):164-171.

[7] Fisher JP, Dean D, Engel PS, Mikos AG. Photoinitiated polymerization of biomaterials. Annual Review of Materials Research 2001;31:171-181.

[8] Leach JB, Bivens KA, Patrick CW, Schmidt CE. Photocrosslinked hyaluronic acid hydrogels: Natural, biodegradable tissue engineering scaffolds. Biotechnology and Bioengineering 2003;82(5):578-589.

[9] Nguyen KT, West JL. Photopolymerizable hydrogels for tissue engineering applications. Biomaterials 2002;23(22):4307-4314.

[10] Smeds KA, Grinstaff MW. Photocrosslinkable polysaccharides for in situ hydrogel formation. Journal of Biomedical Materials Research 2001;54(1):115-121.

[11] Anseth KS, Metters AT, Bryant SJ, Martens PJ, Elisseeff JH, Bowman CN. In situ forming degradable networks and their application in tissue engineering and drug delivery. Journal of Controlled Release 2002;78(1-3):199-209.

[12] Burdick JA, Peterson AJ, Anseth KS. Conversion and temperature profiles during the photoinitiated polymerization of thick orthopaedic biomaterials. Biomaterials 2001;22(13):1779-1786.

[13] Beebe DJ, Moore JS, Yu Q, Liu RH, Kraft ML, Jo BH, et al. Microfluidic tectonics: A comprehensive construction platform for microfluidic systems. Proceedings of the National Academy of Sciences of the United States of America 2000;97(25):13488-13493.

[14] Albrecht DR, Underhill GH, Wassermann TB, Sah RL, Bhatia SN. Probing the role of multicellular organization in three-dimensional microenvironments. Nature Methods 2006;3(5):369-375.

[15] Khademhosseini A, Eng G, Yeh J, Fukuda J, Blumling III J, Langer R, et al. Micromolding of photocrosslinkable hyaluronic acid for cell encapsulation and

entrapment. Journal of Biomedical Materials Research Part A 2006;79A(3):522-532.

[16] Burg KJL, Porter S, Kellam JF. Biomaterial developments for bone tissue engineering. Biomaterials 2000;21(23):2347-2359.

[17] Discher DE, Janmey P, Wang YL. Tissue cells feel and respond to the stiffness of their substrate. Science 2005;310(5751):1139-1143.

[18] Burdick JA, Anseth KS. Photoencapsulation of osteoblasts in injectable RGD-modified PEG hydrogels for bone tissue engineering. Biomaterials 2002;23(22):4315-4323.

[19] Hern DL, Hubbell JA. Incorporation of adhesion peptides into nonadhesive hydrogels useful for tissue resurfacing. Journal of Biomedical Materials Research 1998;39(2):266-276.

[20] Burdick JA, Chung C, Jia XQ, Randolph MA, Langer R. Controlled degradation and mechanical behavior of photopolymerized hyaluronic acid networks. Biomacromolecules 2005;6(1):386-391.

[21] Fisher JP, Holland TA, Dean D, Engel PS, Mikos AG. Synthesis and properties of photocross-linked poly(propylene fumarate) scaffolds. Journal of Biomaterials Science-Polymer Edition 2001;12(6):673-687.

[22] Anseth KS, Shastri VR, Langer R. Photopolymerizable degradable polyanhydrides with osteocompatibility. Nature Biotechnology 1999;17(2):156-159.

[23] Mann BK, Gobin AS, Tsai AT, Schmedlen RH, West JL. Smooth muscle cell growth in photopolymerized hydrogels with cell adhesive and proteolytically

degradable domains: synthetic ECM analogs for tissue engineering. Biomaterials 2001;22(22):3045-3051.

[24] Burdick JA, Mason MN, Hinman AD, Thorne K, Anseth KS. Delivery of osteoinductive growth factors from degradable PEG hydrogels influences osteoblast differentiation and mineralization. Journal of Controlled Release 2002;83(1):53-63.

[25] Sawhney AS, Pathak CP, Hubbell JA. Bioerodible Hydrogels Based on Photopolymerized Poly(Ethylene Glycol)-Co-Poly(Alpha-Hydroxy Acid) Diacrylate Macromers. Macromolecules 1993;26(4):581-587.

[26] Lynn DM, Langer R. Degradable poly(beta-amino esters): Synthesis, characterization, and self-assembly with plasmid DNA. Journal of the American Chemical Society 2000;122(44):10761-10768.

[27] Akinc A, Lynn DM, Anderson DG, Langer R. Parallel synthesis and biophysical characterization of a degradable polymer library for gene delivery. Journal of the American Chemical Society 2003;125(18):5316-5323.

[28] Anderson DG, Tweedie CA, Hossain N, Navarro SM, Brey DM, Van Vliet KJ, et al. A combinatorial library of photocrosslinkable and degradable materials. Advanced Materials 2006;18(19):2614-+.

[29] Soltz MA, Ateshian GA. Experimental verification and theoretical prediction of cartilage interstitial fluid pressurization at an impermeable contact interface in confined compression. Journal of Biomechanics 1998;31(10):927-934.

[30] Agrawal CM, Ray RB. Biodegradable polymeric scaffolds for musculoskeletal tissue engineering. Journal of Biomedical Materials Research 2001;55(2):141-150.

[31] Engler AJ, Sen S, Sweeney HL, Discher DE. Matrix elasticity directs stem cell lineage specification. Cell 2006;126(4):677-689.

[32] Langer R. Drug delivery and targeting. Nature 1998;392(6679):5-10.

[33] Langer R, Peppas NA. Advances in biomaterials, drug delivery, and bionanotechnology. Aiche Journal 2003;49(12):2990-3006.

[34] Bryant SJ, Anseth KS. Hydrogel properties influence ECM production by chondrocytes photoencapsulated in poly(ethylene glycol) hydrogels. Journal of Biomedical Materials Research 2002;59(1):63-72.

[35] Miller MD. Review of Orthopaedics. Philadelphia: Saunders, 2004.

CHAPTER 6: *Controlling Poly(β-amino ester) Network Properties through Macromer Branching*

(Adapted from: DM Brey, JL Ifkovits, RI Mozia, JS Katz, JA Burdick, "Controlling Poly(β-amino ester) Network Properties through Macromer Branching," Acta Biomaterialia, 2008, 4(2): 207-17)

6.1 Introduction

Radically polymerized materials are useful as biomaterials for numerous applications. For instance, bone cements and methacrylate monomers for filling dental caries have a history of use in medicine [1]. Light-initiated photopolymerizations are a type of radical polymerization that occurs at physiologically relevant temperatures (37°C) and with numerous wavelengths of light [2]. Photoinitiated polymerizations also offer spatial and temporal control over the reaction, which is useful in minimizing polymerization exotherms [3] and for fabricating complex structures [4, 5].

Many biomaterials have been developed that are photopolymerizable and degradable, including polyanhydrides [6], poly(propylene fumarate)s [7], poly(ethylene glycol)s [8, 9], and polysaccharides [10, 11]. These materials have been investigated for a wide range of applications, including cartilage and bone regeneration [8, 11, 12], cardiovascular applications [13, 14], drug delivery [15, 16], and in microfluidic devices [17]. One limitation in engineering these materials toward a specific application is that tuning their properties iteratively or predicting their behavior can be tedious and difficult.

To accelerate the identification of potentially useful biodegradable and free-radically polymerized polymers, Anderson et al. developed a combinatorial approach for the synthesis of a library of poly(β-amino ester) (PBAE) macromers that are rapidly synthesized and form networks with a wide range of properties [18]. Specifically, network degradation times ranged from less than one day to over 4 months and the mechanics spanned two orders of magnitude (~2 MPa to ~200 MPa). The synthesis involves the reaction of commercially available diacrylates with amines and no purification of the synthesized macromers is necessary. Brey, et al. [19] further expanded the library by investigating the influence of macromer molecular weight, through changes in the ratio of acrylate to amine, on network properties. This led to changes in network mechanical properties, degradation rates, and cell adhesion.

The primary objective of this work was to examine the importance of macromer branching on network properties, since branching can be easily altered during the synthesis of PBAEs by introduction of a reagent with higher functionality (e.g., triacrylate). This structural feature has only been minimally investigated and little is known about the influence of macromer branching on biodegradable polymers. To this end, one specific composition from the PBAE library was used and a triacrylate group was systematically introduced during synthesis, while maintaining the overall molar ratio of acrylates to amines. The influence of PBAE macromer branching on the overall bulk properties and initial cellular interactions of formed networks was investigated. Information obtained was also used to control scaffold mechanical properties. This will hopefully provide an additional tool to control scaffold properties for tissue regeneration.

6.2 Materials and Methods

6.2.1 Macromer synthesis and characterization

Acrylate terminated PBAEs were synthesized in parallel by the step-growth polymerization of a commercially available primary amine, 3-methoxypropylamine (1, TCI America), and different ratios of 1,6-hexanediol ethoxylate diacrylate (E, Sigma) and pentaerythritol triacrylate (PETA, Sigma). These liquid reagents were mixed at diacrylate:triacrylate ratios of 100:0, 95:5, and 90:10 while holding the molar ratio of acrylate end groups to amines constant (2.4:1) in glass scintillation vials at 90°C overnight while stirring (700 rpm, Telesystem HP15/RM, Variomag USA). The sample notation is consistent with our previous report on the development of the initial PBAE library [18]. Proton NMR spectra were recorded in deuterated chloroform on a Bruker Avance 300 MHz instrument and calibrated to the chloroform (7.27 ppm) impurity as an internal standard.

6.2.2 Photopolymerization

The photoinitiator 2,2-dimethoxy-2-phenyl acetophenone (DMPA, Sigma) was added to the liquid macromers at a final concentration of 0.5% (w/w) by addition of a 10% (w/v) DMPA in methylene chloride. The solvent was removed in a vacuum desiccator overnight and all polymerizations were performed in bulk. The polymerization behavior was monitored using attenuated total internal reflectance – Fourier transform infrared (ATR-FTIR, Nicolet 6700, Thermo Electron) spectroscopy with a zinc selenide crystal collecting a spectrum every 17 seconds with a resolution of 3.86 cm^{-1} for 10 minutes. A drop of the macromer/initiator solution was placed directly

on the horizontal crystal, covered with a glass cover slip, and exposed from above to ultraviolet light (~1.3 W/cm^2 at tip of light guide, distance of 24 cm, 365 nm, Omnicure Series 1000, Exfo). The change in area of the double bond peak (~1630 cm^{-1}) was used to monitor double-bond conversion with light exposure. Values were normalized to the area of the carbonyl peak (~1730 cm^{-1}) and converted to double bond conversion using the initial peak areas. Three samples for each macromer group were tested.

6.2.3 Network characterization

In order to test the bulk polymer properties, the macromer/initiator solution was placed between glass slides with a 1 mm spacer and polymerized with exposure to ~10 mW/cm^2 ultraviolet light (365nm, Blak-Ray B-100 AP, Ultraviolet Products) for 10 minutes. Polymer discs (5 mm diameter x 1 mm thick) were then punched from the resulting networks for testing. The soluble (sol) fraction of the various networks was determined by placing 3 disks of each polymer in methylene chloride. This allowed unreacted macromer to swell from the network. After drying, the sol fraction was calculated as the percent of initial mass lost during 48 hours of swelling. Negligible mass loss was observed with subsequent swelling and drying cycles, indicating that the sol fraction was removed during the first cycle.

For degradation analysis, 4 disks were punched from the slabs and weighed (initial mass). Samples were placed in histology cassettes and degraded in phosphate buffered saline (PBS) at 37°C (pH 7.4) on an orbital shaker with frequent changes of the PBS. Samples were removed after 2, 4, 7, and 10 weeks of degradation, dried in an oven,

and weighed (final mass). The overall mass loss was calculated from the recorded initial and final mass values.

To investigate kinetic chain lengths, a previously reported isolation process was used [20]. Briefly, thin samples (0.56 mm thick x ~1.5 cm diameter) were rapidly degraded in 4 N NaOH over 3 days at 37°C. Thin samples were used to limit depth variations with light attenuation. The pH of the solution was then adjusted to 8-9 with the addition of 4 N HCL and filtered through a 0.45 μm syringe filter. Samples were then dialyzed (Spectra/Por® Biotech Cellulose Ester Membrane, molecular weight cut off: 500, Spectrum Laboratories) and lyophilized (Freezone 4.5, Labconco). Finally, samples were dissolved in DI water at 2μg/ml and run in aqueous gel permeation chromatography (GPC, 1ml/min, 515 HPLC Pump, Ultrahydrogel Linear and 250 columns, 2414 Refractive Index Detector, Waters) to determine the kinetic chain molecular weights compared to PEG standards ($\overline{M_n}$ = 5000, 35000, and 203000).

6.2.4 Mechanical testing

For mechanical testing, slabs were prepared as described above with either a 1 mm (tensile, dynamic, degradation samples) or 2 mm (compression samples) spacer. The polymers were then cut into 25 mm x 5 mm samples for tensile and dynamic testing and 5 mm disks were punched for compression testing. Mechanical properties with degradation were determined through tensile and compressive analysis of samples prepared as described above after 2, 4, and 8 weeks of degradation, using the previously described degradation procedure.

Tensile testing was performed on a materials testing machine (Microtester 5848, Instron) with a constant strain rate of 0.1% per second until macroscopic failure. The elastic modulus was then calculated as the slope of the linear portion of the stress versus strain plot. Unconfined compression testing was completed on a custom made mechanical testing device designed as described in Soltz et al.[21], Samples were creep tested under a 2 gram load until equilibrium and then stressed to 10% strain at 1 μm/sec and allowed to relax. The compressive moduli were calculated as the slope of the stress versus strain plots between 5 and 10% strain.

The viscoelastic behavior of the samples was determined using a Dynamic Mechanical Analyzer (Q800 TA Instruments). Rectangular strips (25 mm x 5 mm x 1 mm) of polymer were cut from polymer slabs and tested in a controlled strain mode at 1 Hz, an amplitude of 10 μm, and a heating rate of 3°C/min from -100°C to 25°C. The glass transition temperature, T_g, is reported as the inflection point of the tan δ (the storage modulus over the loss modulus) curve. The crosslinking density, ν_c, was calculating using the theory of rubber elasticity [22]:

$$\nu_c = E' / 3RT \tag{6.1}$$

where E′ is the storage modulus in the rubbery plateau region at a given temperature T, R is the gas constant (8.314 J K^{-1} mol^{-1}), and assumes that Poisson's ratio for a rubber is 0.5.

6.2.5 Cell interaction studies

To prepare films for cell interaction studies, the macromer/initiator solutions were dissolved in ethanol at a 1:2 (w/v) ratio and pipetted (35 μl) into 24-well plates. The

ethanol was allowed to evaporate off overnight to leave a thin film of the macromer and initiator. The plates were placed in a transparent chamber being purged with nitrogen and polymerized for 10 minutes with ultraviolet light (Blak Ray). To sterilize the films, the plates were placed under a germicidal lamp in a laminar flow hood for 30 minutes. Wells were incubated with PBS overnight to allow unreacted monomer to be removed. After washing with PBS, the wells were incubated with growth media for 30 minutes prior to cell seeding.

Human sarcoma osteoblast-like cells (SaOS-2, ATCC) were grown in media comprised of Modified McCoy's Medium (ATCC) with 10% fetal bovine serum (FBS, Hyclone) and 1% penicillin/streptomycin (Invitrogen). SaOS-2 cells were seeded on the polymer films at 50,000 cells per well (24-well plate). The cells were cultured for 2 and 7 days, fixed in 2.5% glutaraldehyde (Polysciences) for 15 minutes, and cell nuclei were stained with DAPI (1:2500). Phase contrast and fluorescent photomicrographs were taken using an inverted microscope (Axiovert, Zeiss) and a digital camera (Axiovision, Zeiss). The total cell number was determined by counting adhered cell nuclei in at least 5 random fields on 3 individual films for each composition at each time point. Cell area was measured using NIH ImageJ software (3 samples per polymer/ratio, 5 pictures per well, 20 cells per picture, at least 300 cells per composition).

6.2.6 Scaffold fabrication and characterization

Porous scaffolds were fabricated using previously developed techniques of salt leaching [23] and sintered poly(methyl methacrylate) (PMMA) microbeads [24]. Briefly, a solution of 2:1 (w:v) macromer:ethanol containing DMPA and NaCl crystals (sieved to

100-300 μm) were mixed together (80:20 mass ratio NaCl:macromer) and packed into teflon molds. The ethanol was evaporated overnight in a vacuum desiccator, and the resulting salt-macromer mixture was crosslinked with ultraviolet light exposure (as described above) between glass slides. Samples were then cut, the salt was leached with several washes in DI water, frozen in liquid nitrogen, and lyophilized for scanning electron microscopy (SEM) and mechanical testing in compression as describe above.

For spherical porosity, PMMA microbeads (250 μm, Polysciences) were packed into teflon molds, clamped between glass slides, and placed in an oven at 120°C for 22 hours [24]. The glassy top layer was then scraped away, and the voids between the sintered spheres were filled with macromer/DMPA/ethanol solutions. The ethanol was evaporated overnight in a vacuum desiccator, the constructs were crosslinked with ultraviolet light exposure (as described above) between glass slides, the PMMA was removed with several washes in methylene chloride, and the methylene chloride was removed with several washes in water. Samples were then frozen and lyophilized before SEM analysis and compressive mechanical testing as described above.

6.2.7 Statistical analysis

Statistical analysis was performed using ANOVA with Tukey's post-hoc among the groups with significance defined as a confidence level of 0.05. All values are reported as the mean and the standard deviation of the mean.

6.3 Results and Discussion

6.3.1 Synthesis of macromers

Recently, a large library of PBAEs, synthesized via a step growth polymerization of liquid amines and diacrylates, was developed for biomaterial applications [18]. The biggest advantage to this system is that the reaction scheme is simple since there is no purification necessary and that a large number of networks formed from the PBAEs can be rapidly synthesized and screened for applications in tissue regeneration. Although the diversity in properties through alterations in the macromer chemistry and molecular weight [19] was explored, no investigations have been completed on the influence of structural illustrate the diverse properties possible through this structural variation. The macromer made from the diacrylates E and the amine 1 (E1) was selected because it did not have optimal cell interactions, and thus, could illustrate the potential improvement in properties with the addition of branching. The system involved the synthesis of a diacrylate (E) and a primary amine (1) to form a linear diacrylated macromer, or alternatively, a system of branched multiacrylated macromers and linear diacrylated macromer with the features, namely branching, on network properties.

Thus, we synthesized one macromer system (Figure 6.1), with a variety of branching structures, with the addition of small quantities of triacrylate (PETA). This was performed in ratios of diacrylate to triacrylate (E:PETA) of 100:0, 95:5, or 90:0, while maintaining the overall molar ratio of acrylate end groups to amines constant. Higher E:PETA ratios (e.g., 85:15 or 80:20) led to crosslinking during synthesis and could not be examined, as opposed to the tested macromers which were viscous liquids. Incorporation of PETA into the macromer was confirmed by NMR spectroscopy through

the disappearance of the acrylate peak specific to the PETA monomer at 5.9 ppm (Figure 6.2).

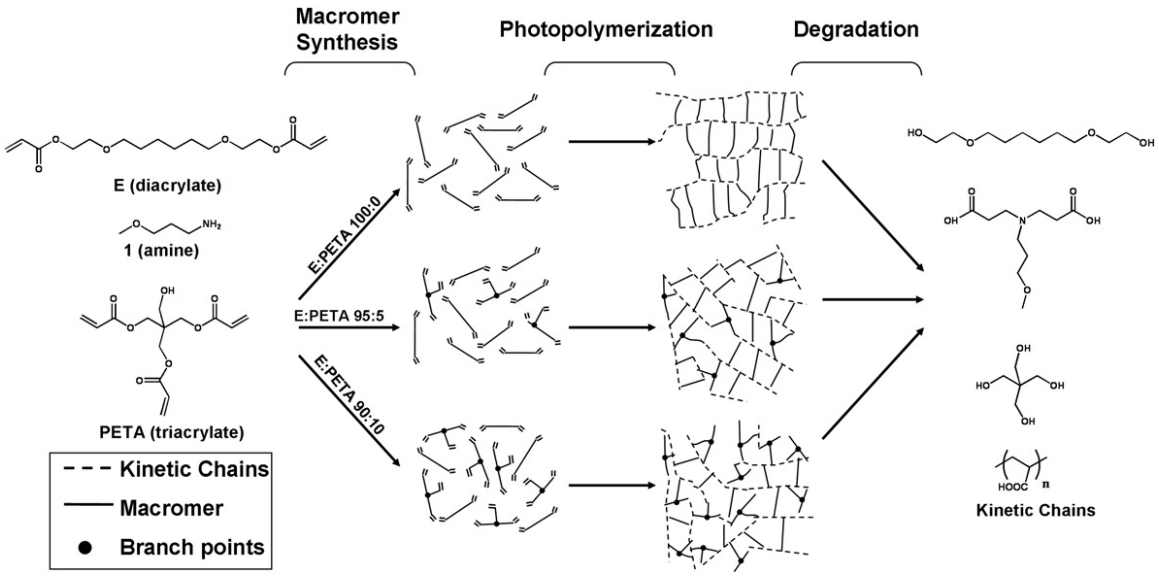

Figure 6.1 Schematic of monomers used in macromer synthesis. Schematic of monomers used in macromer synthesis which is then photopolymerized and degraded in water or base. The kinetic chains are the carbon chains with carboxyl side groups.

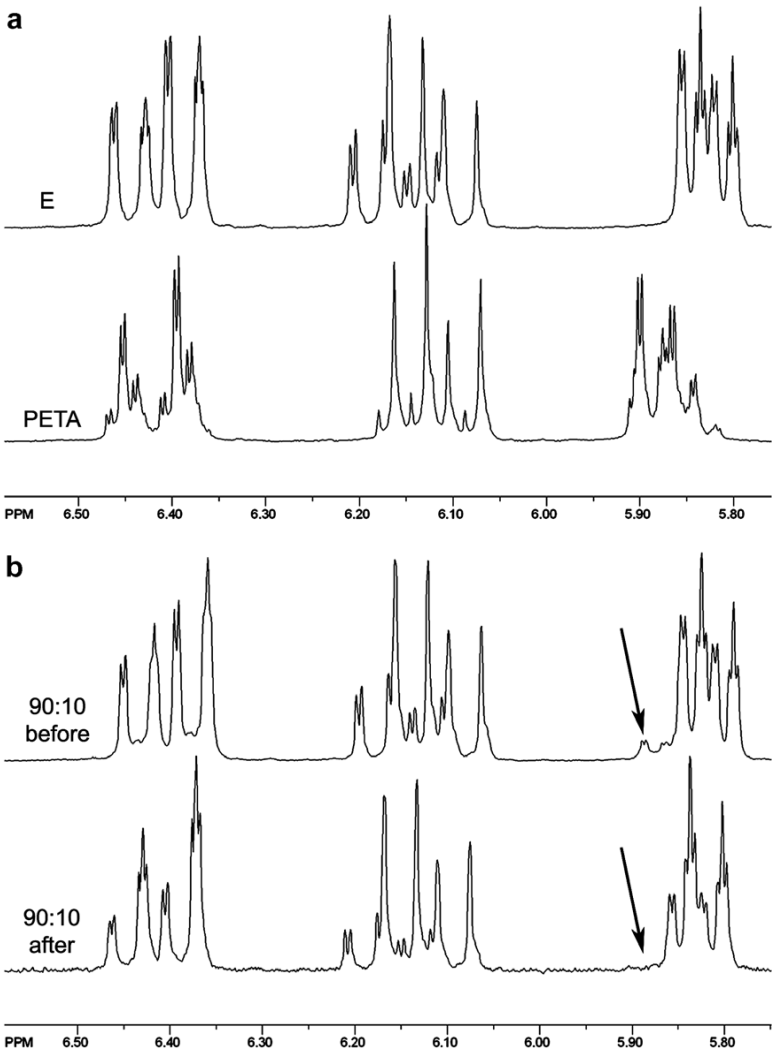

Figure 6.2. ^{1}H-NMR spectra of the E, PETA, and 1 reaction. (A) ^{1}H-NMR spectra of E and PETA acrylate groups. (B) ^{1}H-NMR spectra of acrylate end groups mixture of E, PETA, and 1 before and after synthesis, demonstrating the incorporation of PETA into the macromer structure by the disappearance of the peak at 5.9 ppm (indicated by arrow).

Polymer branch content can be determined using various techniques such as gel permeation chromatography (GPC), NMR, rheology, and small angle scattering [25]. Based on the structures of the starting reagents, it is anticipated that the macromers will

contain short chain branches as opposed to long chain branches. Long chain branches are defined as those, which have a molecular weight indistinguishable from the main chain. GPC and rheology are techniques that are useful for determining long chain branching as opposed to short chain branching [25]. Moreover, previous efforts to obtain GPC data for these macromers were unsuccessful due to their highly cationic nature [19]. Branching is quantified in rheology by using the Dow Rheology Index or the Long Chain Branching Index which are only applicable when a PDI of less than 2 exists. Small angle scattering is also a technique that is more applicable for long chain branching. High frequency (188.6 MHz) ^{13}C NMR can be used to quantify short chain branching. However, it is limited to high levels of short chain branching because it is very difficult to assign chemical shift values to side chains greater than six or more carbon atoms in length [25]. Therefore, based on the chemical structures of the starting reagents, it is very difficult to quantify the branch content of this system via traditional techniques.

6.3.2 Photopolymerization and degradation behavior

The photopolymerization behavior of the macromers was monitored in real time using ATR-FTIR and the results are shown in Figure 6.3. The rate of double bond conversion (Figure 6.3A) was slightly faster for the most branched system (90:10 E:PETA) initially ($\alpha<0.05$ at 2 minutes 50.7±2.0% vs 31.2±6.8% and 32.3±2.5%) and conversion plateaued for all samples at approximately 5 minutes. However, there was no statistical difference between all macromer groups in ultimate double bond conversion after 10 minutes (Figure 6.3B). Although the ultimate conversions are similar, the amount of unreacted macromer molecules may be higher for the less branched system,

since the probability is higher that a branched macromer with a greater number of functional groups is incorporated into the network. This is apparent in our sol fraction calculations shown in Table 6.1. The linear macromer (100:0 E:PETA) had almost twice the sol fraction that our most branched system (90:10 E:PETA) had. The release of unreacted macromer is very important in the application of these polymers to biological systems, where released molecules may be toxic to the surrounding cells and tissue. Thus, macromer branching may be useful in limiting this effect.

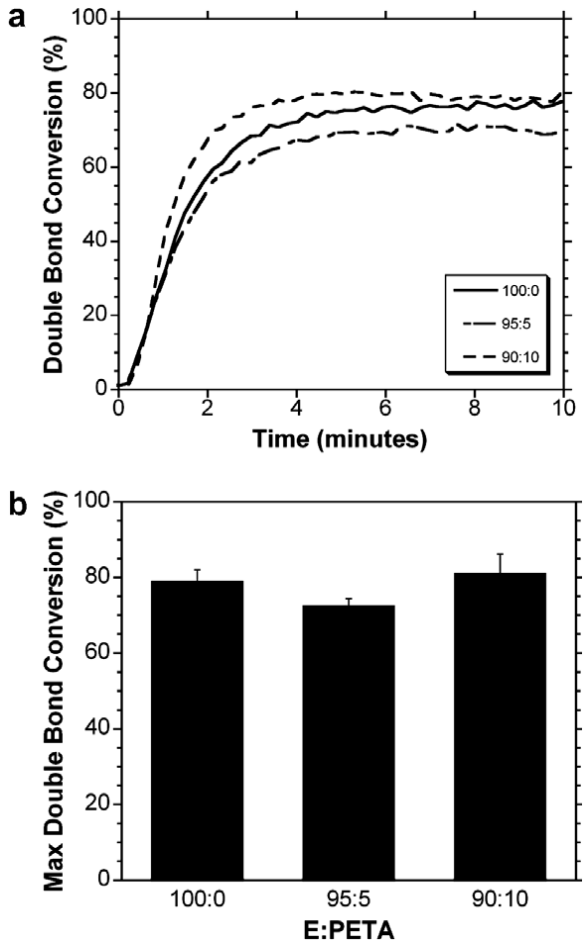

Figure 6.3 Macromer reaction behavior. Real time double bond conversion with ultraviolet light exposure for E:PETA ratios of 100:0, 95:5, and 90:10 (A) and maximum double bond conversion after 10 minutes (B). There was no statistical difference in the maximum conversion with changes in macromer branching.

The mass loss with degradation in PBS at 37°C showed similar profiles between the macromers (Figure 6.4A). In all groups, there was an initial period of more rapid mass loss and then a slowing of the rate of mass loss with time. In the initial 2 weeks there was greater mass loss in the network formed from the linear macromer (E:PETA 100:0), possibly due to the greater amount of sol fraction that is present in that system.

After 10 weeks, networks formed from the E:PETA 90:10 macromers had the greatest mass loss ($a<0.05$), but the difference was still only ~5% between the different networks.

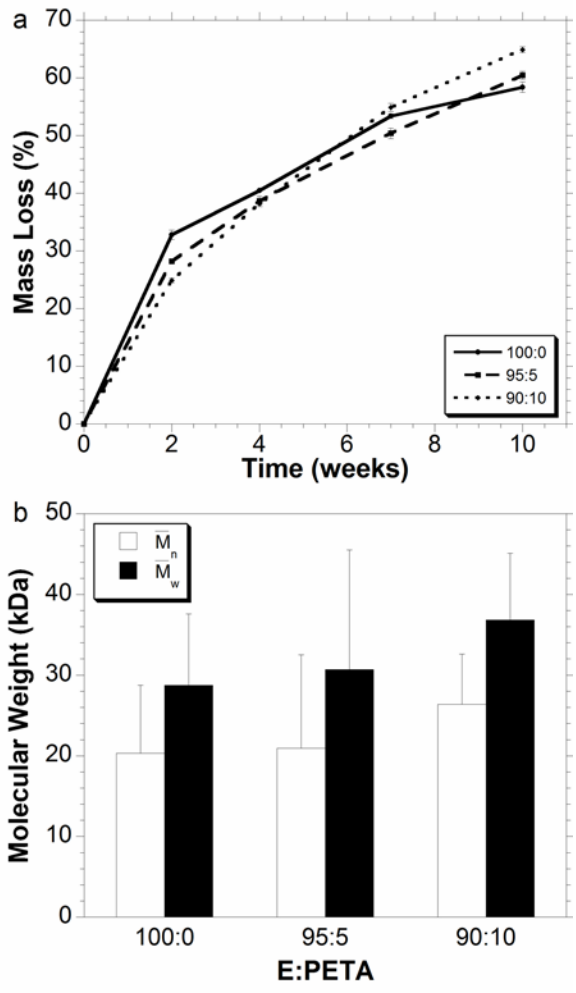

Figure 6.4 Degradation characterization of polymers with triacrylate. (a) Degradation of networks (in PBS at 37°C) formed with various macromers at ratios of E:PETA of 100:0, 95:5, and 90:10, and (b) molecular weights ($\overline{M_n}$ and $\overline{M_w}$) of kinetic chains isolated from degraded networks formed from the same macromers.

During polymerization, nondegradable linear kinetic chains (Figure 6.1) form from the free-radical polymerization of the acrylate groups. These kinetic chains are a degradation product and the molecular weight of these chains can give some insight into the network formation and structure [20]. When isolated and analyzed (Figure 6.4b), a trend of an increase in molecular weight (both $\overline{M_n}$ and $\overline{M_w}$) with an increase in branching was observed; however, there was no statistically significant differences between groups.

6.3.3 Mechanical properties

The mechanical properties of the networks were investigated in both tension and unconfined compression and the results initially as well as with degradation are found in Figure 6.5. A statistically significant difference in moduli was found initially between all of the different macromers used and the 90:10 E:PETA macromer formed networks with a modulus almost double that formed from the 100:0 E:PETA macromer. Similar trends were observed for the networks in both tension and compression. The more complete crosslinking (lower sol fraction) and the greater chance of a macromer forming crosslinks between kinetic chains due to higher functionality likely contribute to this increase.

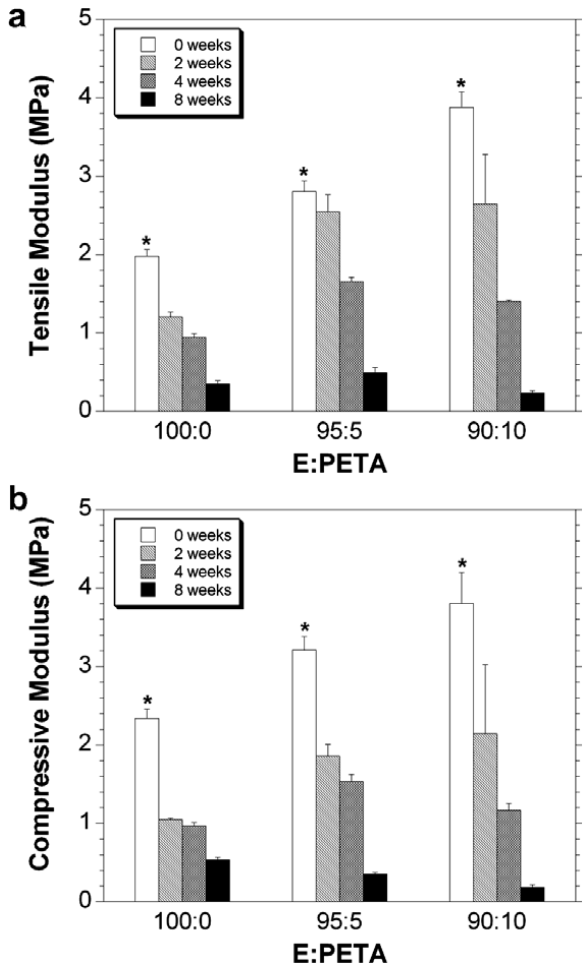

Figure 6.5 Mechanical properties with changes in branching and degradation. Tensile (A) and compressive (B) moduli initially and with degradation for networks formed with various macromers at ratios of E:PETA of 100:0, 95:5, and 90:10. * denotes significance from other groups (0 weeks).

With degradation, the mechanical properties decreased with time. This is expected from bulk eroding networks and was observed regardless of the macromer branching. However, the moduli of the higher branched networks actually decreased more quickly with degradation. For instance, the moduli of networks formed from the

90:10 E:PETA macromer was actually the weakest at 8 weeks, potentially due to the greater mass loss at this point.

The T_g was also measured using dynamic mechanical testing. A representative plot of the temperature dependent mechanics is shown in Figure 6.6 and the data is listed in Table 6.1. There was a trivial, but statistically significant change in T_g between networks formed from the 100:0 and 95:5 E:PETA macromers, and networks formed from the 90:10 E:PETA macromer had a more pronounced, higher T_g ($\alpha<0.05$) than both of the other groups. The crosslinking density (Table 6.1) is also significantly ($\alpha<0.05$) larger as branching increases. This reduces the amount of free volume as the chains are crosslinked together, preventing the microstructure from transitioning freely from the glassy to rubbery state and could explain variations in the T_g between groups.

Table 6.1 Properties of networks formed of E, 1, and PETA with varying ratios of diacrylate and triacrylate.

E:PETA	Sol Fraction (%)	T_g (°C)	Storage Modulus (MPa)	Crosslink Density (mol/m^3)
100:0	19.5 ± 1.1	-46.5 ± 1.0	2.30 ± 0.20	337.6 ± 28.7
95:5	9.4 ± 0.4	-45.1 ± 0.3	2.99 ± 0.05	438.5 ± 7.1
90:10	10.0 ± 1.2	-40.5 ± 0.4	3.92 ± 0.12	575.0 ± 18.0

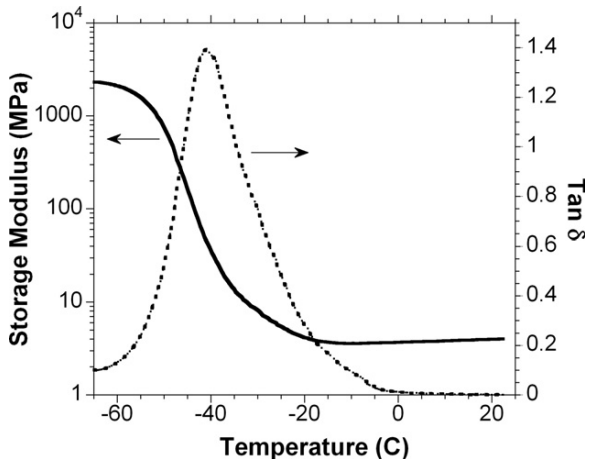

Figure 6.6 Example plot of storage modulus (solid line) and tan δ (dashed line) for networks formed with E:PETA of 90:10. T_g is defined as the temperature at the peak of the tan δ curve.

Others have reported the branching effects on the physical properties of polymers [26-28], yet not in the manner that is reported here. For example, Tian et al. [28] melt grafted PETA and peroxide to linear polypropylene (PP) to form long chain branching PP. They found that increased branching led to increased zero-shear viscosity and shear thinning at lower temperatures. Additionally, the shear modulus (G′) and loss angle (tan δ) were increased and decreased, respectively, at lower temperatures with increased branching. Previous work by Nivasu et al. [27], incorporated PETA as a monomer during network formation, but not into macromer synthesis as is shown here. They found a reduction in polymerization efficiency, but did not investigate the influence of branching on mechanics and degradation. A review by McKee et al. [29], discussed the effect of short chain branching on T_g, where short chain branching was found to lower T_g. These are somewhat different than our case because the end groups are not crosslinked,

so they are able to move. From free volume theory, non-crosslinked branches have increased free volume due to these branches which decreases T_g. In the case of crosslinked polymers, the free volume is reduced since the chains are actually bound together and not allowed to move independent of one another.

6.3.4 Cellular interaction studies

As an initial step towards investigation of branching influences on tissue engineering scaffolds, osteoblast-like cells (SaOS-2) were plated on thin films of networks formed from the various branched macromers and cultured for up to 1 week. Representative photomicrographs of the cells after 2 and 7 days are shown in Figure 6.7. While cells do adhere to the films in all cases, the attachment was much greater and the cells were more spread as the branching increased. After one week, a clear difference can be seen in cellular morphology, where almost all of the cells on films formed from the 100:0 E:PETA are rounded, as opposed to many viable and spread cells are found on films formed from the 90:10 E:PETA macromers. These observations are also inherent in the quantification of cell adhesion and spreading reported in Figure 6.8. There is a statistical increase in adhesion (2 days) and proliferation (7 days) on networks formed from the branched macromers over the linear macromer at both time points, but none of the values reach that of control TCPS. Again, the attachment and spreading are most similar to TCPS for that of the most branched macromer (90:10 E:PETA). For spreading results, the percentage of cells that are less than 300 μm^2 drops from 88% to virtually zero on films formed from the 100:0 to 90:10 E:PETA macromers. There are still not as

many large cells (>1500 μm^2) as there are on the controls, but the cell morphology is much more similar.

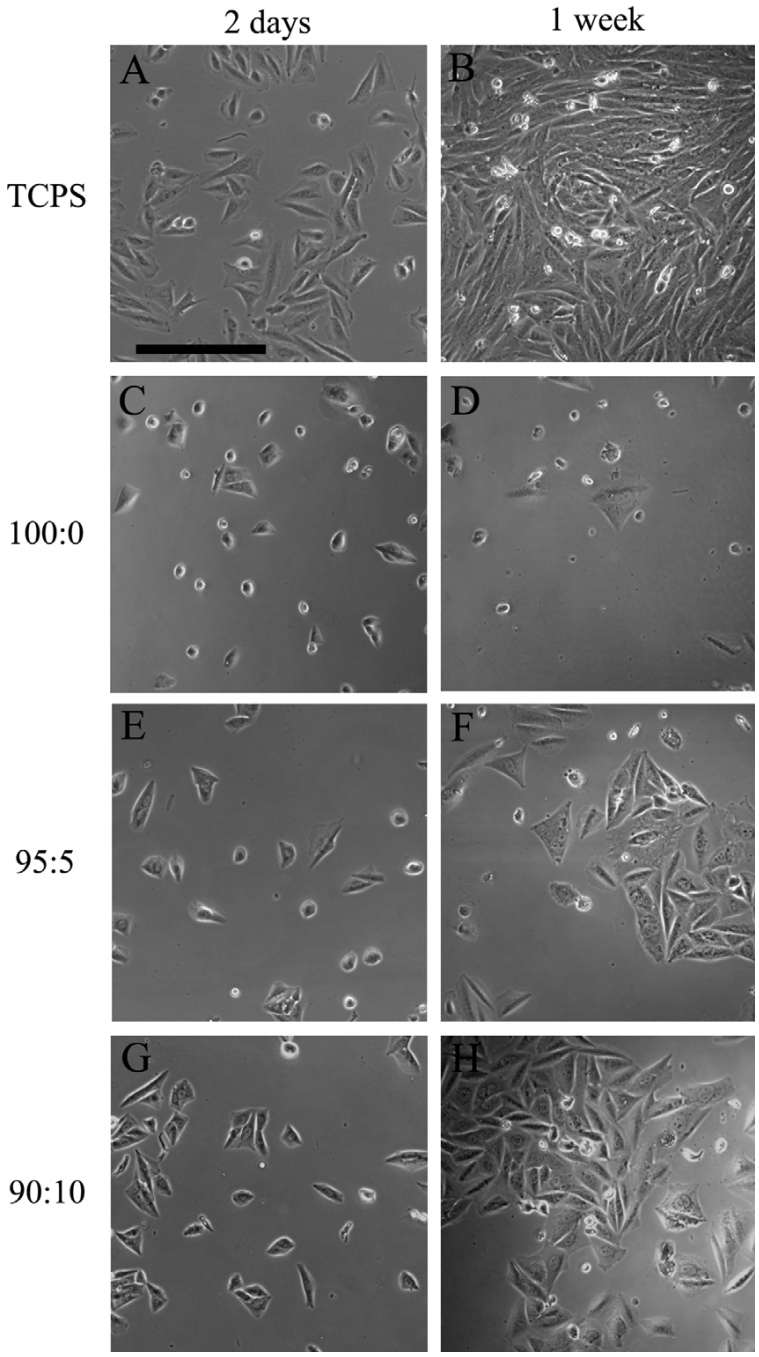

Figure 6.7 Osteoblast-like cells on control TCPS (A,B) and on films formed from macromers with E:PETA ratios of 100:0 (C,D), 95:5 (E,F), and 90:10 (G,H) after 2 days (A,C,E,G) and 1 week (B,D,F,H). The scale bar represents 100μm.

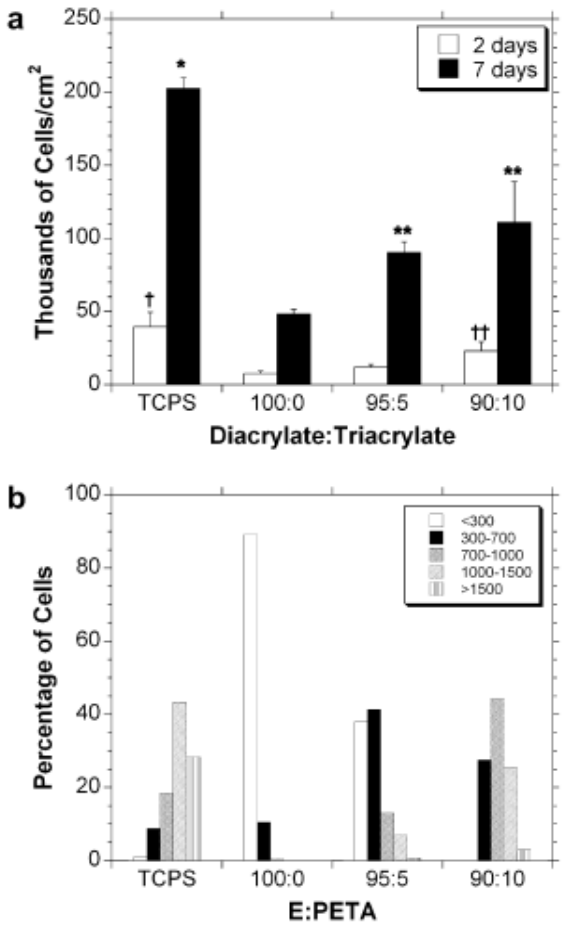

Figure 6.8 (a) Thousands of cells per cm^2 after 1 week, † denotes significance from other groups, †† denotes significance from all other groups, * denotes significance to all other groups, and ** denotes significance from 100:0 at 7 days. (b) Histogram of cell areas (μm^2) after 24 hours.

These changes in cellular interactions with macromer branching may be attributed to a number of factors such as the presence of unreacted end groups (as demonstrated by FTIR conversion < 100%) and the mechanics of the polymer. As shown here, the linear macromers led to networks with a greater amount of potentially unreacted molecules, which may be toxic to cells. Additionally, others have reported the relationship between

substrate mechanical properties and cellular attachment and function [30-32], which may play a limited role. Ultimately, these results illustrate the potential in using macromer branching to manipulate mechanical properties without altering other properties or unreacted end groups. Mechanical properties can control cellular interactions, an important factor in the success of scaffolding in many tissue engineering approaches. It should be noted that these networks were not chosen based on their superior interactions with cells, but because they are useful in illustrating these branching effects. This approach will be useful for many polymers, and especially, for candidates from the PBAE library.

6.3.5 Tissue engineering scaffolds

As a final step towards illustration of the impact of macromer branching on the development of scaffolds for tissue regeneration, two different methods were investigated to develop interconnected, porous scaffolds. These include both poragen leaching [23, 33] and sintered-PMMA microbead [24] techniques that have been used successfully for scaffold fabrication from other polymers and are particularly appropriate for the formation of scaffolds from photoreactive macromers. The polymerization around poragens allowed for simple control over the size of pores through the size of the salt crystals or microbeads and the interconnectivity was created by the packing of the salt-macromer mixture or through the sintering of the beads. The porosity, pore size, and pore interconnectivity are important for the transport of nutrients and waste by diffusion, as well as the infiltration and growth of cells and vasculature [34-36].

The scaffolds created with the sintered microspheres are shown in Figure 6.9A. These scaffolds contain very regular, interconnected pores, created by the sintering of PMMA beads together, photocrosslinking of the macromer in the void space, and dissolution of the PMMA using a solvent. The use of spheres may lead to a more regular structure than alternate poragens, and consequently, greater connectivity and mechanical properties [37]. When the scaffolds were tested in compression (Figure 6.9C), similar mechanical property trends were noted that were found with the slabs, with the 90:10 samples significantly ($\alpha<0.05$) greater than the 95:5 and 100:0. Specifically, an increase in macromer branching led to scaffolds with greater moduli (though not significantly between 100:0 and 95:5), illustrating that the effects of macromer structure translate to scaffold properties.

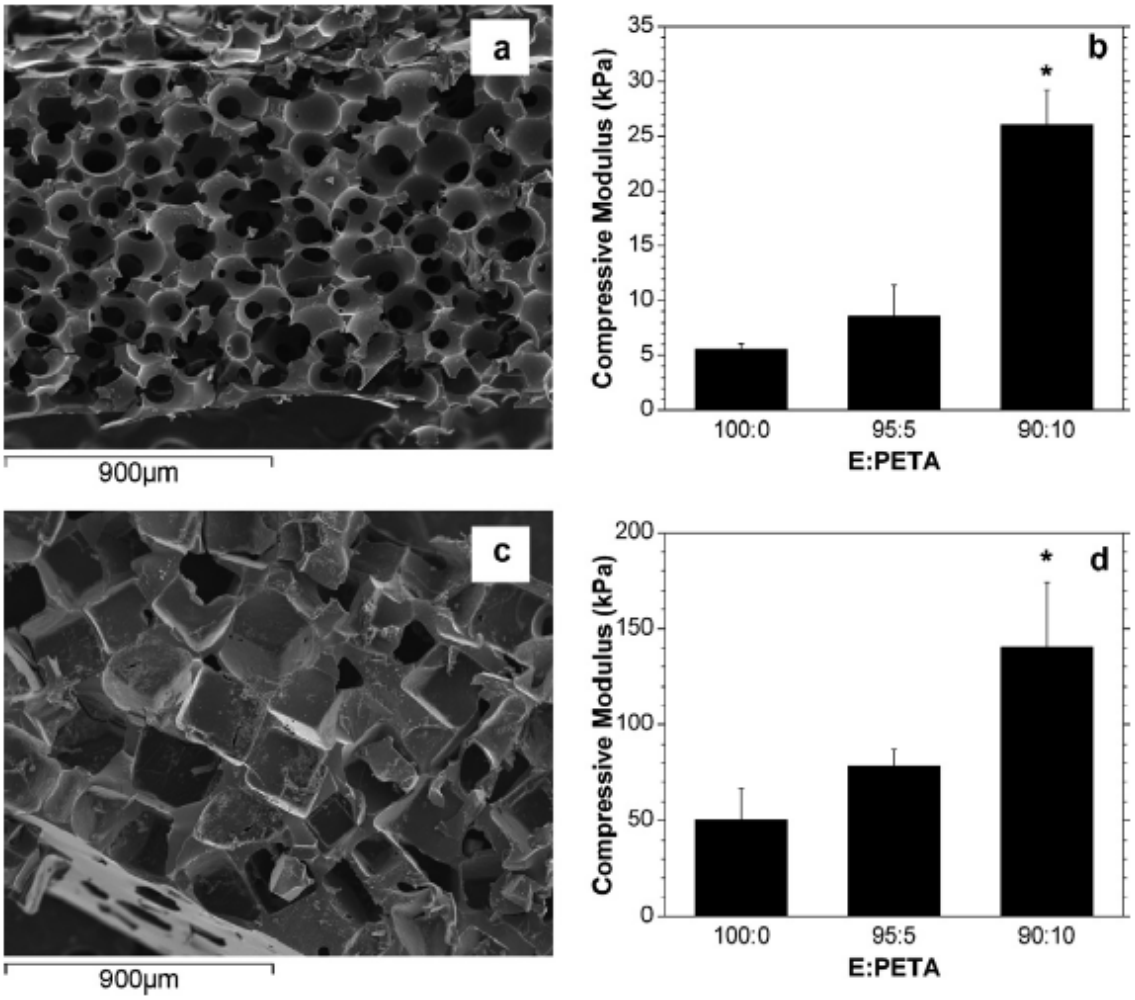

Figure 6.9 Representative scaffolds fabricated with E:PETA of 95:5 for the sintering technique (a) and salt leaching techniques (c) and compressive moduli of scaffolds from the sintering (b) and salt leaching techniques (d) from various E:PETA ratios. * denotes significance from the all other groups.

As an alternate technique, a salt leaching process was also used to obtain porous scaffolds. Figure 6.9B shows an example of the porous structure obtained with this technique, with most of the pores following the shape of the salt crystals and an interconnectivity in the structure. Again, the compressive moduli (Figure 6.9D) follows

the same trend seen in the bulk polymer with an increase in moduli with increased branching. The overall values are greatly reduced from the bulk polymer, but this is expected as there is only ~20% of the polymer remaining. The samples made from the salts were considerably stronger than their PMMA microbead counterparts. Observations of the SEM images indicate that the scaffolds formed from salt crystals are less interconnected and more polymer (and therefore lower porosity) than the sintered microsphere scaffolds. There have been methods for more uniform interconnected pores [37] which may aid in strengthening the resulting material, but the microspheres here were randomly arranged.

While the sintered microspheres lead to the desired scaffold microstructure and the material able to support cell growth in 2D culture, this is not possible as an injectable system. The PMMA spheres must be formed into a rigid sintered structure prior to implantation and removed using toxic solvents. The use of salt leaching may not be optimal, but alternate poragens, such as cytocompatible sugar crystals, may be explored. Thus, the composite could be used to fill a tissue defect, polymerized *in situ*, and then the porogen would dissolve to leave an interconnected porous structure behind.

6.4 Conclusions

The enhanced branching of network precursors, through the introduction of reagents with higher functionality during macromer synthesis, allows for further diversity of properties from a library of PBAEs. Increased macromer branching led to an increase in the initial polymerization rate, but little change in the ultimate double bond conversion and degradation behavior were. However, macromer branching significantly ($\alpha<0.05$)

decreased the network sol fraction and increased the mechanical properties of networks and adherence and spreading of osteoblast-like cells on polymer films. Finally, the macromers were used to form interconnected porous scaffolds using poragen leaching techniques, and scaffold properties followed the same trends in mechanical properties that were found in the bulk polymers. Ultimately, this work indicates that the introduction of branching during macromer synthesis can lead to variations in scaffold properties towards tissue engineering applications.

References:

[1] Anseth KS, Goodner MD, Reill MA, Kannurpatti AR, Newman SM, Bowman CN. The influence of comonomer composition on dimethacrylate resin properties for dental composites. Journal of Dental Research 1996;75(8):1607-1612.

[2] Bryant SJ, Nuttelman CR, Anseth KS. Cytocompatibility of UV and visible light photoinitiating systems on cultured NIH/3T3 fibroblasts in vitro. Journal of Biomaterials Science-Polymer Edition 2000;11(5):439-457.

[3] Burdick JA, Peterson AJ, Anseth KS. Conversion and temperature profiles during the photoinitiated polymerization of thick orthopaedic biomaterials. Biomaterials 2001;22(13):1779-1786.

[4] Khademhosseini A, Eng G, Yeh J, Fukuda J, Blumling J, Langer R, et al. Micromolding of photocrosslinkable hyaluronic acid for cell encapsulation and entrapment. Journal of Biomedical Materials Research Part A 2006;79A(3):522-532.

[5] Liu VA, Bhatia SN. Three-dimensional photopatterning of hydrogels containing living cells. Biomedical Microdevices 2002;4(4):257-266.

[6] Anseth KS, Shastri VR, Langer R. Photopolymerizable degradable polyanhydrides with osteocompatibility. Nature Biotechnology 1999;17(2):156-159.

[7] Fisher JP, Holland TA, Dean D, Engel PS, Mikos AG. Synthesis and properties of photocross-linked poly(propylene fumarate) scaffolds. Journal of Biomaterials Science-Polymer Edition 2001;12(6):673-687.

[8] Burdick JA, Mason MN, Hinman AD, Thorne K, Anseth KS. Delivery of osteoinductive growth factors from degradable PEG hydrogels influences osteoblast differentiation and mineralization. Journal of Controlled Release 2002;83(1):53-63.

[9] Sawhney AS, Pathak CP, Hubbell JA. Bioerodible Hydrogels Based on Photopolymerized Poly(Ethylene Glycol)-Co-Poly(Alpha-Hydroxy Acid) Diacrylate Macromers. Macromolecules 1993;26(4):581-587.

[10] Chung C, Mesa J, Miller GJ, Randolph MA, Gill TJ, Burdick JA. Effects of auricular chondrocyte expansion on neocartilage formation in photocrosslinked hyaluronic acid networks. Tissue Engineering 2006;12(9):2665-2673.

[11] Chung C, Mesa J, Randolph MA, Yaremchuk M, Burdick JA. Influence of gel properties on neocartilage formation by auricular chondrocytes photoencapsulated in hyaluronic acid networks. Journal of Biomedical Materials Research Part A 2006;77A(3):518-525.

[12] Elisseeff J, McIntosh W, Anseth K, Riley S, Ragan P, Langer R. Photoencapsulation of chondrocytes in poly(ethylene oxide)-based semi-interpenetrating networks. Journal of Biomedical Materials Research 2000;51(2):164-171.

[13] DeLong SA, Moon JJ, West JL. Covalently immobilized gradients of bFGF on hydrogel scaffolds for directed cell migration. Biomaterials 2005;26(16):3227-3234.

[14] Hillwest JL, Chowdhury SM, Slepian MJ, Hubbell JA. Inhibition of Thrombosis and Intimal Thickening by in-Situ Photopolymerization of Thin Hydrogel

Barriers. Proceedings of the National Academy of Sciences of the United States of America 1994;91(13):5967-5971.

[15] Anseth KS, Metters AT, Bryant SJ, Martens PJ, Elisseeff JH, Bowman CN. In situ forming degradable networks and their application in tissue engineering and drug delivery. Journal of Controlled Release 2002;78(1-3):199-209.

[16] Piantino J, Burdick JA, Goldberg D, Langer R, Benowitz LI. An injectable, biodegradable hydrogel for trophic factor delivery enhances axonal rewiring and improves performance after spinal cord injury. Experimental Neurology 2006;201(2):359-367.

[17] Beebe DJ, Moore JS, Bauer JM, Yu Q, Liu RH, Devadoss C, et al. Functional hydrogel structures for autonomous flow control inside microfluidic channels. Nature 2000;404(6778):588-+.

[18] Anderson DG, Tweedie CA, Hossain N, Navarro SM, Brey DM, Van Vliet KJ, et al. A combinatorial library of photocrosslinkable and degradable materials. Advanced Materials 2006;18(19):2614-2618.

[19] Brey DM, Erickson IE, Burdick JA. Influence of macromer molecular weight and chemistry on poly(β-amino ester) network properties and intitial cell interactions. Journal of Biomedical Materials Research Part A 2007 (in press).

[20] Burdick JA, Lovestead TM, Anseth KS. Kinetic chain lengths in highly cross-linked networks formed by the photoinitiated polymerization of divinyl monomers: A gel permeation chromatography investigation. Biomacromolecules 2003;4(1):149-156.

[21] Soltz MA, Ateshian GA. Experimental verification and theoretical prediction of cartilage interstitial fluid pressurization at an impermeable contact interface in confined compression. Journal of Biomechanics 1998;31(10):927-934.

[22] Xu JW, Shi WF, Pang WM. Synthesis and shape memory effects of Si-O-Si cross-linked hybrid polyurethanes. Polymer 2006;47(1):457-465.

[23] Mikos AG, Thorsen AJ, Czerwonka LA, Bao Y, Langer R, Winslow DN, et al. Preparation and Characterization of Poly(L-Lactic Acid) Foams. Polymer 1994;35(5):1068-1077.

[24] Bryant SJ, Cuy JL, Hauch KD, Ratner BD. Photo-patterning of porous hydrogels for tissue engineering. Biomaterials 2007;28(19):2978-2986.

[25] Kulkarni AS, Beaucage G. Quantification of branching in disordered materials. Journal of Polymer Science Part B-Polymer Physics 2006;44(10):1395-1405.

[26] Li XR, Su YL, Chen QY, Lin Y, Tong YJ, Li YS. Synthesis and characterization of biodegradable hyperbranched poly(ester-amide)s based on natural material. Biomacromolecules 2005;6(6):3181-3188.

[27] Nivasu VM, Yarapathi RV, Tammishetti S. Synthesis, UV photo-polymerization and degradation study of PEG containing polyester polyol acrylates. Polymers for Advanced Technologies 2004;15(3):128-133.

[28] Tian JH, Yu W, Zhou CX. The preparation and rheology characterization of long chain branching polypropylene. Polymer 2006;47(23):7962-7969.

[29] McKee MG, Unal S, Wilkes GL, Long TE. Branched polyesters: recent advances in synthesis and performance. Progress in Polymer Science 2005;30(5):507-539.

[30] Burdick JA, Anseth KS. Photoencapsulation of osteoblasts in injectable RGD-modified PEG hydrogels for bone tissue engineering. Biomaterials 2002;23(22):4315-4323.

[31] Discher DE, Janmey P, Wang YL. Tissue cells feel and respond to the stiffness of their substrate. Science 2005;310(5751):1139-1143.

[32] Hern DL, Hubbell JA. Incorporation of adhesion peptides into nonadhesive hydrogels useful for tissue resurfacing. Journal of Biomedical Materials Research 1998;39(2):266-276.

[33] Burdick JA, Philpott LM, Anseth KS. Synthesis and characterization of tetrafunctional lactic acid oligomers: A potential in situ forming degradable orthopaedic biomaterial. Journal of Polymer Science Part a-Polymer Chemistry 2001;39(5):683-692.

[34] Karageorgiou V, Kaplan D. Porosity of 3D biornaterial scaffolds and osteogenesis. Biomaterials 2005;26(27):5474-5491.

[35] Freed LE, Vunjaknovakovic G, Biron RJ, Eagles DB, Lesnoy DC, Barlow SK, et al. Biodegradable Polymer Scaffolds for Tissue Engineering. Bio-Technology 1994;12(7):689-693.

[36] Yang SF, Leong KF, Du ZH, Chua CK. The design of scaffolds for use in tissue engineering. Part 1. Traditional factors. Tissue Engineering 2001;7(6):679-689.

[37] Stachowiak AN, Bershteyn A, Tzatzalos E, Irvine DJ. Bioactive hydrogels with an ordered cellular structure combine interconnected macroporosity and robust mechanical properties. Advanced Materials 2005;17(4):399-403.

CHAPTER 7: *Screening PBAE Library for Osteoconductive Materials*

(Adapted from: DM Brey, C Chung, KD Hankenson, JP Garino, JA Burdick. Identification of Osteoconductive and Biodegradable Polymers from a Combinatorial Polymer Library. J Biomed Mater Res A. 2010;93A(2):807-816.)

7.1 Introduction

Traditional polymer development for tissue engineering applications has been a time consuming and tedious process, as polymer synthesis often requires multiple reactions and purification steps. Fortunately, technology is continuously being developed to accelerate various steps in the tissue engineering process, including the high-throughput screening of materials and small molecule mediators of cellular behavior, the use of microdevices to screen cellular microenvironments, the technology to rapidly assess material properties, and the use of combinatorial polymer syntheses [1]. In general, combinatorial synthesis is a method to produce large libraries of compounds and materials through simplified single-step reactions [2]. This approach has been used widely in the pharmaceutical industry to greatly expand the pool of drugs for investigation, and to help identify structure-property relationships of bioactive molecules [3].

More recently, combinatorial libraries are being utilized to develop materials for biomedical applications; including gene delivery vehicles [4, 5], substrates for the culture

of stem cells [6, 7], and potential biodegradable materials for tissue engineered scaffolds [8-12]. For scaffold development, combinatorial syntheses are used to produce libraries of materials that can be screened and developed for a specific application based on desired properties. For example, Brocchini *et al.* developed a library of 112 polyarylates that exhibited a range of physical and cellular characteristics [9]. This library has been used to develop predictive computational models of chemical structures and physical properties [13], cell growth [14], and the adsorption of fibronectin [15]. These models were then utilized to virtually design a polymethacrylate combinatorial library that predicted cell attachment, cell growth, and fibrinogen adsorption [13]. Experimentally measured values showed agreement in many of the predicted properties, which opens the door for future, faster and cheaper biomaterial development procedures.

Beyond distinct chemical libraries, gradients of materials may also be used to identify optimal formulations to meet a given set of criteria. Using these approaches, both Meredith *et al.* and and Yang *et al.* were able to optimize the combination of poly(D,L-lactide) and poly(ε-caprolactone) [10] and tyrosine-derived polycarbonates [11], respectively, for desirable osteoblast interactions. Additionally, combinatorial synthesis on the nanoliter scale can greatly accelerate material discovery. For example, 3456 different individual combinations and ratios of 24 polymers were mixed in nanoliter spots on an array in order to determine cell-material interactions [7].

An important step in this approach is the identification of effective criteria that permit material selection for specific applications. For tissue engineering, these criteria may include properties such as: degradation rate, mechanics, cell attachment, cytotoxicity, and biocompatibility [16]. Degradation allows a material to be replaced

with cells and tissue over time, but is also important for the temporal mechanical properties and the release of degradation products. Mechanical properties are important for the stability of a scaffold, but have also been implicated in the differentiation of cells (e.g., mesenchymal stem cells, MSCs).[17] Additionally, mechanical mismatching can lead to issues such as stress shielding, which weakens the surrounding bone in orthopaedic applications [18]. Cell attachment is needed for matrix deposition by anchorage dependent cells and can be facilitated through protein adsorption, such as fibronectin, or through the incorporation of known cell binding peptides (i.e., RGD) [19]. Biocompatibility means that the material does not incur any significant inflammatory or immune response when implanted into the body [20]. Also, it is desirable for a material to not just be isolated from the body through a foreign body response, but to also integrate with tissues [20]. 'Bioactive' materials can be designed to support certain tissues or even be used to help drive differentiation with the addition of functional groups [21].

We have recently developed a combinatorial library of acrylate-terminated poly(β-amino ester)s (PBAEs) that form networks with a wide range of mechanical properties (3-300 MPa) and degradation rates (<24 hours to >100 days) based on chemical variations [8]. The macromers are formed through simple addition reaction without the need for purification, and thus meet the criteria for combinatorial synthesis. Additionally, the size and branching of the macromers can be modified to introduce further material control for a desired application [22, 23]. These macromers can be crosslinked into networks using a radical polymerization (e.g., photopolymerization) to form scaffolds for biomedical applications, which introduces further spatial and temporal

control over the materials [24]. Also, they can be processed into scaffolds using basic templating/poragen techniques [23] or through electrospinning into fibrous structures [25].

The diversity of this PBAE library allows for exploration for a range of tissue engineering applications, and in this work, the library was screened to identify an osteoconductive material for use in mineralized tissue regeneration. The candidates were first assessed for material properties and *in vitro* cellular interactions and an optimal candidate was processed into 3-dimensional scaffolds and implanted into rat cranial defects assess the bone regeneration potential. An osteoinductive factor was also introduced to further illustrate the potential of the scaffold for mineralized tissue growth. This work has identified a novel biomaterial with beneficial characteristics for promoting bone regeneration; but perhaps more importantly, it illustrates a process that can be used for developing tissue engineering scaffolds from combinatorial libraries of biodegradable polymers.

7.2 Materials and Methods

7.2.1 PBAE synthesis

PBAEs were synthesized as described previously [8]. Briefly, 10 combinations of diacrylates and primary amines (all reagents were purchased from Sigma, Scientific Polymer Products, or TCI America) were chosen from previous data [8] according to their degradation rate to meet design criteria and mixed together in a molar ratio of 1.2:1, respectively, overnight at 90°C. The reaction scheme and monomers used are shown in Figure 7.1 and the sample notation is from the original study on the library development [8]. The macromers were characterized with proton nuclear magnetic resonance (^{1}H NMR, Bruker DMX360, 360 MHz) and were determined to be ~2000 Da. The photoinitiator 2,2-dimethoxy-2-phenyl acetophenone (DMPA, Sigma) was added to the liquid macromers at a final concentration of 0.5% (w/w). The viscous macromer solutions were then polymerized with exposure to ultraviolet light (~10 mW/cm^2, 365 nm, 10 min, Blak-Ray B-100 AP).

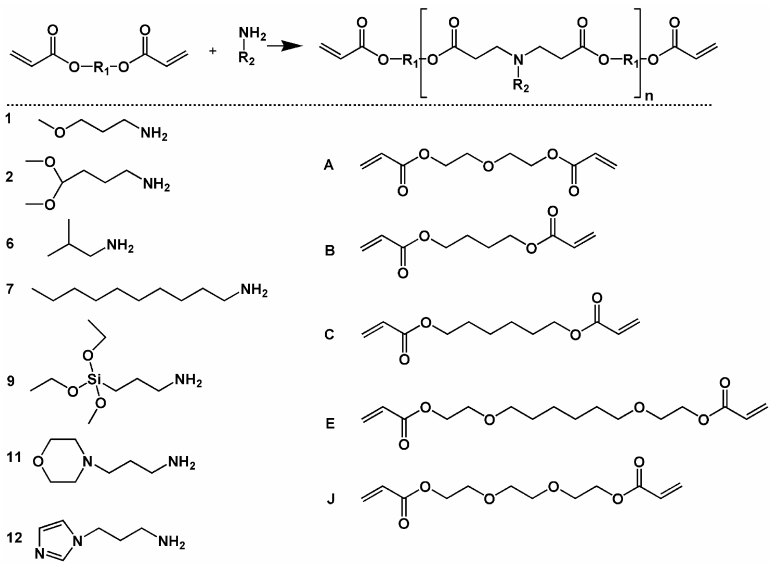

Figure 7.1 Reaction scheme for the synthesis of photopolymerizable and degradable poly(β-amino ester)s (top) and amines (numbered monomers, determines R_2) and diacrylates (lettered monomers, determines R_1) used in the synthesis (bottom). The molecule notation is from the original report of the combinatorial library.[8]

7.2.2 In vitro characterization

Bulk slabs were obtained by polymerizing the macromers between two glass slides with a 1 mm thick spacer and cutting samples to a desired size. Mass loss was monitored by placing 8 x 12 mm samples into phosphate buffered saline (PBS) at a pH of 7.4 on an orbital shaker at 37°C. At desired time points, the samples were removed, lyophilized, and the final mass compared to the initial mass. The mechanical properties of the materials were assessed by compression of 5 mm diameter disks with a dynamic mechanical analyzer (Q800 TA Instruments) at a strain rate of 10%/min with the modulus determined as the slope of the stress/strain curve at low strains (<20%).

To form thin films, macromers were dissolved in ethanol at 1:2 (macromer:EtOH), added to 24-well plates (30 μl), the ethanol was allowed to evaporate overnight, and the macromer was crosslinked with UV exposure in a nitrogen environment. Human MSCs (Lonza) were seeded on the films at a density of 5000 cells/cm^2 and cultured for up to 7 days. MSCs were grown in growth media (αMEM, 17% fetal bovine serum, 1% penicillin/streptomycin, 1% l-glutamine) or osteogenic media (growth media, 10mM β-glycerol phosphate, 25 μg/mL ascorbic acid-2-phosphate, 10 nM dexamethasone). Viability was measured using a metabolic activity assay (Alamar Blue, Invitrogen), by adding 50 μl of the reagent to each well, incubating for 4 hours, and reading the fluorescence in a plate reader (Bio-Tek Synergy HT, excitation-545nm, emission-590 nm). Osteogenic differentiation and activity of the MSCs in osteogenic media was measured with an alkaline phosphatase fluorescent assay (APF, Sigma), as alkaline phosphatase is an early indicator of bone formation.

Cells were then cultured on the best candidate material over 3 weeks to further characterize the osteoconductivity of the materials. RNA was extracted at 7, 14, and 19 days using TRIzol® (Invitrogen), and isolated according to manufacturer's instructions. RNA concentration and quality were determined using an ND-1000 spectrometer (Nanodrop Technologies), and 1 ug of RNA was reverse transcribed into cDNA using reverse transcriptase (Superscript II, Invitrogen) and OligoDT (Invitrogen). Relative gene expression was determined using an Applied Biosystems 7300 Real-Time Polymerase Chain Reaction system for osteocalcin and normalized to the housekeeping gene glyceraldehyde 3-phosphate dehydrogenase (GAPDH, Table 7.1) followed by normalization to the cell pellet gene expression levels at day 0 using the $\Delta\Delta C_T$ method.

Table 7.1 Quantitative PCR primers and probes.

Gene	Forward Primer	Reverse Primer	Probe
GAPDH	AGGGCTGCTTTTAACTCTGGTAAA	GAATTTGCCATGGGTGGAAT	CCTCAACTACATGGTTTAC
Osteocalcin	CTGGCCGCACTTTGCAT	CTGCACCTTTGCTGGACTCT	CACCTGCCTGGCCAGC

7.2.3 In vivo characterization

Sprague Dawley (250-275 g, Charles River) rats were used for the animal models. NIH guidelines for the care and use of laboratory animals (NIHPublication #85-23 Rev. 1985) were observed. Polymer disks (n=3, 8 mm diameter, 1 mm thick) were implanted subcutaneously into dorsal pockets in rats for 2, 4, and 8 weeks in order to monitor *in vivo* degradation and investigate the inflammatory response of the local tissue as in [26]. Scaffolds were prepared using a bead sintering and extraction procedure as described previously [23]. Briefly, 200 μm diameter PMMA beads (Polysciences) were sintered overnight in an 8 mm x 1.5 mm teflon mold, the macromer/initiator was added to fill the void spaces, and the sample was photopolymerized with UV exposure between two glass slides. The PMMA beads were removed with serial washings in methylene chloride and then the methylene chloride was evaporated from scaffolds in a fume hood. Scaffolds (n=3) were characterized with scanning electron microscopy (SEM, JEOL 7500 HR-SEM) and were implanted subcutaneously to confirm tissue infiltration and tissue response.

Scaffold composites (1.5 mm thick) were then made by adding a small amount of collagen (Inamed Biomaterials) either alone or loaded with 2 μg of rhBMP-2 (R&D

systems). The collagen solution (61 μl) was allowed to gel at 37°C for 1.5 hours and the scaffolds were frozen and lyophilized. Scaffolds were then implanted either intramuscularly (6 mm diameter) or into a critical-sized cranial defect (8 mm diameter) in rats. For the intramuscular implants, scaffolds were implanted bilaterally into the adductor thigh muscle for 4 weeks [27]. For cranial implants, an 8 mm defect was made using a hand trephine across the sagittal suture, and compression fit with the A6 scaffold. Four groups were investigated (n=5/group) consisting of empty defects, defects filled with porous scaffold alone, defects filled with porous scaffold containing a small amount of collagen gel, and defects filled with polymer scaffold containing a small amount of collagen gel loaded with BMP-2. Calvaria were removed at 6 weeks and fixed in 4% formalin.

High-resolution x-rays were obtained using a MX-20 Faxitron (Faxitron) at 15 s and 25 kV. The radiopacity was measured as the percent intensity of the defect area over the intensity of intact bone and analyzed with ImageJ software. Calvaria were then scanned using a VivaCT40 uCT scanner (Scanco) with X-ray acquisition settings set at 55 kVp and 145 mA and an integration time of 200 ms. Scans were performed with an isotropic voxel size of 10.5 μm and images were reconstructed in 1,024 x 1,024 pixel matrices. A lower threshold of 743.4 mg/cm^3 and an upper threshold of 2000 mg/cm^3 were determined by visual inspection to best distinguish between bone and non-bone material. Scanco computer software was used to calculate the bone volume and the connectivity index. Samples were then decalcified in 10% EDTA for 3 weeks, dehydrated, and then mounted in paraffin wax for histology. Samples were processed using standard techniques for hematoxylin and eosin staining.

7.2.4 Statistics

Statistical analysis was performed using ANOVA with Tukey's post-hoc among the groups with significance defined as p-value less than 0.05. All values are reported as the mean and the standard deviation of the mean.

7.3 Results and Discussion

7.3.1 Polymer development

As technology to rapidly produce large numbers of materials (e.g., combinatorial libraries) is developed, it is important to understand the process to identify optimal materials for desired applications. For this paper, a previously developed library of PBAEs was assessed to identify osteoconductive materials for use as scaffolding in mineralized tissue regeneration. The PBAE macromers are synthesized by the conjugate addition of commercially available amines and diacrylates (Figure 7.1), without the production of byproducts that would need purification; thus, large numbers of molecules are rapidly produced. The availability of vasculature and progenitor cells in bone [16] affords potential acellular approaches that rely on the recruitment of these localized resources to scaffolding that is conducive to cellular interactions and may also include inductive cues to stimulate osteogenesis. This may be advantageous for many instances over cellular approaches that would be patient specific and require additional steps prior to implantation to isolate and culture cells. Thus, our approach is to identify an osteoconductive material from the library with the appropriate physical properties and

cellular interactions and then to include osteoinductive molecules to further improve tissue regeneration.

For tissue engineering, the scaffold supports cell attachment and acts as a template to control the geometry and extent of produced tissue. Ideally, this material would degrade with time and be replaced with new tissue. This can be a delicate balance as losing mass too quickly could prevent adequate cell adhesion and support, whereas too slowly could inhibit the normal growth and replacement of natural tissue [28]. With this in mind, the desired degradation behavior for this application was determined to be gradual mass loss and complete degradation within approximately 3-5 months. This will hopefully allow for minimal toxicity from the degradation products and support during the approximate time for a fracture to heal and the bony callus to resorb [29, 30].

From the original PBAE library of 120 polymers, 10 macromers (Figure 7.1: A6, A7, B1, B2, C11, C12, E1, E2, E9, and J6) were identified as forming polymer networks that meet this mass loss criteria. The shapes of the degradation profiles (Figure 7.2A) ranged from fairly linear to a more rapid initial release followed by a slower plateau region. Differences may be attributed to variability in the hydrophobicity of the polymers, which could affect the rate ofwater uptake, or the presence of a soluble fraction that may be released rapidly. A slower initial degradation may also be preferable as it allows cells to populate scaffolds before the substrate begins to degrade.

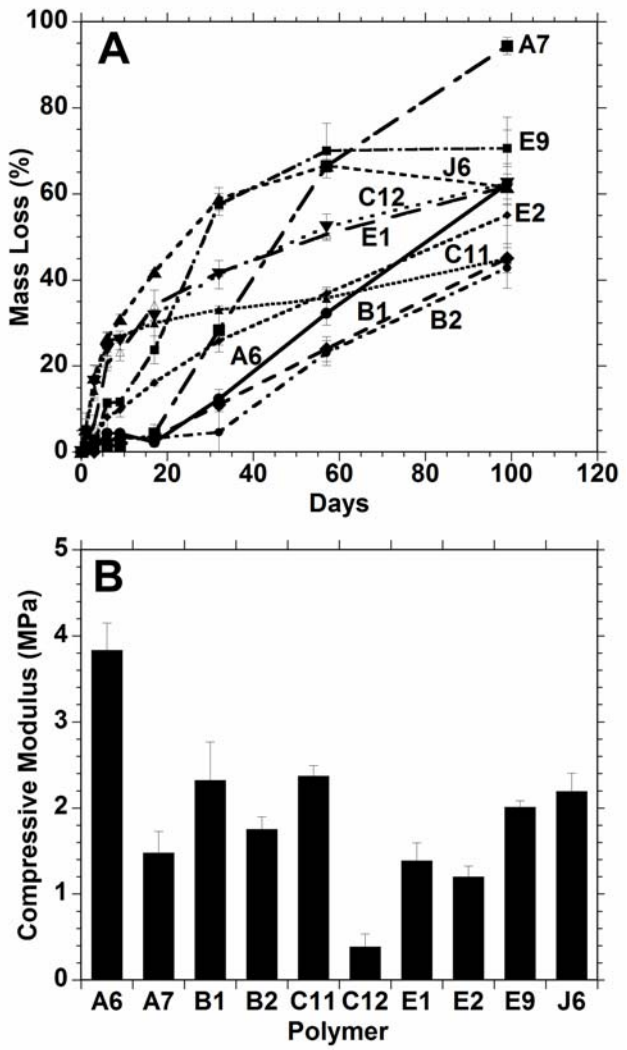

Figure 7.2 Bulk polymer degradation (A) and compressive moduli (B) of 10 candidate polymers formed from PBAE macromers that met design criteria from the initial combinatorial polymer library. The A6 group possessed a statistically higher ($p<0.05$) modulus than all other groups.

The compressive moduli for slabs of these 10 polymer networks are shown in Figure 7.2B. The variation of this subset of materials was all in the same order of magnitude (~0.5 to 4.0 MPa), in contrast to the entire library which ranged over 2 orders

of magnitude [8]. The mechanical properties are important to the cellular microenvironment, as previous studies have shown that stem cells grown on stiffer substrates differentiate towards an osteogenic pathway, while cells that are grown on very soft surfaces differentiate towards other lineages [17]. The low modulus of these materials with respect to bone, as with all synthetic polymer systems, will restrict utility to non-load bearing defects or use in conjunction with other fixation techniques. The A6 network had the highest moduli of the 10 polymers, at 3.8 ± 0.3 MPa; however, since all of these samples possessed moduli in the same magnitude, mechanics were not used to exclude any candidates from the group.

Next, the ability of cells to adhere and remain viable on the surfaces of these materials was investigated by growing MSCs on thin films of polymers and measuring the cellular metabolic activity (with the Alamar Blue assay), as reported in Figure 7.3A. The media in the wells with C11 and C12 quickly changed to yellow, indicating an acidic environment in which the cells did not survive. Similarly, cells grown on A7 did not remain viable and the polymer E9 prematurely crosslinked. Therefore, these four materials were removed from further testing. Cellular mitochondrial activity increased for other groups (B1, B2, E2, J6), but decreased between the 4 and 7 day time points. However, the mitochondrial activity steadily increased for polymers E1 and A6 over the entire week of culture. Variations in the mitochondrial activity between polymers may be attributed to a number of factors including changes in protein adsorption, which can affect initial adhesion events, or the toxicity of degradation products that are eluted at different times in culture. However, the presence of cells at the 7 day time point and

proliferation with culture has generally been a good indicator of non-toxicity in these environments.

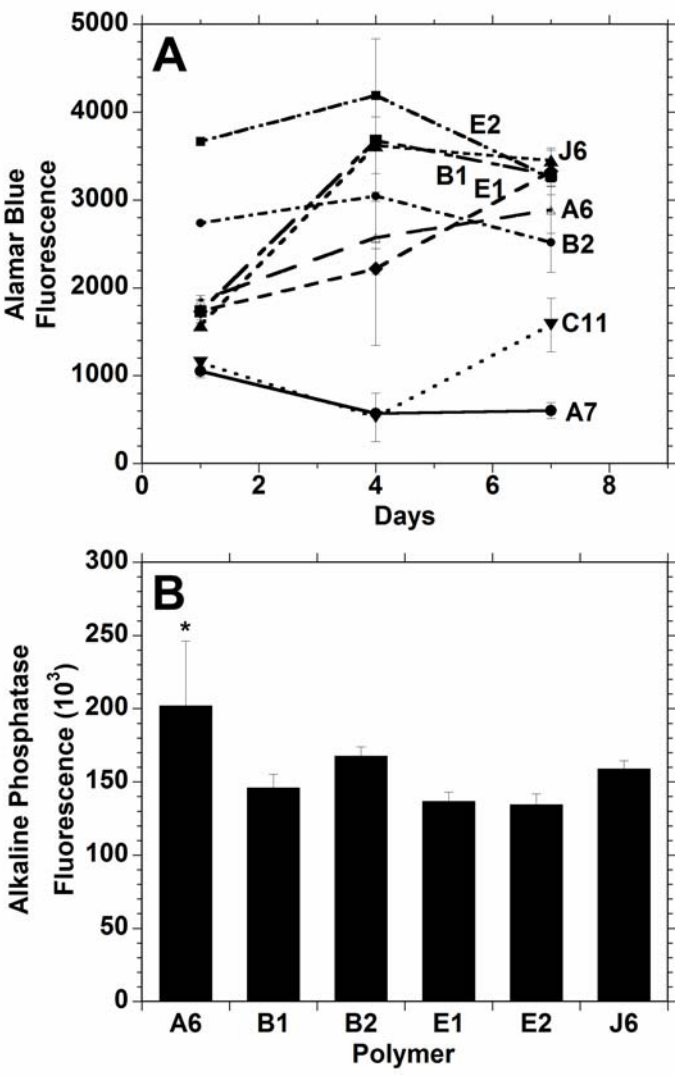

Figure 7.3 Mesenchymal stem cell viability (measured with Alamar Blue) (A) and alkaline phosphatase activity after 3 days (B) after seeding onto films of candidate polymers formed from PBAE macromers. * indicates significant difference ($p < 0.05$) from all other groups except B2.

Alkaline phosphatase (ALP) activity of MSCs grown on polymer thin films after 3 days in osteogenic media (Figure 7.3B) was used as one measure of the osteoconductivity of these polymers. Although ALP activity was observed by cells on all of these polymers, the ALP activity of the cells grown on A6 was significantly greater than the activity of the cells on all other polymers except B2. Comparing the A6 and B2 polymers, the A6 supported a steady increase in cell viability throughout the 1 week period and was higher after 7 days. B2 and A6 had relatively similar linear degradation profiles, but A6 had a modulus that was roughly double that of polymer B2. With these factors in mind, A6 was selected for further analysis as an osteoconductive polymer from the library.

Osteoconductivity was also assessed by measuring osteocalcin gene expression of MSCs cultured on films of A6. The osteocalcin expression (Figure 7.4A) greatly increased from the initial level throughout the duration of the experiment, and was significantly greater than MSCs grown on control tissue culture polystyrene (TCPS) at 2 and 3 weeks. Osteocalcin is an important non-collagenous matrix protein specific to bone, and an increased expression of 17.4 ± 11.0 and 3.95 ± 1.17 fold at 2 and 3 weeks, respectively, should indicate increased mineralized tissue production. The up-regulation in osteocalcin is supported by the increase in ALP expression found in the shorter term studies.

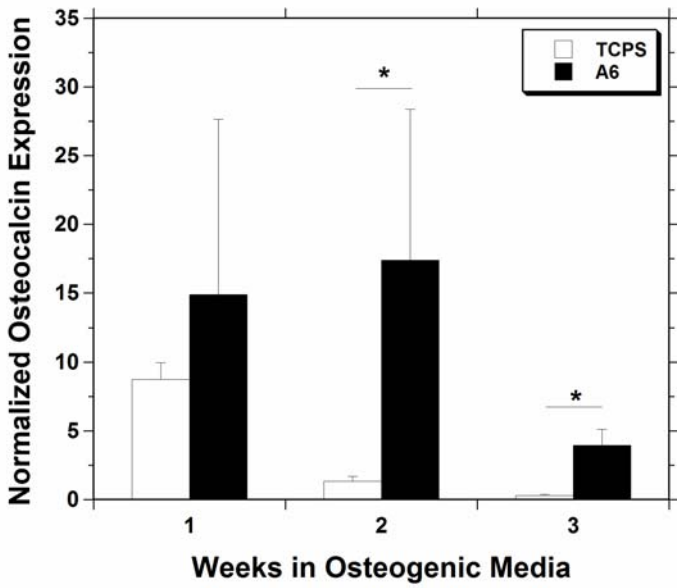

Figure 7.4 Osteocalcin gene expression in mesenchymal stem cells cultured up to 3 weeks in osteogenic media on TCPS (white) or A6 thin films (black), normalized to the expression of the same gene in cells at time of seeding. * indicates a significant difference ($p < 0.05$) between the two groups at that time point.

7.3.2 Subcutaneous implantation

A longer term degradation study showed that the A6 polymer was completely degraded after 17 weeks in PBS (Figure 7.5A), which fits our 3-5 month degradation criteria. For comparison, bulk slabs of A6 were implanted subcutaneously in rats to measure their inflammatory response, as well as the *in vivo* degradation profile. The degradation of these samples was similar to what was seen *in vitro*, especially at 2 and 8 weeks (Figure 7.5A), with ~50% mass lost after 8 weeks. Histology of the A6 implants after 4 and 8 weeks are shown in Figure 7.5B and C, respectively. The polymer elicited a mild inflammatory response in the first 2 weeks with some new blood vessel formation

and macrophage recruitment to the polymer-tissue interface. With time, the polymer was encapsulated with a thin fibrous tissue, and there is no evidence of inflammation or necrosis within the adjacent subcutaneous fibroadipose tissue, skin adnexal structures or deep skeletal muscle. In general, these results indicate a mild inflammatory response, typical of commonly used biodegradable polymers.

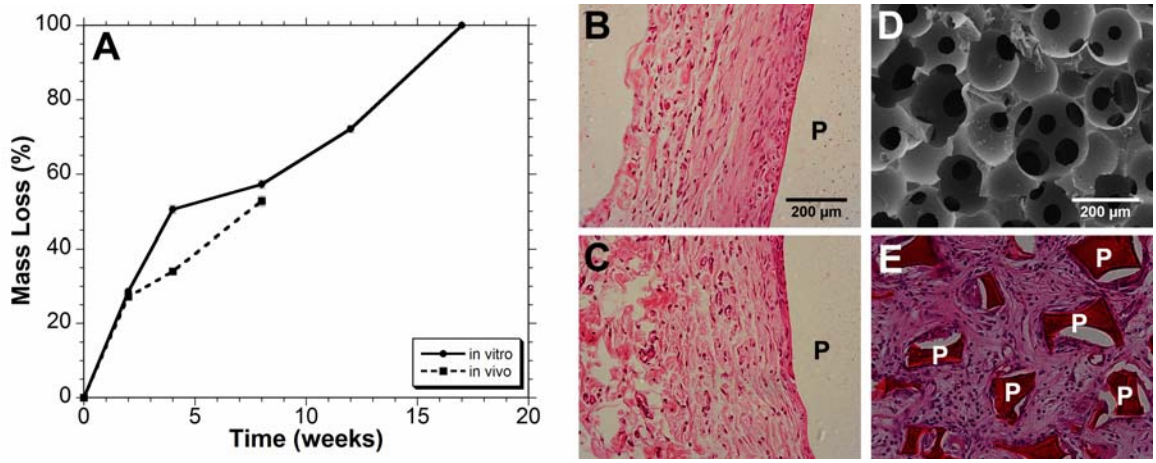

Figure 7.5 Mass loss profiles of bulk A6 slabs *in vitro* (solid line) or after subcutaneous implantation (dashed line) (A) and representative tissue response to the A6 slabs 4 (B) and 8 weeks (C) after subcutaneous implantation. SEM of A6 porous scaffolds showing large, interconnected porosity (D) and representative tissue response to A6 porous scaffolds 4 weeks after subcutaneous implantation (E), illustrating complete fibrous tissue infiltration. P = Polymer.

Towards utility in 3-dimensional tissue engineering, porous A6 scaffolds (Figure 7.5D) were fabricated using a previously described poragen leaching technique [23]. Scaffolds exhibited large pores (~200 µm) and pore interconnectivity, both of which are

important design parameters for musculoskeletal tissue scaffolds [16, 31]. When implanted subcutaneously, minimal inflammation was observed and tissue fully infiltrated the acellular scaffolds (Figure 7.5E). Histological assessment revealed that this tissue was fibrous and vascularized and there was no indication of mineralized tissue production within the scaffold, which is not expected without incorporation of inductive cues.

7.3.3 In vivo assessment

An important component for many tissue engineering approaches is the incorporation of inductive factors, such as direct recombinant growth factor delivery or through gene therapy [32]. In many cases, scaffolds incorporating these inductive factors improve their ability to produce functional tissue. In this work, we introduced a known, FDA-approved osteoinductive factor (BMP-2) [33, 34] into the porous scaffolds by loading the molecule within a very small amount of collagen. The collagen solution is simply pipetted into the porous scaffold and gelled with elevated temperature. The collagen is easily remodeled by cells and the BMP-2 is released through both diffusion and cell-mediated degradation. This made it difficult to quantify the specific release profiles obtained with this technique.

Two models were used for the evaluation of these BMP-2 loaded osteoconductive scaffolds. First, the scaffolds were implanted into an intramuscular implant site, as described by Hartman *et al* [27], to assess their ability to form ectopic mineralized tissue. For this preliminary experiment, only two groups were tested, A6 scaffold with BMP-2 loaded collagen and the A6 scaffold with collagen alone, implanted for 4 weeks. The

radiographs in Figure 7.6A (no BMP-2) and Figure 7.6B (with BMP-2, looking from a side view) indicate that ectopic mineralized tissue is formed, but only in the scaffolds incorporating the osteoinductive factor. Likewise, histology of these implants show no evidence of bone formation in the unloaded samples (Figure 7.6C), yet mineralized tissue is observed in the BMP-2 loaded scaffolds (Figure 7.6D). 3D reconstruction of the newly produced bone using μCT demonstrates extensive mineralization with a pattern that resembles the interconnected pores of the scaffold.

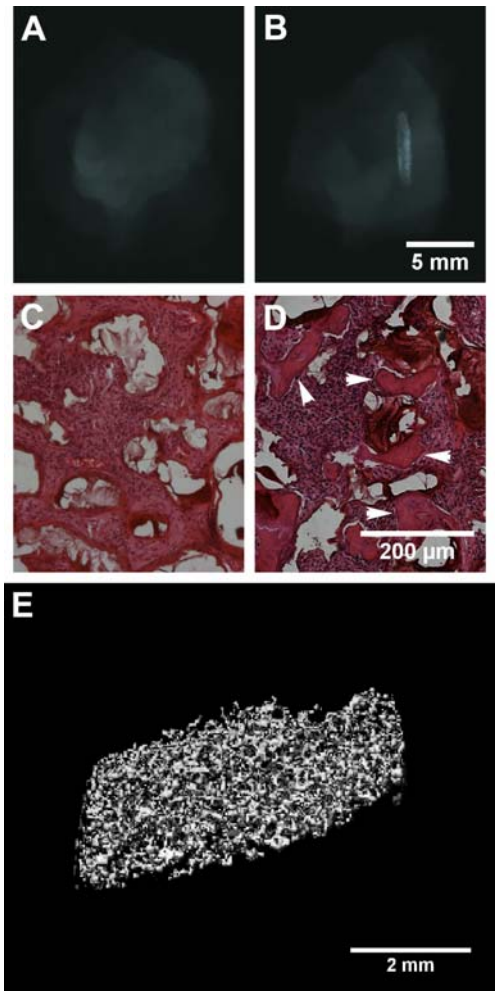

Figure 7.6 Radiographs (A, B), histology (C, D, mineralized tissue identified with arrows), and micro-CT (E) of A6 scaffolds 3 weeks after intramuscular implantation alone (A, C) or when loaded with BMP-2 (B, D, E). Ectopic mineralized tissue formation was only evident in samples that contained BMP-2 and the tissue formed a porous structure that templated the implanted scaffolds.

The scaffolds were further assessed in a critical-sized cranial defect (8 mm) model in rats that does not support extensive healing without intervention [35]. The defect is not load bearing, and is common to the intramembranous bone healing of fractures that

are rigidly fixed [36, 37]. Four groups were assessed; the negative control of an empty defect, the A6 scaffold alone, the A6 scaffold plus collagen gel filling the pores, and the A6 scaffold plus collagen gel loaded with 2 μg of BMP-2. Treatments of collagen gel alone were not assessed since it would involve significantly more collagen to fill the defect site than what is used as a BMP-2 carrier. After 6 weeks, radiographs (Figure 7.7A) indicate that only the samples loaded with BMP-2 had consistent bone growth throughout the scaffold, while the other groups showed minimal growth, mostly at the outer edges. The radiopacity (Figure 7.7B) of samples with BMP-2 was significantly greater than the other 3 groups, and there were no significant differences between these other groups.

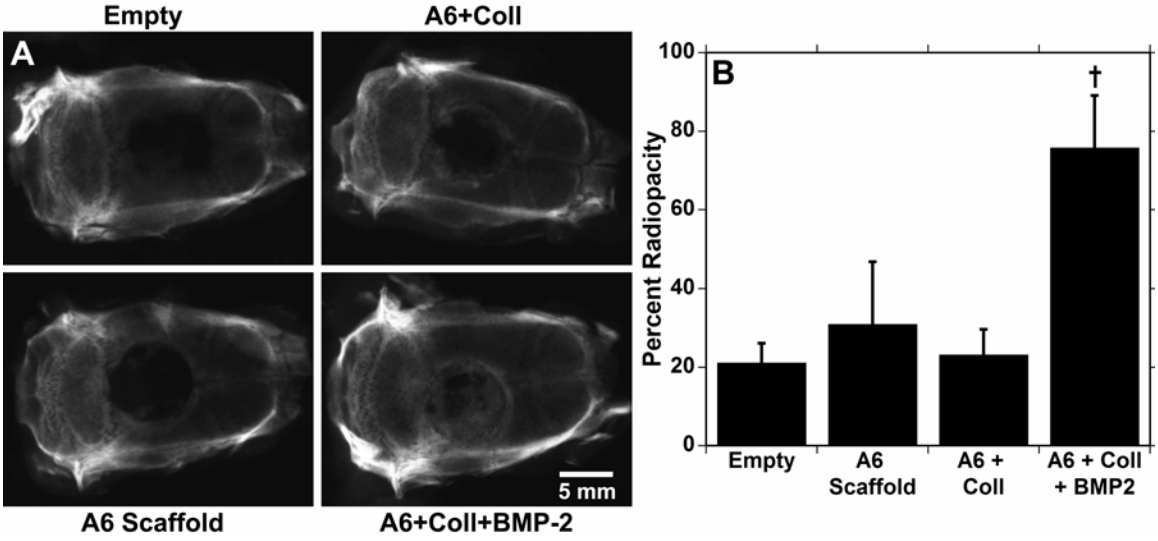

Figure 7.7 Radiographs of rat calvaria 6 weeks after 8 mm defect creation and either left empty or filled with A6 scaffolds alone or loaded with collagen or collagen and BMP-2 (A). The percent radiopacity of the defect/scaffold radiographs compared to intact bone (B). † indicates significant difference ($p < 0.05$) from all other groups.

Similarly, μCT images (Figure 7.8A) show consistent bone growth in the samples with BMP-2. Again, while there is some growth in the empty defects, the cross sections show that this is very thin and only at the edges. The bone volume (Figure 7.8B) showed similar results to the radiographic data, with significantly greater bone volume in the BMP-2 containing samples at 16.4 ± 4.1 mm^3 compared to other groups. The connectivity index (Figure 7.8C), a measure of the interconnectivity of the bone, is significantly higher in the BMP-2 samples as well. Finally, histological samples of A6 scaffolds (Figure 7.9) reinforced the μCT data. In the untreated defects group, there is some growth of bone, but the majority of the defect is filled with thin fibrous tissue. In

the groups of scaffolds without growth factor (regardless of the presence of collagen), there is tissue infiltration throughout the scaffolds, but the only bone growth is observed at the edges of the scaffold. In the BMP-2 scaffolds, there is bone formation within the scaffold consistently from the outer edge all the way through to the middle.

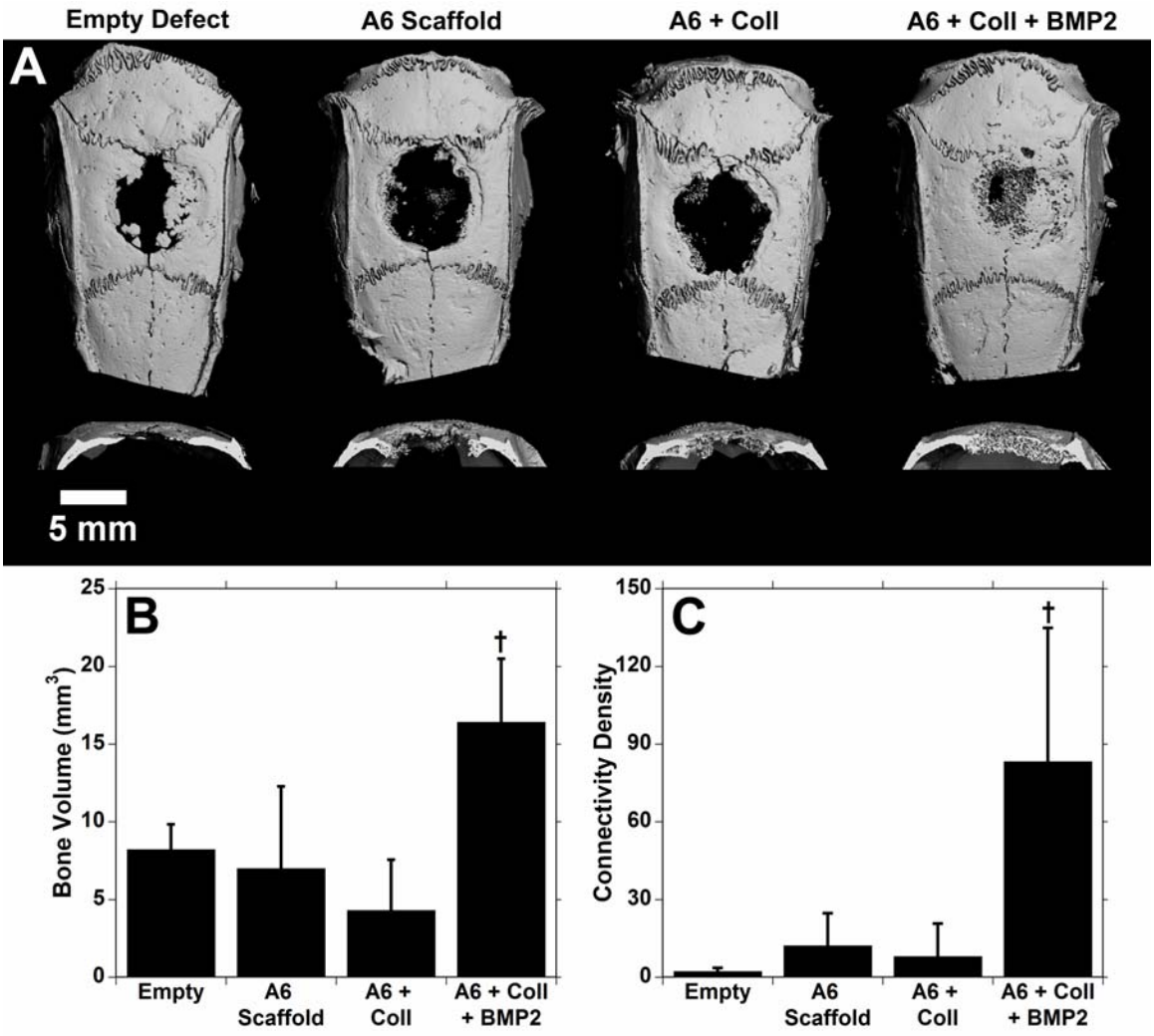

Figure 7.8 3-dimensional reconstructions (A) and quantification of the bone volume (B) and connectivity index (C) from μCT analysis of the groups 6 weeks after implantation in the calvarial defects. † indicates significant difference ($p < 0.05$) from all other groups.

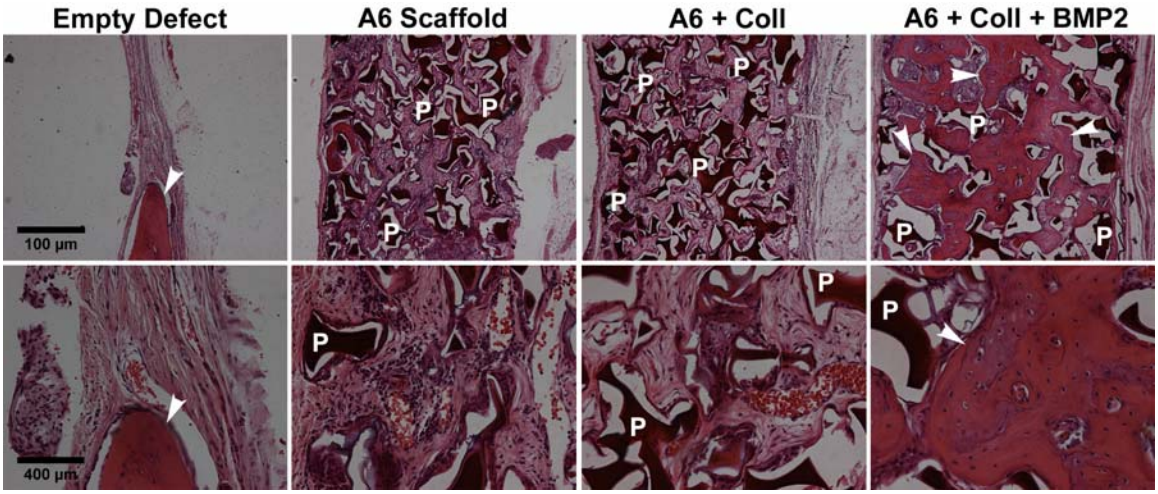

Figure 7.9 Histological sections of calvarial defects 6 weeks after treatment (top: 5x, bottom: 20x). Only samples with BMP-2 show bone formation throughout the scaffold (labeled with arrows) and polymer scaffold remains at this time point (labeled by P).

The samples with BMP-2 showed bone formation throughout the scaffold and the bone was connected throughout due to the interconnectivity of the pores created by the sintered microbeads. At 6 weeks, the new bone is still interdispersed within the remaining A6 scaffold. There is no evidence of cartilage, potentially since the bone is forming through intramembranous ossification or perhaps because of the later time points of harvest. BMP-2 greatly enhanced new bone formation within the scaffold, and could have recruited progenitor cells in the area to differentiate along an osteogenic lineage to produce mineralized tissues. There was no significant difference in the amount of bone formed in any of the other groups, and the bone that was formed was largely restricted to the perimeter of the defect. Thus, it is believed that while the porous scaffolds identified as being inductive supported tissue growth and did not possess a highly inflammatory response, they do not have any inherent osteoinductive capabilities.

The use of combinatorial libraries can greatly increase the pool of materials for use in biomedical applications. In this case, a relatively small but diverse set of PBAEs was screened for use in mineralized tissue engineering, but this library could also be used in the development of materials for drug delivery, gene delivery [4], or other tissue engineering applications [25]. The tunability of the properties through control of macromer synthesis [22, 23] and the flexibility afforded to the processing of photopolymerizable materials reflect the advantages of this particular library.

This screen was accomplished with a relatively straight-forward approach using traditional bulk measurements of degradation, mechanics, and cell viability. The complexity of this system can be quickly increased by investigating copolymers of the library constituents or investigating gradients of monomers. The use of techniques that more rapidly screen these parameters, including with microdevices, will be important in identifying materials for given applications in the future.

7.4 Conclusions

By screening a library of 120 photocrosslinked PBAEs against design parameters (bulk properties, cellular adhesion and toxicity) for an application of mineralized tissue engineering, an osteoconductive material was identified. Cells cultured on this optimal material exhibited enhanced viability profiles and alkaline phosphatase activity compared to other polymers. When implanted subcutaneously, the material elicited minimal inflammation, and porous scaffolds were fully infiltrated with tissue. While this material has no inherent osteoinductive properties, it was loaded with a known osteoinductive factor, BMP-2, which led to bone formation ectopically in an intramuscular location and

within a critical-sized bone defect. This work presents a process for identifying potential scaffolding material for tissue engineering applications using a combinatorial library of biodegradable macromers that can be crosslinked into networks.

References:

[1] Peters A, Brey DM, Burdick JA. High-throughput and Combinatorial Technologies for Tissue Engineering Applications. Tissue Engineering, Part B 2009;[Epub ahead of print].

[2] Hoogenboom R, Meier MAR, Schubert US. Combinatorial methods, automated synthesis and high-throughput screening in polymer research: Past and present. Macromolecular Rapid Communications 2003;24(1):16-32.

[3] Goldberg M, Mahon K, Anderson D. Combinatorial and rational approaches to polymer synthesis for medicine. Advanced Drug Delivery Reviews 2008;60(9):971-978.

[4] Lynn DM, Anderson DG, Putnam D, Langer R. Accelerated discovery of synthetic transfection vectors: Parallel synthesis and screening of degradable polymer library. Journal of the American Chemical Society 2001;123(33):8155-8156.

[5] Putnam D. Polymers for gene delivery across length scales. Nature Materials 2006;5(6):439-451.

[6] Anderson DG, Levenberg S, Langer R. Nanoliter-scale synthesis of arrayed biomaterials and application to human embryonic stem cells. Nature Biotechnology 2004;22(7):863-866.

[7] Anderson DG, Putnam D, Lavik EB, Mahmood TA, Langer R. Biomaterial microarrays: rapid, microscale screening of polymer-cell interaction. Biomaterials 2005;26(23):4892-4897.

[8] Anderson DG, Tweedie CA, Hossain N, Navarro SM, Brey DM, Van Vliet KJ, et al. A combinatorial library of photocrosslinkable and degradable materials. Advanced Materials 2006;18(19):2614-2618.

[9] Brocchini S, James K, Tangpasuthadol V, Kohn J. A combinatorial approach for polymer design. Journal of the American Chemical Society 1997;119(19):4553-4554.

[10] Meredith JC, Sormana JL, Keselowsky BG, Garcia AJ, Tona A, Karim A, et al. Combinatorial characterization of cell interactions with polymer surfaces. Journal of Biomedical Materials Research Part A 2003;66A(3):483-490.

[11] Yang Y, Bolikal D, Becker ML, Kohn J, Zeiger DN, Simon CG. Combinatorial polymer scaffold libraries for screening cell-biomaterial interactions in 3D. Advanced Materials 2008;20(11):2037-+.

[12] Khademhosseini A, Langer R, Borenstein J, Vacanti JP. Microscale technologies for tissue engineering and biology. Proceedings of the National Academy of Sciences of the United States of America 2006;103(8):2480-2487.

[13] Brocchini S, James K, Tangpasuthadol V, Kohn J. Structure-property correlations in a combinatorial library of degradable biomaterials. Journal of Biomedical Materials Research 1998;42(1):66-75.

[14] Abramson SD, Alexe G, Hammer PL, Kohn J. A computational approach to predicting cell growth on polymeric biomaterials. Journal of Biomedical Materials Research Part A 2005;73A(1):116-124.

[15] Gubskaya AV, Kholodovych V, Knight D, Kohn J, Welsh WJ. Prediction of fibrinogen adsorption for biodegradable polymers: Integration of molecular dynamics and surrogate modeling. Polymer 2007;48(19):5788-5801.

[16] Agrawal CM, Ray RB. Biodegradable polymeric scaffolds for musculoskeletal tissue engineering. Journal of Biomedical Materials Research 2001;55(2):141-150.

[17] Engler AJ, Sen S, Sweeney HL, Discher DE. Matrix elasticity directs stem cell lineage specification. Cell 2006;126(4):677-689.

[18] Konttinen YT, Zhao DS, Beklen A, Ma GF, Takagi M, Kivela-Rajamaki M, et al. The microenvironment around total hip replacement prostheses. Clinical Orthopaedics and Related Research 2005(430):28-38.

[19] Hubbell JA. Biomaterials in Tissue Engineering. Bio-Technology 1995;13(6):565-576.

[20] Ratner BD. A paradigm shift: biomaterials that heal. Polymer International 2007;56(10):1183-1185.

[21] Benoit DSW, Schwartz MP, Durney AR, Anseth KS. Small functional groups for controlled differentiation of hydrogel-encapsulated human mesenchymal stem cells. Nature Materials 2008;7(10):816-823.

[22] Brey DM, Erickson I, Burdick JA. Influence of macromer molecular weight and chemistry on poly(beta-amino ester) network properties and initial cell interactions. Journal of Biomedical Materials Research Part A 2008;85A(3):731-741.

[23] Brey DM, Ifkovits JL, Mozia RI, Katz JS, Burdick JA. Controlling poly(beta-amino ester) network properties through macromer branching. Acta Biomaterialia 2008;4(2):207-217.

[24] Ifkovits JL, Burdick JA. Review: Photopolymerizable and degradable biomaterials for tissue engineering applications. Tissue Engineering 2007;13(10):2369-2385.

[25] Tan AR, Ifkovits JL, Baker BM, Brey DM, Mauck RL, Burdick JA. Electrospinning of photocrosslinked and degradable fibrous scaffolds. Journal of Biomedical Materials Research Part A 2008;87A(4):1034-1043.

[26] Ifkovits JL, Padera RF, Burdick JA. Biodegradable and radically polymerized elastomers with enhanced processing capabilities. Biomedical Materials 2008;3(3).

[27] Hartman EHM, Vehof JWM, de Ruijter JE, Spauwen PHM, Jansen JA. Ectopic bone formation in rats: the importance of vascularity of the acceptor site. Biomaterials 2004;25(27):5831-5837.

[28] Chung C, Beecham M, Mauck RL, Burdick JA. The influence of degradation characteristics of hyaluronic acid hydrogels on in vitro neocartilage formation by mesenchymal stem cells. Biomaterials 2009;30(26):4287-4296.

[29] Burkoth AK, Burdick J, Anseth KS. Surface and bulk modifications to photocrosslinked polyanhydrides to control degradation behavior. Journal of Biomedical Materials Research 2000;51(3):352-359.

[30] Kakudo N, Kusumoto K, Kuro A, Ogawa Y. Effect of recombinant human fibroblast growth factor-2 on intramuscular ectopic osteoinduction by

recombinant human bone morphogenetic protein-2 in rats. Wound Repair and Regeneration 2006;14(3):336-342.

[31] Karageorgiou V, Kaplan D. Porosity of 3D biomaterial scaffolds and osteogenesis. Biomaterials 2005;26(27):5474-5491.

[32] Langer R, Vacanti JP. Tissue Engineering. Science 1993;260(5110):920-926.

[33] Hammonds RG, Schwall R, Dudley A, Berkemeier L, Lai C, Lee J, et al. Bone-Inducing Activity of Mature Bmp-2b Produced from a Hybrid Bmp-2a/2b Precursor. Molecular Endocrinology 1991;5(1):149-155.

[34] Sasano Y, Ohtani E, Narita K, Kagayama M, Murata M, Saito T, et al. Bmps Induce Direct Bone-Formation in Ectopic Sites Independent of the Endochondral Ossification Invivo. Anatomical Record 1993;236(2):373-380.

[35] Burdick JA, Frankel D, Dernell WS, Anseth KS. An initial investigation of photocurable three-dimensional lactic acid based scaffolds in a critical-sized cranial defect. Biomaterials 2003;24(9):1613-1620.

[36] Brighton CT, Hunt RM. Early histological and ultrastructural changes in medullary fracture callus. Journal of Bone and Joint Surgery 1991;73(6):832-847.

[37] Einhorn TA, O'Keefe RJ, Buckwalter JA. Orthopaedic Basic Science: Foundations of Clinical Practice. Third ed. Rosemont, IL: American Academy of Orthopaedic Surgeons, 2007.

CHAPTER 8: *Evaluation of Bone Formation in a Rat Femur Window Defect using Scaffolds from the Combinatorial Library*

8.1 Introduction

Bone is one of the most regenerative tissues in the body and is capable, unlike most tissues, of healing without the formation of scar tissue and into tissue that has many properties of healthy bone [1]. Due to this fact, bone tissue has long been a target for tissue engineering technology in applications to accelerate bone healing, induce mineralization of critically sized defects and non-unions, and for reconstructive surgery [2, 3]. Schemes for regenerating mineralized tissue for bone tissue engineering are often based on principles identified during normal bone formation and healing (e.g., scaffold structure and soluble factor delivery). During development and fracture healing, bone forms through either endochondral ossification (EO) or intramembranous ossification (IO) [1].

IO occurs in bones such as the calvaria and clavicle, and is characterized by osteoblasts that directly form bone matrix [1, 4]. The growth occurs from the center and grows outward between the bone and the periosteum. Conversely, EO occurs in long bones, and is distinguished by the formation first of cartilage. This cartilage then becomes hypertrophic and mineralizes, which then is used as a template for osteoblasts as they infiltrate and form bone tissue. This process is typical of long bone formation embryologically, as well as at the growth plate of children as they grow. In the end, the

final product of either process is histologically similar mineralized tissue, even though they arrive by very different steps [1].

Naturally, most fractures in bones heal through a combination of IO or EO. After a break, there is an inflammatory phase in which macrophages release several cytokines to recruit osteoprogenitor cells to localize, proliferate, and begin to differentiate [1, 4] and new vasculature begins to form. This stage is followed by the formation of a fibrous callus for stabilization and the formation of vasculature at the fracture site during the reparative phase. This callus hardens with time into a bony callus as mineralization produces woven bone. Finally, the remodeling phase replaces the woven bone with lamellar bone and the callus is resorbed [4, 5].

The type of ossification that dominates a fracture depends on the fixation and movement at the fracture site [4-9]. In cases where the fracture is rigidly fixed, such as the use of plates and nails, IO is likely the main process of mineralization. The stable surroundings of the callus allow for the direct production of bone matrix since there is no strain on the newly formed structures [7]. In contrast, if fracture sites are allotted some movement, such as in casting, then the dominant form of bone formation is through EO. The cartilage forms a more flexible environment that is slowly strengthened as the matrix is calcified and osteoblasts then further remodel the bone and mineralize [8].

In tissue engineering paradigms, there are several other factors that can drive bone regeneration, and these strategies can influence the type of ossification that occurs. In a study by Tortelli, et al [10], when porous ceramic scaffolds were seeded with MSCs an EO process took place; however, IO occurred when these same scaffolds were seeded with mature osteoblasts. In scaffolds that deliver BMPs and other growth factors, results

have been mixed. In cellular laden implants that released both BMP and VEGF, bone was formed via EO [9, 11, 12], while the release of BMP-2 from acellular therapies found evidence of both IO and EO [13, 14]. Similarly, pore geometry influenced the path of bone formation [9, 14], with larger, more interconnected pores, which allows for a better flow of nutrients that prefers direct bone formation. When the pores were smaller or the diffusion of nutrients was impeded, there was usually the formation of cartilage first.

Several small animal models exist for evaluating bone regeneration paradigms. One common method is the use of a critical-sized cranial defect which creates a large defect in the calvaria of rats (8 mm) or mice (4-6 mm) [15-21] (as presented in Chapter 7). Calvarial defects are convenient since they are not a load-bearing bone and therefore require no external fixation and there is a large surface area to assess. Some of the difficulties include the proximity to the brain that increases risks during surgery and there are conflicting reports of whether the mineralization is through EO [20] or IO [18, 20]. For surgeries using long bones, segmental defects are the most common [11, 22-24]. These models usually involve a critical-sized (>5 mm) section of long bone that is removed, usually the femur [11, 22, 24], although the model has been performed with the radius. The long bone model is associated with EO [11, 22, 24], but requires fixation, which adds to the complexity of the model.

Previous studies by our lab (see Chapter 7) have involved a critical-sized cranial defect model to study bone regeneration with a poly(β-amino ester) scaffold [16] and IO appeared to be the process of bone formation. An alternate animal model was used in this study, namely a rat femur window model [25], to investigate bone healing in a long bone, which develops through EO. These bones are load-bearing, so for this study, rather than

remove an entire cylinder of the bone, a window was cut into the bone shaft, still allowing the remaining bone to function. Upon euthanasia of the animal, the femur was excised and imaged using contact radiographs and μCT, processed histologically, and tested mechanically.

8.2 Materials and Methods

8.2.1 Polymer synthesis and scaffold fabrication

PBAEs were synthesized as described previously [26] (Figure 8.1A, see previous Chapters). To form the A6 macromer, isobutylamine (Sigma) and diethylene glycol diacrylate (Scientific Polymer Products) were mixed together in a molar ratio of 1.2:1, respectively, overnight at 90°C. The reaction scheme and monomers used are shown in Figure 8.1 and the sample notation is from the original study on the library development [26]. The macromers were characterized with proton nuclear magnetic resonance (^{1}H NMR, Bruker DMX360, 360 MHz) and were determined to be ~2000 Da. The photoinitiator 2,2-dimethoxy-2-phenyl acetophenone (DMPA, Sigma) was added to the liquid macromers at a final concentration of 0.5% (w/w). The viscous macromer solutions were then used to fabricate macroporous scaffolds.

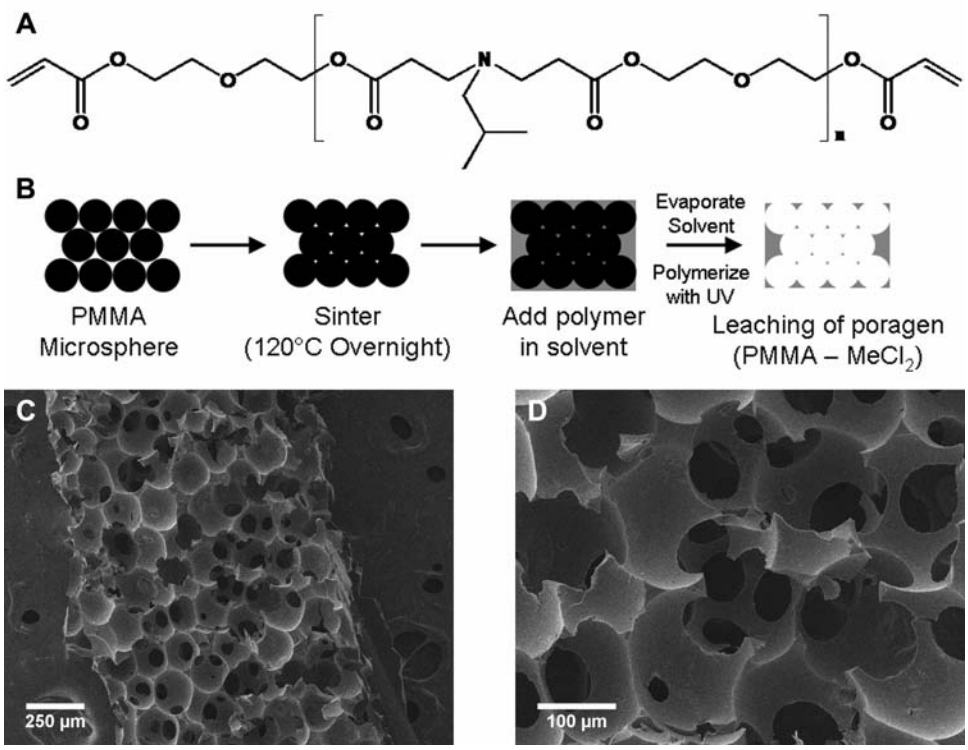

Figure 8.1 (A) A previously identified osteoconductive PBAE, A6, is used to make (B) porous scaffolds using a poragen leaching technique. The scaffolds (C,D) produced this way are shown to be highly porous with a high amount of interconnectivity.

Porous scaffolds were fabricated using previously developed techniques of sintered poly(methyl methacrylate) (PMMA) microbeads [27, 28] as shown in Figure 8.1B. For spherical porosity, PMMA microbeads (200 µm, Polysciences) were packed into teflon molds, clamped between glass slides, and placed in an oven at 120°C for 22 hours. The glassy top layer was then scraped away, and the voids between the sintered spheres were filled with macromer/DMPA solutions. The constructs were crosslinked with ultraviolet light exposure (~10 mW/cm^2, 365 nm, 10 min, Blak-Ray B-100 AP) between glass slides, the PMMA was removed with several washes in methylene

chloride, and the methylene chloride was removed with several washes in water. Samples were then frozen and lyophilized before SEM analysis. These scaffolds were cut to defect size (6.5 mm x 1.2 mm x 1.5 mm) and a small amount (21 μL) of 3% collagen (Inamed Biomaterials) was added into the pores either alone or loaded with 500 ng of rhBMP-2 (R&D systems). The collagen solution was allowed to gel at 37ºC for 1.5 h and the scaffolds were frozen and lyophilized for implantation.

8.2.2 Femur window defect

NIH guidelines for the care and use of laboratory animals (NIH Publication #85-23 Rev. 1985) were observed. A bilateral surgical approach was made to the anterolateral, femoral diaphysis of Fisher 344 rats (Charles River Laboratories International, 325–400 g) [25]. A large, oblong unicortical window defect, measuring 1.2 mm in width and 6.5 mm in length, was created in each femur using a 1.6 mm fissure burr (Small battery drive, Synthes) as shown in Figure 8.2. The defect was then left empty or filled with a porous A6 scaffold with or without BMP-2 by an interference fit. No external or internal limb fixation devices were used postoperatively and animals were allowed to function without restriction immediately following surgery. The operated femora were dissected at 3 (n = 5 femora/group) and 10 (n = 10 femora/group) weeks postoperatively. At 3 weeks, all samples were scanned for μCT, and 3 samples/group were fixed in formalin, decalcified in 10% EDTA, and processed for histology. For samples at 10 week, all samples were scanned for μCT, 3 samples/group were fixed in formalin, decalcified in 10% EDTA, and processed for histology. Meanwhile the remaining samples were not fixed and reserved for mechanical testing.

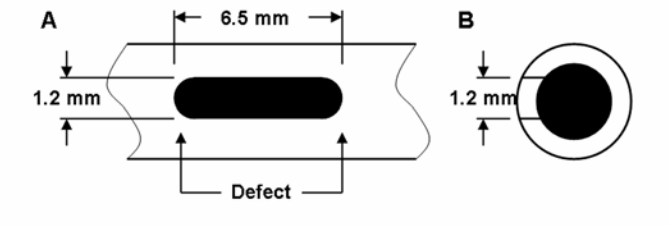

Figure 8.2 View of unicortical femur window defect from (A) the side and (B) a cross-section. This defect requires no fixation and will normally heal on its own with time.

8.2.3 Micro computed tomography

For μCT scanning, all specimens were kept moist, wrapped in saline saturated gauze, and stored in air tight containers at -20°C until scanned. Cortical zones of the femora were scanned using a VivaCT40 μCT scanner (Scanco) with X-ray acquisition settings set at 55 kVp and 145 mA with an integration time of 200 ms. Scans were performed with an isotropic voxel size of 10.5 μm and images were reconstructed in 1,024 x 1,024 pixel matrices. A lower threshold of 697.4 mg of HA/cm^3 and an upper threshold of 2000 mg of HA/cm^3 were determined by visual inspection to best distinguish between bone and non-bone material. Scanco software was used to calculate the average density of the new bone, the bone volume, and total volume of the defect.

8.2.4 Mechanical testing

After μCT scanning, all specimens were kept moist, wrapped in saline saturated gauze, and stored in air tight containers at -20°C until the day of testing. On the day of testing, femora were then mounted in a specially designed jig that ensured proper

alignment, leaving a 1.5 cm length of the diaphysis subject to mechanical testing. This jig was designed to convert translational displacement to angular displacement using an Instron hydraulic materials testing machine (model #1321). Each femur was tested in torsion at 239°/min until failure. Load-displacement curves were continuously recorded. Ultimate torque (N-m), stiffness (N-m/deg), and angle of deformation to failure (deg) were calculated.

8.2.5 Histology

Samples were then decalcified in 10% EDTA for 3 weeks, dehydrated, and then mounted in paraffin wax for histology. Samples were processed using standard techniques for hematoxylin and eosin staining. Images were acquired with an upright microscope (Olympus BX-51, with Olympus DP2-BSW software).

8.2.6 Statistical analysis

Statistical analysis was performed using ANOVA with Tukey's post-hoc among the groups with significance defined as a confidence level of 0.05. All values are reported as the mean and the standard deviation of the mean.

8.3 Results and Discussion

8.3.1 Scaffold fabrication

Scaffolds were produced using a poragen leaching method of sintered PMMA microspheres (Figure 8.1B). An advantage of using free radical polymerization is the control over the polymerization process for a range of scaffold fabrication processes. In

this case, a liquid monomer with photoinitiator was able to fill the void space of the sintered microspheres and was then crosslinked in a mold to create a negative of the PMMA structure. This technique allows for great control over the pore size by altering the size of the poragen. The sintering allows for the microspheres to fuse together and to form interconnected pores in the PBAE scaffolds (Figure 8.1C and D). The size and extent of the interconnectivity can be varied by altering the temperature or time of the sintering. Both pore size and connectivity are important to osteogenesis *in vivo* in allowing cells, nutrients, and capillaries to infiltrate the entire scaffold [14]. In this work, a uniform scaffold was used for all studies that had a pore size of 200 μm and was fabricated out of the A6 material that was deemed cytocompatible and osteoconductive (see Chapter 7).

8.3.2 Three week femur window healing

The femur window defect was created by drilling a unicortical hole through the femur of a rat. Since an entire segment of bone was not removed, no external fixation was required. However, the defect is not of a critical size so there is healing that occurs in the bone, even without treatment. Yet, the goal was to illustrate the potential of the porous scaffolds to heal bone in an alternative model to the cranial defect.

At 3 weeks, the rat femur defects were still visible by inspection during excision of the femur. The samples were first scanned using μCT to inspect the formation of bone throughout the wound and scaffold. Three dimensional renderings of the cortical femurs are shown in Figure 8.3A. The healing in the Empty and A6 with BMP-2 groups appear to span the entire wound, with new bone formed that looks similar to trabecular bone and

is almost even with the surface of the original bone. However, the A6 without BMP-2 shows very little new bone growth within the defect. The cross sections in the same figure show similar results with both the Empty and A6 with BMP-2 groups showing bone growth in the defect, but also some bone growth within the medullary canal, unlike the center of the no surgery control. In the A6 without BMP-2 group, there is some bone growth around the defect, but there is limited mineralization at the defect site.

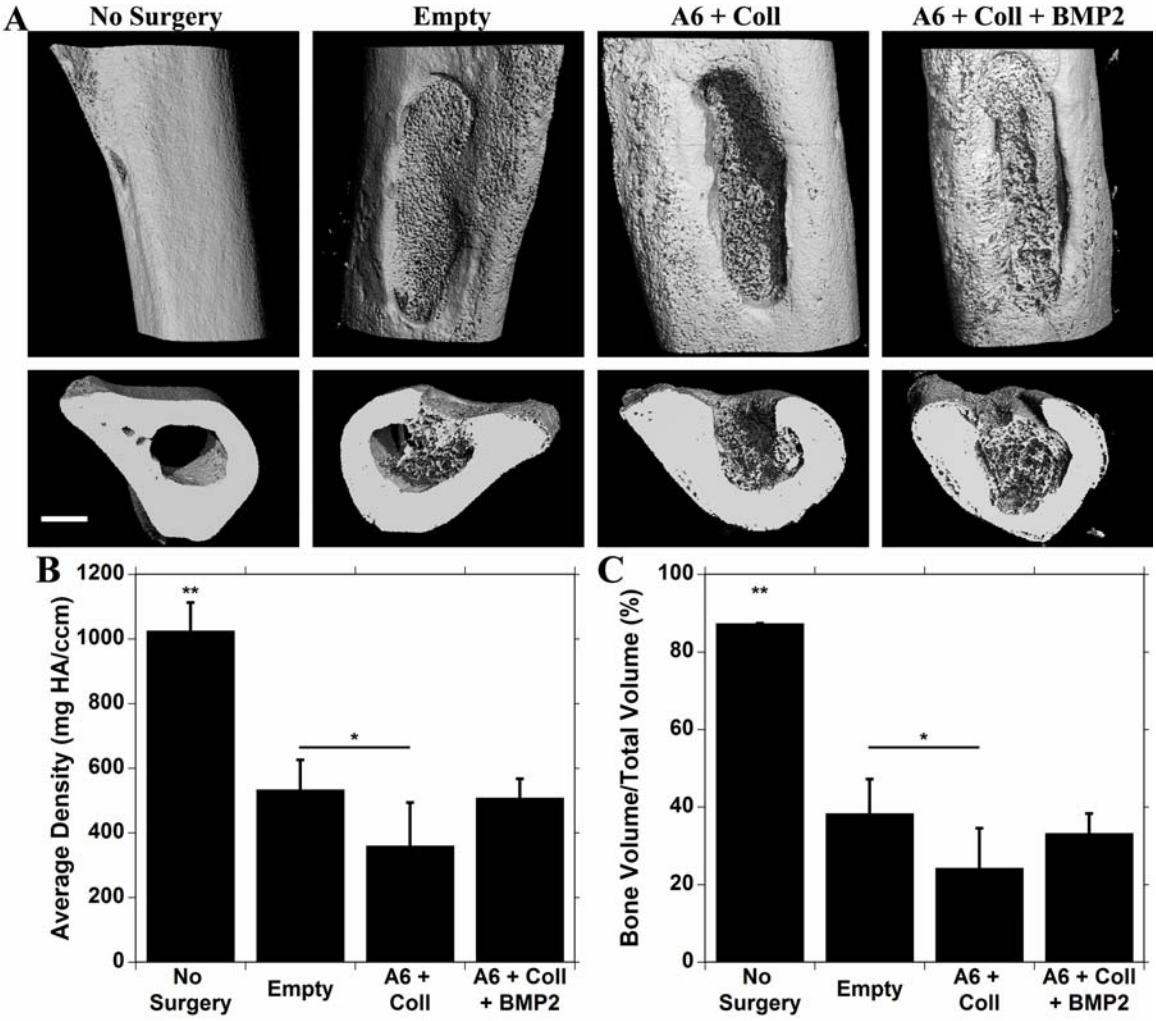

Figure 8.3 MicroCT data of implants 3 weeks post sugery. (A) MicroCT created 3D images of femurs and cross-sections for each of the four groups tested , as well as (B) the average density of the new bone and (C) the ratio of bone volume to total volume of the defect region. (* denotes significant difference from A6 + Coll, ** denotes significance from all groups)

The average density of the tissue in the defect region is shown in Figure 8.3B. The density for the Empty and A6 with BMP-2 were similar and roughly 50% of the value for intact bone. There was a significant difference between the Empty and A6

without BMP-2, but not between the A6 with and without BMP-2 groups. This was the same for the percentage of bone volume over the total volume of the wound (Figure 8.3C), and these results were similar to the average density results.

The histology of the samples shows that in all surgical cases the bone that forms is accompanied by fibrous tissue growth as well (Figure 8.4). The A6 without BMP-2 groups shows some bone growth deep inside the scaffold, but at the surface, there is mostly fibrous tissue. The Empty healing looks similar to the healing in the A6 with BMP-2 group with branched bone formation throughout the defect. Both are also accompanied with bone growth within the medullary canal, and the bone growth for the A6 scaffold without BMP-2 appears to initiate at the center. This could be due to the large number of stem cells that are present in the bone marrow that are recruited to differentiate by the cytokines that are released due to the formation of the injury and the BMP-2 released from the scaffold. Presumably this bone will be resorbed as the wound heals and this bone is no longer carrying any load.

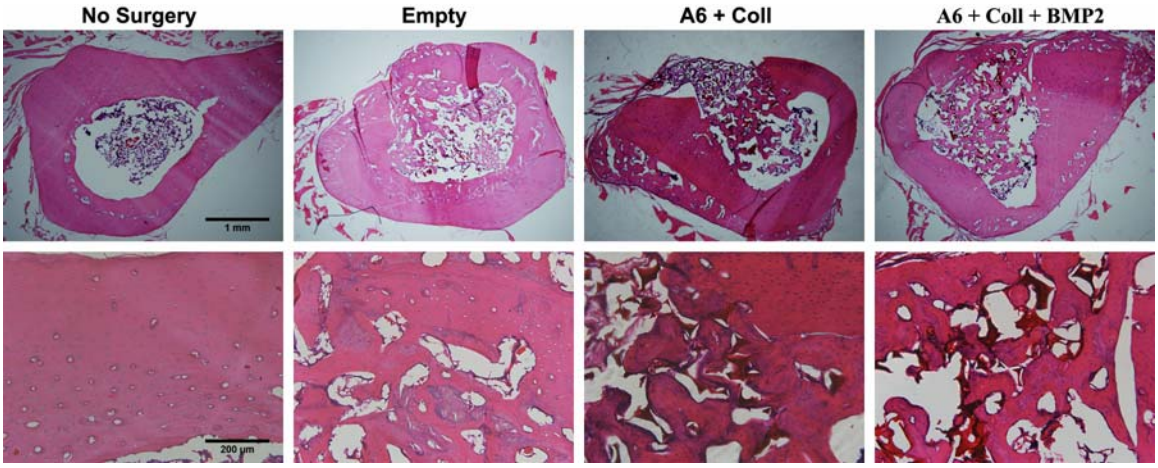

Figure 8.4 H & E staining of femurs 3 weeks after surgery at 4x (top row) and 20x (bottom row) for all four groups.

8.3.3 Ten week femur window healing

At 10 weeks, the defects in the Empty and A6 with BMP-2 groups were difficult to determine upon macroscopic inspection. The µCT scans revealed that new bone had grown to the surface in these cases to where they were nearly flush with the surrounding uninjured bone (Figure 8.5A). The A6 scaffold without BMP-2 demonstrated more bone growth than at 3 weeks, but the healing was clearly lagging to the other groups. Cross sections of the µCT scans reveal that the growth within the medullary canal was now largely central to the wound area. For the A6 scaffold without BMP-2, there may be some thickening of the uninjured cortical bone. The average quantity (mg) of hydroxyapatite per cm^3 (Figure 8.5B) for the Empty and A6 with BMP-2 cases were greater than 80% of intact bone (850.8 ± 50.7 and 800.7 ± 43.3, respectively), and both were significantly greater than the A6 without BMP-2 (636.9 ± 92.3). The same results were observed in the bone volume to the total volume of the defect (Figure 8.5C).

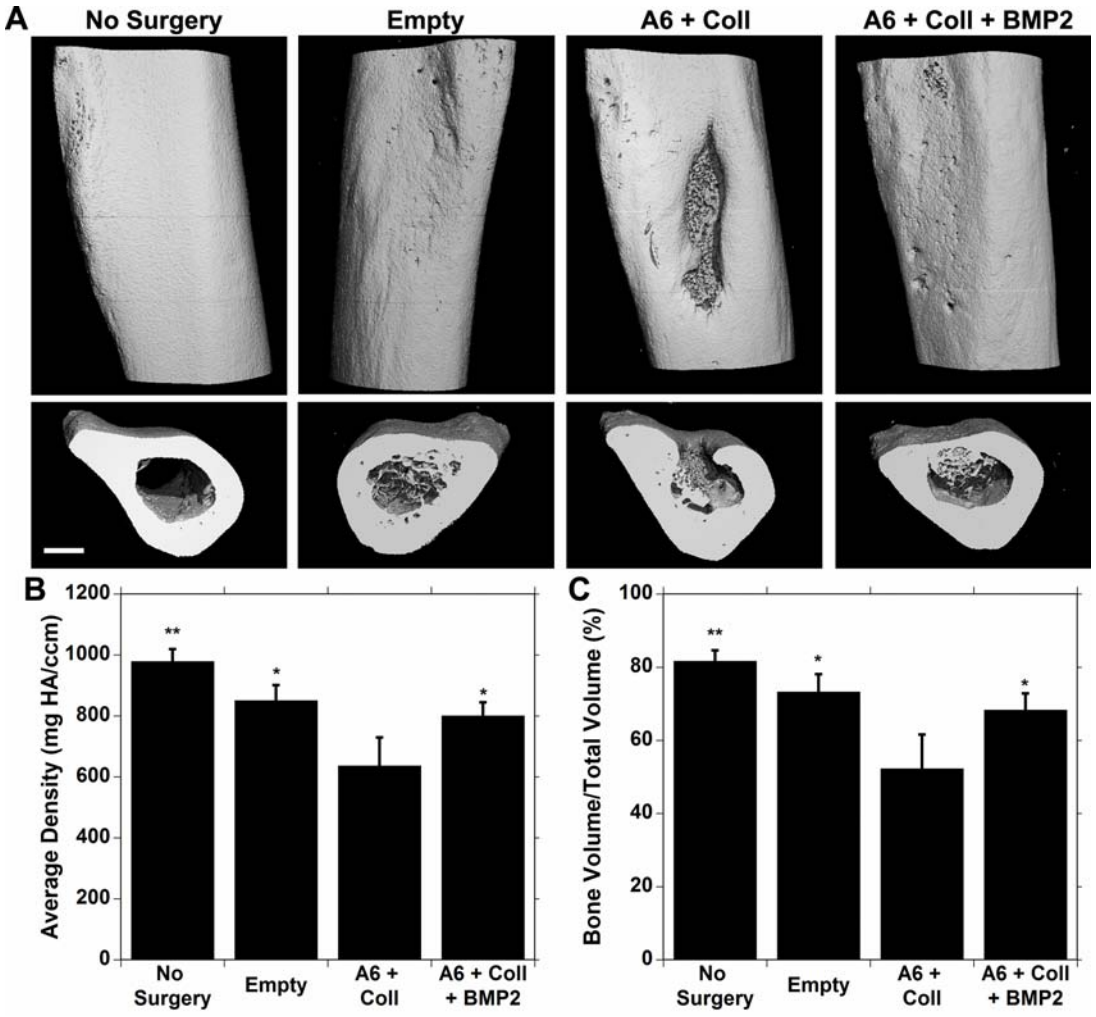

Figure 8.5 μCT data of implants 10 weeks post-surgery. (A) μCT created 3D images of femurs and cross-sections for each of the four groups tested , as well as (B) the average density of the new bone and (C) the ratio of bone volume to total volume of the defect region. (* denotes significant difference from A6 + Coll, ** denotes significance from all groups)

The samples at 10 weeks were tested in torsion using a jig to convert axial displacement to rotational strain on the bone (Figure 8.6). The apparent stiffness of the

bone shaft was calculated as the slope of the torque against the angle of deformation, and there was wide variability between the samples in this study (Figure 8.6A). There was no apparent trend and no significant differences between the groups. The angle turned by the bone at fracture also showed much variation, and again no significant differences between groups were observed (Figure 8.6B). In this case, intact bone was anticipated to be significantly lower, due to the brittleness of the bone, while the window defect allow for more flexibility of the bone in torsion. While the bone with no surgery was lower on average than all other groups, this difference was not significant. The amount of healing at 10 weeks likely prevented this effect from being apparent. Finally, the ultimate torque at failure was calculated, and this too showed no significant differences between the groups (Figure 8.6C). The lack of difference was likely due to the sample to sample variability, as well as the extensive healing at 10 weeks that was already completed. Perhaps mechanics at earlier time points would demonstrate more separation between the groups.

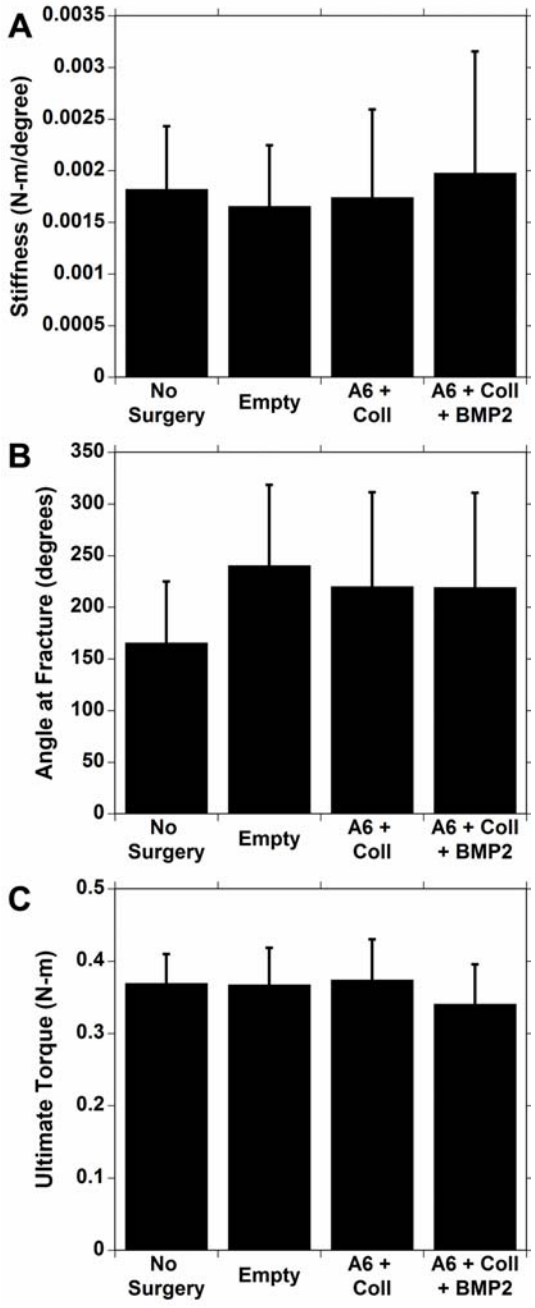

Figure 8.6 Mechanical data on femurs tested in torsion 10 weeks after surgery, showing the (A) stiffness of the femurs, (B) the angle of the bending femur at fracture, and (C) the ultimate torque reached before failure.

The histology showed substantial bone growth at the defect for the Empty defect and the A6 with BMP-2, but the healing in the Empty defect is more continuous at this point like normal bone. The A6 scaffold without BMP-2 has some bone growth, but the defect still has fibrous tissue at the outer edge. The new bone formed in both A6 scaffolds appears more like trabecular bone, likely due to the porous nature of the scaffold which was not completely degraded at this point. Interestingly, there is substantial thickening of the cortical bone into the medullary, which is especially apparent in the Empty group. This could be due to the new bone growth observed at 3 weeks growing into the rest of the bone, which likely is also aided in carrying the extra load until the defect is healed. This explains why bone volume, as calculated by μCT, did not show any significant difference between groups, even though there were differences in BV/TV and average density. This thickening may also explain why there were not clear differences in mechanical properties of the different groups.

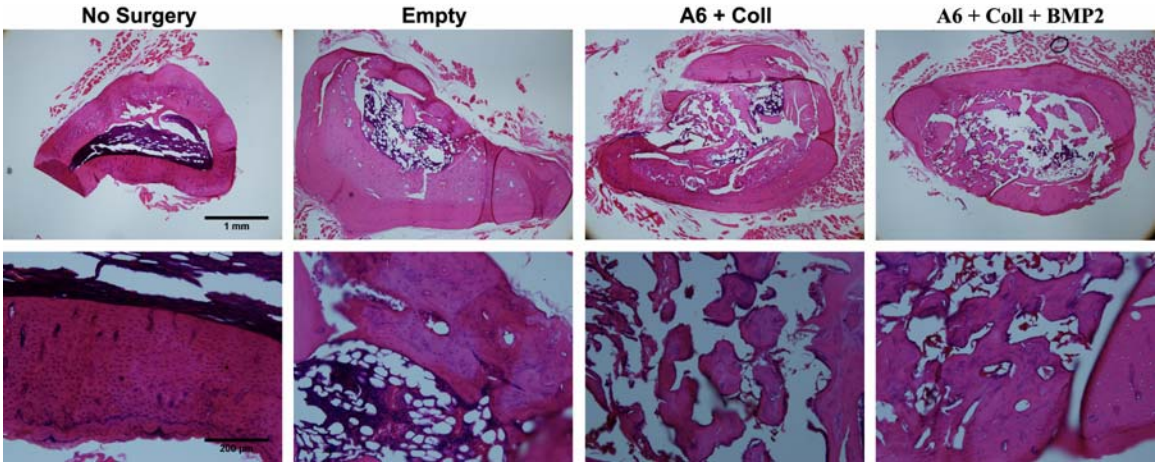

Figure 8.7 H & E staining of femurs 10 weeks after surgery at 4x (top row) and 20x (bottom row) for all four groups.

From the H&E staining, there is no clear evidence that the bone is being formed through EO. Distinct shapes and forms of hypertrophic cartilage was not apparent in the histology of any of these groups. The 10 week time point is likely too late to catch the EO phase if it occurs, but the 3 week results should be short enough to capture the intermediate chondrocyte phase [11-13]. The reasons could be due to the structure of the scaffolding used, as higher porosity and larger pores have been linked to direct bone formation [14]. Previous usage of this model investigated scaffolds that had large pores (200-300 μm), but very low porosity (21%) [25]. The lower porosity often leads to reduced flow of nutrients or formation of capillaries, which often helps trigger chondrocyte hypertrophy [14].

The bone regeneration of the A6 scaffold with BMP-2 was better than the case of A6 scaffold alone, but there was no separation from the natural healing of the Empty defect. In fact, at 10 weeks the bone in the Empty defect was more continuous like the non-surgical controls. The bone formed in the A6 scaffolds looks to have formed in the original pores of the scaffold, and may actually be impeded from forming more continuous bone until the scaffold completely degrades. The presence of additional cells in the area does not accelerate degradation because it is hydrolytically degradable. These results highlight the ability of 3-dimensional scaffolds to template bone tissue formation and limitations in the use of a non-critical sized defect model for comparisons.

One of the original design criteria for the A6 material was for a material that degraded in 3-5 months to be used in a critical-sized cranial defect. In a critical-sized situation, there is only fibrous healing of the defect, so a slower degrading scaffold can

both impede the infiltration of a fibrous scar as well as provide a stable platform for the proliferation of cells and production of mineralized matrix. In this application, the A6 scaffold load with BMP-2 demonstrated substantially improved bone formation over the other groups. In this non-critical-sized defect, the body can naturally form the needed matrix, so perhaps the materials should be faster degrading, or able to be degraded by the cells as needed. A better test for this polymer may be a segmental defect which is decidedly more surgically complex as it requires fixation, but it has been linked to the EO. This particular model would likely be better to test at shorter time periods to investigate methods for rapid healing improvements.

8.4 Conclusions

Highly porous scaffolds were produced via a poragen leaching technique for use in a rat femur window defect. Three tested groups of empty defects, A6 scaffolds without BMP-2, and A6 scaffolds with BMP-2 were implanted in the window to investigate extent of bone regeneration, using histology, imaging techniques, and mechanical testing. Throughout the study, the empty scaffolds performed better than the A6 scaffold without BMP-2, and were equivalent to the A6 scaffold with BMP-2. Also, there was no significant improvement of mechanics between any of the groups. For the case of a non-critical-sized defect, there is no evidence that this treatment improves bone regeneration compared to natural healing.

References:

[1] Einhorn TA, O'Keefe RJ, Buckwalter JA. Orthopaedic Basic Science: Foundations of Clinical Practice. Third ed. Rosemont, IL: American Academy of Orthopaedic Surgeons, 2007.

[2] Kneser U, Schaefer DJ, Munder B, Klemt C, Andree C, Stark GB. Tissue engineering of bone. Minimally Invasive Therapy & Allied Technologies 2002;11(3):107-116.

[3] Laurencin CT, Ambrosio AMA, Borden MD, Cooper JA. Tissue engineering: Orthopedic applications. Annual Review of Biomedical Engineering 1999;1:19-46.

[4] Lieberman JR, Friedlander GE. Bone regeneration and repair : biology and clinical applications. Totowa, N.J.: Humana Press, 2005.

[5] Bucholz RW, Heckman JD, Court-Brown CM. Rockwood and Green's fractures in adults. 6th ed. Philadelphia, PA: Lippincott Williams & Wilkins, 2006.

[6] Brighton CT, Hunt RM. Early histological and ultrastructural changes in medullary fracture callus. Journal of Bone and Joint Surgery 1991;73(6):832-847.

[7] Dimitriou R, Tsiridis E, Giannoudis PV. Current concepts of molecular aspects of bone healing. Injury-International Journal of the Care of the Injured 2005;36(12):1392-1404.

[8] Ferguson C, Alpern E, Miclau T, Helms JA. Does adult fracture repair recapitulate embryonic skeletal formation? Mechanisms of Development 1999;87(1-2):57-66.

[9] Sundelacruz S, Kaplan DL. Stem cell- and scaffold-based tissue engineering approaches to osteochondral regenerative medicine. Seminars in Cell & Developmental Biology 2009;20(6):646-655.

[10] Tortelli F, Tasso R, Loiacono F, Cancedda R. The development of tissue-engineered bone of different origin through endochondral and intramembranous ossification following the implantation of mesenchymal stem cells and osteoblasts in a murine model. Biomaterials;31(2):242-249.

[11] Kanczler JM, Ginty PJ, White L, Clarke NMP, Howdle SM, Shakesheff KM, et al. The effect of the delivery of vascular endothelial growth factor and bone morphogenic protein-2 to osteoprogenitor cell populations on bone formation. Biomaterials;31(6):1242-1250.

[12] Li GH, Corsi-Payne K, Zheng B, Usas A, Peng HR, Huard J. The Dose of Growth Factors Influences the Synergistic Effect of Vascular Endothelial Growth Factor on Bone Morphogenetic Protein 4-Induced Ectopic Bone Formation. Tissue Engineering Part A 2009;15(8):2123-2133.

[13] Hou LT, Liu CM, Liu BY, Chang PC, Chen MH, Ho MH, et al. Tissue engineering bone formation in novel recombinant human bone morphogenic protein 2-atelocollagen composite scaffolds. Journal of Periodontology 2007;78(2):335-343.

[14] Karageorgiou V, Kaplan D. Porosity of 3D biomaterial scaffolds and osteogenesis. Biomaterials 2005;26(27):5474-5491.

[15] Advani S, LaFrancis D, Bogdanovic E, Taxel P, Raisz LG, Kream BE. Dexamethasone suppresses in vivo levels of bone collagen synthesis in neonatal mice. Bone 1997;20(1):41-46.

[16] Brey DM, Chung C, Hankenson KD, Garino JP, Burdick JA. Identification of osteoconductive and biodegradable polymers from a combinatorial polymer library. Journal of Biomedical Materials Research Part A 2010;93A(2):807-816.

[17] Burdick JA, Anseth KS. Photoencapsulation of osteoblasts in injectable RGD-modified PEG hydrogels for bone tissue engineering. Biomaterials 2002;23(22):4315-4323.

[18] Huang YC, Simmons C, Kaigler D, Rice KG, Mooney DJ. Bone regeneration in a rat cranial defect with delivery of PEI-condensed plasmid DNA encoding for bone morphogenetic protein-4 (BMP-4). Gene Therapy 2005;12(5):418-426.

[19] Meinel L, Fajardo R, Hofmann S, Langer R, Chen J, Snyder B, et al. Silk implants for the healing of critical size bone defects. Bone 2005;37(5):688-698.

[20] Peng HR, Usas A, Olshanski A, Ho AM, Gearhart B, Cooper GM, et al. VEGF improves, whereas sFlt1 inhibits, BMP2-induced bone formation and bone healing through modulation of angiogenesis. Journal of Bone and Mineral Research 2005;20(11):2017-2027.

[21] Winn SR, Schmitt JM, Buck D, Hu YH, Grainger D, Hollinger JO. Tissue-engineered bone biomimetic to regenerate calvarial critical-sized defects in athymic rats. Journal of Biomedical Materials Research 1999;45(4):414-421.

[22] Yasko AW, Lane JM, Fellinger EJ, Rosen V, Wozney JM, Wang EA. The Healing of Segmental Bone Defects, Induced by Recombinant Human Bone

Morphogenetic Protein (Rhbmp-2) - a Radiographic, Histological, and Biomechanical Study in Rats. Journal of Bone and Joint Surgery-American Volume 1992;74A(5):659-670.

[23] Geiger F, Bertram H, Berger I, Lorenz H, Wall O, Eckhardt C, et al. Vascular endothelial growth factor gene-activated matrix (VEGF(165)-GAM) enhances osteogenesis and angiogenesis in large segmental bone defects. Journal of Bone and Mineral Research 2005;20(11):2028-2035.

[24] Fang JM, Zhu YY, Smiley E, Bonadio J, Rouleau JP, Goldstein SA, et al. Stimulation of new bone formation by direct transfer of osteogenic plasmid genes. Proceedings of the National Academy of Sciences of the United States of America 1996;93(12):5753-5758.

[25] Livingston T, Ducheyne P, Garino J. In vivo evaluation of a bioactive scaffold for bone tissue engineering. Journal of Biomedical Materials Research 2002;62(1):1-13.

[26] Anderson DG, Tweedie CA, Hossain N, Navarro SM, Brey DM, Van Vliet KJ, et al. A combinatorial library of photocrosslinkable and degradable materials. Advanced Materials 2006;18(19):2614-2618.

[27] Brey DM, Ifkovits JL, Mozia RI, Katz JS, Burdick JA. Controlling poly(beta-amino ester) network properties through macromer branching. Acta Biomaterialia 2008;4(2):207-217.

[28] Bryant SJ, Cuy JL, Hauch KD, Ratner BD. Photo-patterning of porous hydrogels for tissue engineering. Biomaterials 2007;28(19):2978-2986.

CHAPTER 9: *High-throughput Screening of a Small Molecule Library for Promoters and Inhibitors of Mesenchymal Stem Cell Osteogenic Differentiation*

9.1 Introduction

As research has expanded toward the application of stem cells as a cell source for tissue regeneration and cell replacement therapies, the importance of driving differentiation and cell behavior in a controlled fashion has increased. Human mesenchymal stem cells (hMSCs) are readily available adult stem cells that have been investigated extensively in recent years as an autologous cell source. hMSCs have been shown to differentiate along chondrogenic [1-3], adipogenic [4, 5], osteogenic [4-10], and neuronal [11-13] lineages when provided the right chemical or physical cues. Physical cues may include mechanical stiffness of the surrounding matrix [9], the presentation of functional groups in the encapsulating cell environment [4], or even the shape of the cell [14]. These are important signals that maybe incorporated into scaffold design for regenerative medicine to obtain specific differentiation paths by interacted on delivered cells.

The assessment of the proper chemical cues has also been extensively investigated, and can be divided between the use of either growth factors or the use of small molecules. Growth factors can naturally drive cell differentiation, such as during development and wound repair, through interactions with cell receptors and via cell signaling cascades. For example, transforming growth factor beta (TGF-β) is crucial for

the chondrogenic differentiation of MSCs [1, 3], while combinations of basic fibroblast growth factor, epidermal growth factor, and platelet-derived growth factor may lead to neuronal differentiation [11].

Bone morphogenetic proteins (BMPs) have been important drivers of osteogenic differentiation [15, 16]. Of the many variations in the BMP family, the use of BMP-2, -4, and -7 have all been shown to stimulate osteoblast markers in osteoprogenitor cells [17-20]. However, this effect appears mitigated when explored in human MSCs [16, 19, 21-23]. Similarly, while BMPs have shown great bone growth in rat and rabbit models [7, 15, 24-29], there has only been limited success in human clinical studies [30, 31], which often require large quantities of expensive proteins for even modest improvements. BMP-6 has also been shown to drive osteogenic differentiation of hMSCs [16, 22, 32] *in vitro* as well as in animal models, though these treatments have not progressed to any reported human clinical trials.

These limitations have directed many researchers to the identification of small molecules as osteogenic promoters [6, 8, 33]. In particular, dexamethasone (Dex) is commonly used for *in vitro* cell studies. Dex is a synthetic glucocorticoid, often used as an anti-inflammatory drug and in cancer treatments, but in 2D culture has acted as a potent osteopromoter. Dex has been shown to induce osteogenic differentiation in MSCs, pericytes, bovine vascular smooth muscle cells, and mouse NIH3T3 fibroblasts [34]. Several studies have shown optimal Dex concentrations to be between 10-100 nM [8, 35-38] in the presence of 5-10 mM beta-glycerol phosphate (βGP) and ascorbic acid (or ascorbic acid-2-phosphate, AA2P). Our lab has previously used a formulation of 10 nM

dexamethasone, 10 mM βGP, and 25 μg/mL AA2P to drive robust MSC osteogenic differentiation [7].

Unfortunately, these osteogenic effects studied *in vitro* have not translated into clinical practice. First, while Dex, like many glucocorticoids, are potent anti-inflammatories, prolonged treatment can actually lead to osteoporosis [39-42]. This is suspected to be due to the suppression of the proliferation of osteoblastic precursors, which allows osteoclasts to break down bone without subsequent replacement with new bone [42]. Next, intramuscular injections of Dex at the site of a spinal fusion actually inhibited bone graft incorporation [40]. Finally, while there has been some success with implanted Dex releasing, hMSC-seeded scaffolds [43, 44], this technique of delivery adds a level of clinical complexity, cost, and time that could be better avoided if native progenitor cells could be recruited and differentiated *in situ*.

While tissue engineering investigates ways to stimulate tissue formation, there are some diseases where the prevention of differentiation and matrix may be desired. In the case of bone, progenitor cells have been found to form heterotopic bone in models for fibrodysplasia ossificans progressiva (FOP) [45]. This disease is caused by a mutation to a BMP receptor, ACVR1, that causes connective tissues to spontaneously form bone [46]. Interestingly, Dex has also been implicated in stimulating osteogenic differentiation of pericytes that can lead to the formation of vascular calcification present in many cardiovascular diseases [34]. Therefore, new therapies to inhibit progenitor cells from differentiating into osteoblasts could be beneficial for common cardiovascular diseases, as well as rare skeletal disorders.

These limitations of Dex and the high cost and limited effectiveness of BMP therapy motivates the need for the identification of alternative factors that stimulate osteogenic differentiation, as well as the need that exists for molecules that may inhibit osteogenesis. Little effort has been made to identify new soluble factors for their osteogenic potential in stem cells [6]; however, high-throughput screening (HTS) tools and techniques are being developed to explore large libraries of materials for a variety of applications [1, 33, 47-49]. Traditional techniques to identify molecules for stem cell differentiation have often relied on a small number of molecules and limited combinations of factors. This is due to the time, cost, and complexity of these combinations and assessment of outcomes. The advantages of HTS methods allows for more combinations to be assessed faster, and with fewer reagents, so that new compounds can be discovered and more complex delivery schemes can be tested.

In this study, we developed techniques for the assessment of a library of soluble factors for promoters and inhibitors of the osteogenic differentiation of MSCs using HTS tools. Hits were identified using statistical relationships to controls, as well as meeting criteria related to viability. Towards our interests in tissue engineering, promoters were then screened further to confirm these effects using traditional cell culture techniques. The most promising of these factors were then tested in conjunction with a previously identified osteoconductive poly(β-amino ester), A6 (see Chapter 7), for potential future use *in vivo* [7].

9.2 Materials and Methods

9.2.1 HTS assay development

Human MSCs (Lonza) were cultured in growth media (αMEM, 17% fetal bovine serum, 1% penicillin/streptomycin, 1% l-glutamine) and plated onto 384 well, flat bottom plates (Corning) at passage 3 or 4 in 40 µl of media per well using a microplate dispenser (Matrix Wellmate, Thermo Scientific). Plates were sealed with Breath-Easy gas permeable membranes (Research Products International Corp) to minimize evaporative losses. The following day, media was changed to incomplete osteogenic media (OG-, growth media plus 10 mM β-glycerol phosphate and 25 µg/mL ascorbic acid-2-phosphate) or complete osteogenic media (OG+, OG- plus 10 nM dexamethasone), depending on the goal of identifying either promoters or inhibitors.

After 7 days of culture, 4 µl of Alamar Blue was added to each well and the fluorescence was measured (535 nm excitation/595 nm emission, EnVision, Perkin Elmer) after incubation for 15 and 30 minutes. Cells were then washed with PBS, and lysed in the wells with 5 µl of CelLytic M (Sigma) at 37° C for 15 minutes. Plates were cooled for 5 minutes on ice before the addition of 45 µl of the fluorescent ALP detection reagents (40 µl fluorescent buffer, 5 µl dilution buffer, 0.25 µl 4-Methylumbelliferyl phosphate disodium salt, APF, Sigma). Plates were then read every 10 minutes for 1 hour at 355 nm excitation/450 nm emission to determine ALP activity.

Various aspects of this protocol were optimized prior to the library screening. These included the timing of media change (no change for the entire 7 days versus changing once after 4 days), the cell seeding density (24, 18, 12, and 6 thousand cells/cm^2), and the concentration of DMSO (1.0%, 0.75%, 0.50%, 0.25%, 0.10%, and 0%

DMSO) used for addition of the small molecules. Ultimate ALP activity, separation between ALP activity in cells grown in OG- media (negative controls) and OG+ media (positive controls) using Z-factor analysis [50] (see Statistics), and viability were used to identify the optimal conditions.

9.2.2 NINDS library screen

Once the HTS assay optimization was complete, the approach was used with the National Institute of Neurological Disorders and Stroke (NINDS) chemical library of 1040 small molecules (provided and listed by Microsource Discovery Systems, Inc, www.msdiscovery.com/ninds.html). The specific procedure used is shown in Figure 9.1. Cells were plated in each well at 12,000 cells/cm^2 (~720 cells per well) in 40 µl of growth media. The next day, the media was switched to OG- (for promoter studies) or OG+ (for inhibitor studies). Soluble factors were diluted in DMSO and added using a robotic liquid handling system (Evolution P3 Pipetting Platform, PerkinElmer) for a final concentration of 10 µM and 0.1% DMSO. In each plate the first and last two columns were reserved for positive (OG+ with 0.1% DMSO) and negative (OG- with 0.1% DMSO) controls. At day 5 (4 days in differentiating media), the media and soluble factors were refreshed. Finally, 7 days after soluble factors were added, cell viability and ALP activity were measured as described above.

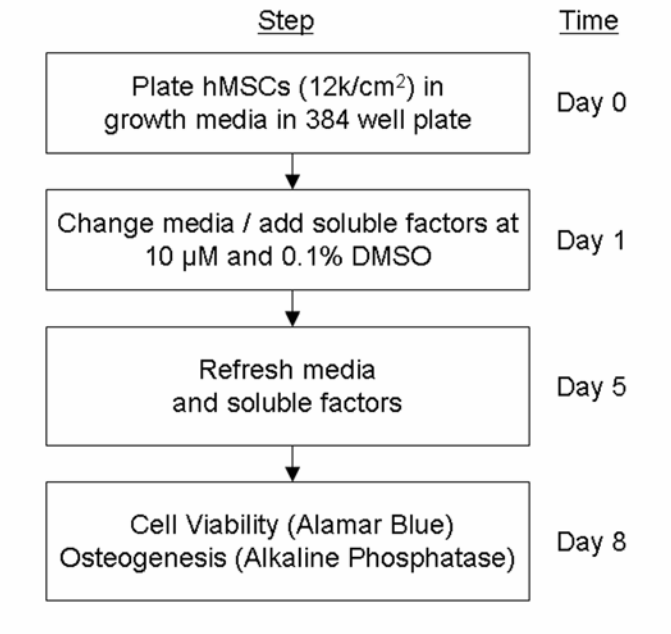

Figure 9.1 Flow chart for the HTS experiments. First, cells were plated in 384 well plates overnight to allow for attachment. On the next day, the media was changed to OG- for promoter and OG+ for inhibitor experiments, and soluble factors were added at a concentration of 10 µM. Four days later, the media was refreshed and factors were added again. After 7 days the cell viability was assessed using Alamar Blue and then the cells were lysed to determine their ALP activity.

Hits were determined only in plates with a Z-factor greater than 0.50 (see statistical analysis section below). For promoters, hits were wells that had an ALP activity level greater than 3 times the coefficient of variation (CV) above the negative control and a cell viability greater than 75% of the negative controls. For the inhibitors, hits were in wells that had an ALP activity level less the 3 times the CV below the

positive control and a cell viability greater than 75% of the positive controls. Promoters were then studied in a dose response experiment (3 to 100,000 nM) to confirm the osteogenic effects and determine the most potent hits.

9.2.3 Traditional cell culture

The most potent hits were studied further using traditional cell culture techniques. From the initial library, three factors were selected for further study: triamcinolone diacetate (TD), fludrocortisone acetate (FC), and Medrysone (Med). For these studies, hMSCs were plated on 6, 12, or 24 well plates at 6000 cells/cm^2 and cultured for up to 3 weeks. Cells were cultured in OG- (negative control), OG+ (positive controls), and 1, 10, and 100 nM concentrations of TD, FC, and Med. Cells were lysed in 150 µl of CelLytic M at 37° C for 20 minutes at 3, 7, 11, 14, and 21 days, spun down at 12,000 G for 15 minutes and the supernatant collected for analysis.

Cell proliferation was measured using the Quant-iT™ PicoGreen dsDNA assay (Invitrogen) in a 384 well plate. Samples were prepared by diluting 2 µl of cell lysate in 23 µl of TE buffer and reacting with 25 µl of working solution (40 µl of PicoGreen reagent with 8 ml TE buffer) and read at 480 nm excitation and 520 nm emission. The ALP activity was measured using the procedure as described previously with 5 µl of lysate. On some plates, cells were fixed in formalin after 3 weeks and calcium deposits were stained with Alizarin Red [51]. RNA was extracted at 14 and 21 days using TRIzol® (Invitrogen). Gene activation was measured using quantitative PCR for the osteogenic markers osteocalcin and CBFA1/Runx2 and normalized to the housekeeping

gene GAPDH (Table 9.1) followed by normalization to the cell pellet gene expression levels at day 0.

Table 9.1 Quantitative PCR primers and probes.

Gene	Forward Primer	Reverse Primer	Probe
GAPDH	AGGGCTGCTTTTAACTCTGGTAAA	GAATTTGCCATGGGTGGAAT	CCTCAACTACATGGTTTAC
Osteocalcin	CTGGCCGCACTTTGCAT	CTGCACCTTTGCTGGACTCT	CACCTGCCTGGCCAGC
CBFA1/Runx2	TGGACCTCGGGAACCCA	GCGGTCAGAGAACAAACTAGGTT	AAGGCACAGACAGAAGC

9.2.4 Culture on osteoconductive polymer

MSCs were also plated on thin films of the previously identified osteoconductive poly(β-amino ester), A6, synthesized by the reaction of isobutylamine and diethylene glycol diacrylate [7]. To form thin films, A6 macromer with photoinitiator 2,2-dimethoxy-2-phenyl acetophenone (DMPA, 0.5% (w/w), Sigma) was dissolved in ethanol at 1:2 (macromer:EtOH), added to 24-well plates (30 µl) and 6-well plates (125 µl), the ethanol was allowed to evaporate overnight, and the macromer was crosslinked with UV exposure in a nitrogen environment. MSCs were seeded on the films at a density of 6000 cells/cm^2 and cultured for up to 21 days. Cell proliferation, ALP activity, mineralization staining, and RNA were all assessed as described above.

9.2.5 Statistical analysis

The quality of assay was determined using Z-Factor analysis [50] comparing the positive controls to the negative controls.

$$Z = 1 - 3 * \frac{\sigma_p + \sigma_n}{\mu_p - \mu_n} \tag{9.1}$$

where σ_p and σ_n are the standard deviation of the positive and negative control values, respectively, and μ_p and μ_n are their means. A score > 0.5 indicates an excellent assay which delineates possible hits from statistical noise on a given plate. The percent activity of a given well was determined as:

$$\%Activity = \frac{x - \mu_n}{\mu_p - \mu_n} \times 100 \tag{9.2}$$

where x was the fluorescence reading of a given well. A 'hit' was determined as a factor whose percent activity was more than 3 times the (CV) above the negative control values for promoters and 3 times the CV below the positive control for inhibitors.

Statistical analysis for non-HTS studies were performed using ANOVA with Tukey's post-hoc among the groups with significance defined as a p-value less than 0.05. All values are reported as the mean and the standard deviation of the mean.

9.3 Results and Discussion

9.3.1 HTS assay development

The advantage of HTS is the ability to rapidly test many conditions while using fewer reagents on smaller platforms. This requires the optimization of assays and culture techniques that may not parallel larger scale procedures. For this study, the optimization of MSC culture conditions was completed to best demonstrate osteogenic differentiation, as shown in Figure 9.2. In normal culture, cell media is change once every 2-4 days to remove waste and provide new nutrients, but in HTS, because of the scale, these changes

are not always necessary. In this study, MSCs grown for 7 days in OG+ media with a media change at 4 days showed nearly a 3-fold increase in ALP expression than MSCs grown in OG+ media without refreshing the media (Figure 9.2A).

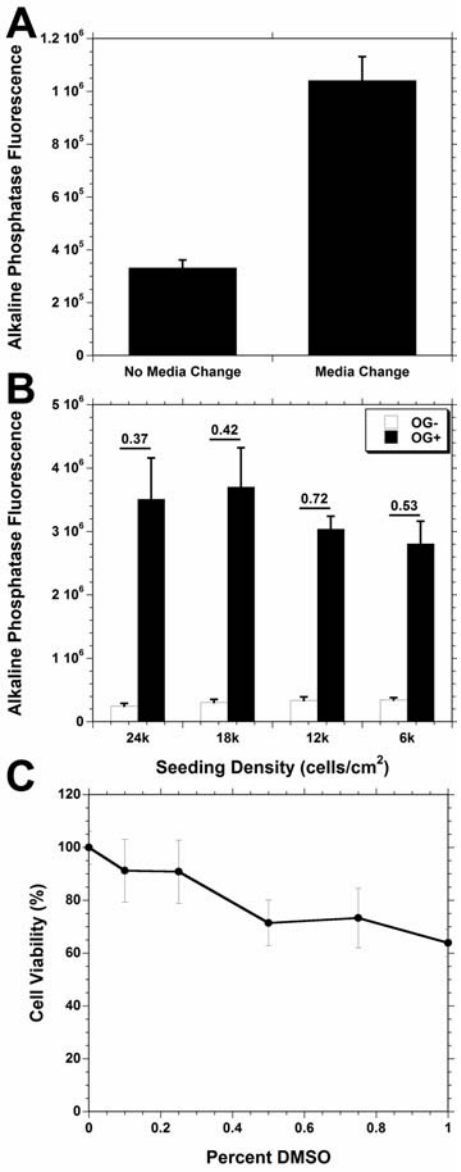

Figure 9.2 Assessment of conditions for optimal osteogenesis and viability of MSCs in 384-well plates. (A) ALP levels of MSCs grown in OG+ media for 7 days with a media change at 4 days and without. (B) Differences in ALP activity of the positive and negative controls for osteogenesis for various cell seeding densities, the Z-factor for each pairing is reported above each bar. (C) MSC sensitivity (reported as viability assessed with Alamar Blue) to DMSO since the small molecules are added in a DMSO solution.

Cell seeding density has been shown to be important in determining stem cell differentiation [5, 14], so cells were plated at 24, 18, 12, and 6 thousand cells/cm^2 in OG- and OG+ media to determine the density for optimal distinction of osteogenic differentiation. While there was several fold differences in ALP expression in all cases (Figure 9.2B), the lower variability of the cells seeded at 12000 cells/cm^2 led to a Z-factor of 0.72, while samples at a higher density failed to achieve a Z-factor score > 0.5. Finally, the soluble factors are dissolved in DMSO so the DMSO toxicity to MSCs was tested using a cell viability dose response study (Figure 9.2C). The cells were still ~90% viable at 0.1% and 0.25%, but dropped below 75% as DMSO quantities increased. To minimize cell death from DMSO, the final concentration of DMSO in all studies was 0.10%.

9.3.2 Identification of osteogenic promoters and inhibitors

After the cell culture conditions were optimized for HTS, the screening of the NINDS library was performed to identify potential promoters and inhibitors of hMSC osteogenic differentiation, sample plots are shown in Figure 9.3. From the screen of 1040 compounds, 36 potential promoters and 20 potential inhibitors were identified, as shown in Table 9.2, which met the requisite requirements as a 'hit'. Many of the inhibitors that met the criteria for low ALP, did so only by killing the cells, illustrating the importance of assessing cell viability. Many of the compounds stimulated cell viability greater than 100%, indicating potential proliferative changes due to the small molecules.

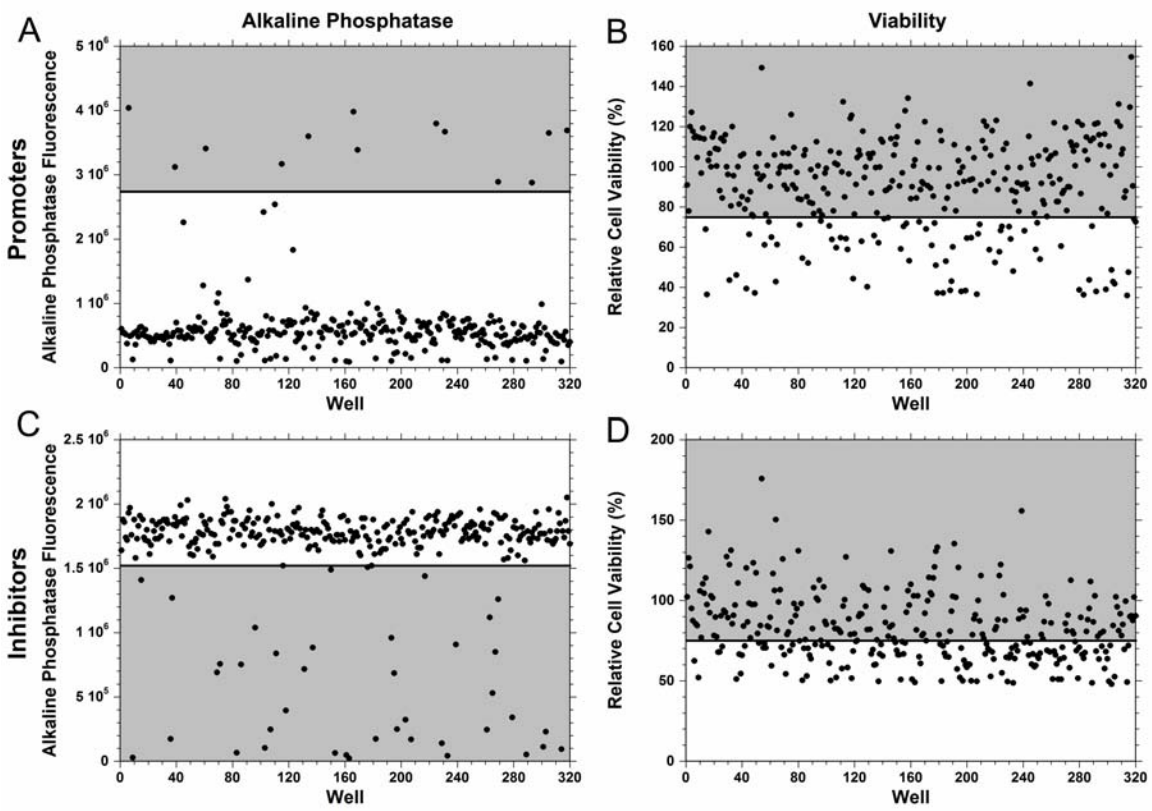

Figure 9.3 Sample plots of plates for promoter (A, B) and inhibitor (C, D) experiments. 'Hits' for promoters (gray) needed to have (A) ALP levels greater than 3 standard deviations above cells in OG- and (B) cell viability at least 75% of cells in OG-. 'Hits' for inhibitors (gray) needed to have (B) ALP levels less than 3 standard deviations below cells in OG+ and a (B) cell viability at least 75% of cells in OG+.

Table 9.2 Osteogenic promoters and inhibitors of hMSCs identified by the initial screen of the NINDS library.

Promoters	Inhibitors
Fludrocortisone Acetate	Griseofulvin
Triamcinolone Diacetate	Desoxycorticosterone Acetate
Avobenzone	Testosterone Propionate
Tuaminoheptane Sulfate	Testosterone
Trimebutine Maleate	Cyproterone Acetate
Fuorometholone	Ethacrynic Acid
Dienestrol	Hydroxyprogesterone Caproate
Halcinonide	Mechlorethamine
Isopropamide Iodide	Norethindrone
Medrysone	Norethynodrel
Chloroguanide Hydrochloride	Norgestrel
Protoveratrine A	Phentolamine Hydrochloride
Zolpidem	7,4'-Dihydroxyflavone
Ropinirole	Isotrentinon
Nateglinide	Menadione
Clopamide	Anethole
Minocycline Hydrochloride	Tannic Acid
Valacyclovir Hydrochloride	Clorsulon
Inositol	Securinine
Cholecalciferol	Hydroxyprogesterone
Nalbuphine Hydrochloride	
Olanzapine	
Aspirin	
Doxycycline Hydrochloride	
γ-Aminocutyric Acid	
Gentamicin Sulfate	
Medroxyprogesterone Acetate	
Furegrelate Sodium	
Antipyrine	
Acetanilide	
Ebselen	
Fenthion	
Cephalexin	
Tolazamide	
Aminohippuric Acid	
Spiperone	

The inhibitors display a wide range of molecules that include antifungals (griseofulvin), anticancer drugs (mechlorethamine, isotretinoin), and sex hormones. Interestingly, there are several progestins (hydroxyprogesterone, norgestrel, norethynodrel, norethindrone, cyproterone acetate) which act similarly as estrogens and

are often elevated during pregnancy. There is some indication that FOP disease is inhibited during pregnancy [52, 53], and these hits may be an indicator of how that occurs. Estrogen has been implicated as being beneficial to coronary heart disease (CHD) [54, 55] and inhibition of osteogenesis of pericytes could prevent vascular calcification [34], although recent concerns with CHD associated with hormone replacement therapy has further complicated this picture. At the same time, testosterone is also a potential inhibitor, even though testosterone and estrogen have both been shown to help prevent osteoporosis [56-58].

The promoters of hMSC osteogenic differentiation were also a diverse collection of factors. These included several glucocorticoids (hydrocortisone acetate, metamethasone, fluorometholone, halcinonide, medrysone) that could act along the same pathways as Dex. While many of the hits for osteopromoters were statistically improved from negative controls, many did not necessarily show improvement from OG+ media. The top hits were then screened again using the HTS assay for a dose response study which confirmed which factors were potent even at low concentrations.

9.3.3 Traditional cell culture

The most potent hits from the dose response study were mainly glucocorticoids, similar to Dex, though with different levels of potency [59] for the glucocorticoid receptor (GCR). Therefore, three compounds were chosen that had low GCR potency (Med), medium GCR potency (TD), and a potent mineralocorticoid (FC) to further investigate with traditional cell culture techniques. These compounds were tested for up to 21 days at 1, 10 and 100 nM concentrations and compared to the OG+ media with the

highly GCR potent 10 nM Dex. The cell proliferation was very similar in all cases (Figure 9.4A), but in samples with less than 100 nM of drug, the cells eventually detached from the tissue culture polystyrene (TCPS) in a sheet. This is common in MSCs grown in growth media if they are allowed to reach over confluency. Interestingly, this does not occurs in cells in OG+ media, likely due to the mineralized matrix being produced that alters how the cells are attached. Similarly, cells treated with 100 nM of the FC, TA, and Med all remained attached throughout the 3 week study. The ALP activity (Figure 9.4B) showed a slight increase in all of the 100 nM samples at 14 days and ~25% increase at 21 days as compared to cells grown in OG+ media.

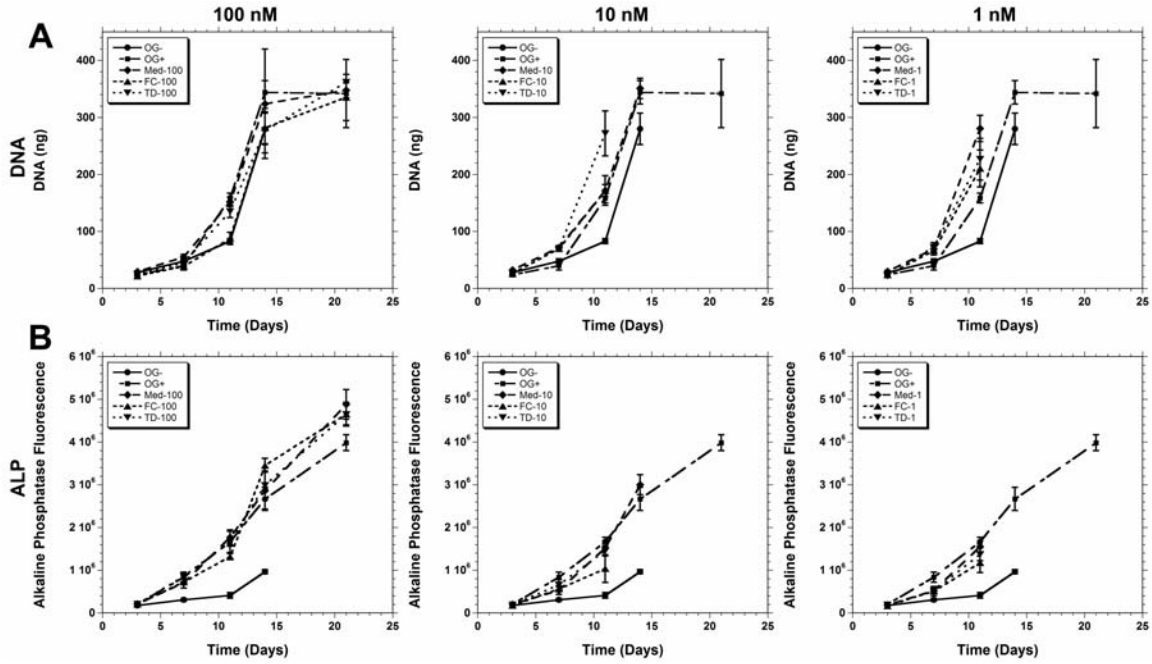

Figure 9.4 Temporal response of three of the top osteopromoters at various concentrations. The amount of (A) DNA and (B) ALP expression with exposure to 100, 10, and 1 nM of medrysone (Med), fludrocortisone acetate (FC), and triamcinolone diacetate (TD) is shown over a period of 21 days.

RNA expression of osteoblast genes of interest provides additional (Figure 9.5). CBFA1 is a transcription factor that has been associated with osteoblast differentiation, and while these levels are slightly elevated from the starting levels in MSCs, there does not appear to be much variation between the different inducers. While CBFA1 levels may be marginally increased, this assay does not investigate the activity post-translation, which is even more important in human cells [60]. Conversely, OC is a bone specific matrix protein, and the expression levels improve with time. At 21 days, the OC expression in the 100 nM TD samples was ~2.5 fold better than OG+ levels, which could indicate increased matrix production.

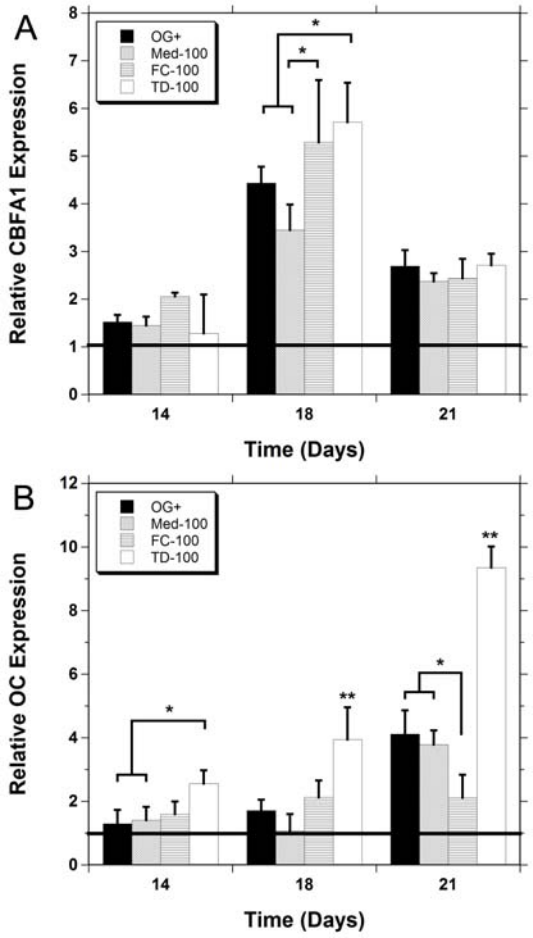

Figure 9.5 RNA expression of osteogenic markers. Expression of (A) CBFA1 and (B) osteocalcin after culture in OG+ media and 100 nM of medrysone (Med), fludrocortisone acetate (FC), and triamcinolone diacetate (TD) for 14, 18, and 21 days. * denotes significance between indicated groups, ** denotes significance from all groups at that time point.

Alizarin Red staining for calcium deposits, a component of bone matrix, show that only the MSCs grown in FC media deposit comparable matrix to OG+ positive controls (Figure 9.6). Very minimal staining was observed on the Med and TD samples, even though osteogenic genes were upregulated. Once again, this difference could be

due to a post-translational change in the cells that could further activate CBFA1. While levels of CBFA1 may be equal, their activity could be hampered or enhanced accordingly.

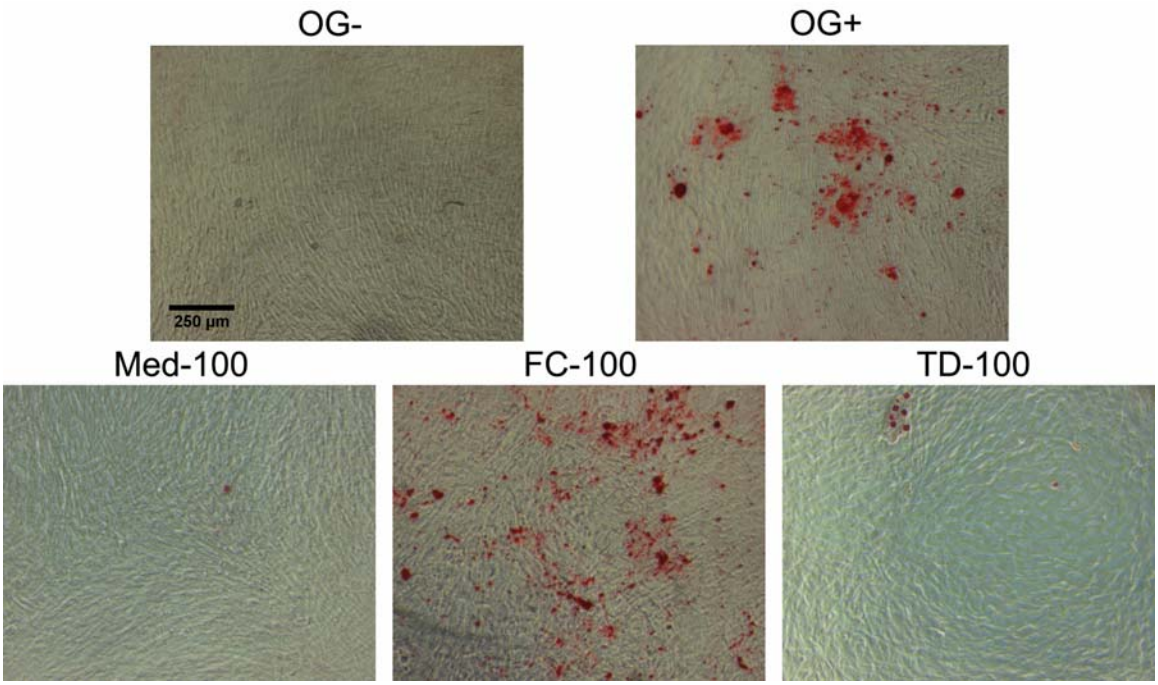

Figure 9.6 Alizarin Red staining of MSCs on TCPS. MSCs were grown for 21 days in OG-, OG+, and OG- media supplemented with 100 nM Med, FC, or TD and stained for calcium deposits, indicating mineralized matrix production.

These results show that in various ways, these new factors show improvement in some of the general indicators of osteogenic differentiation and mineralized matrix production from Dex. ALP expression is elevated 2 and 3 weeks for all 3 factors studied, with comparable cell survival and proliferation. Osteocalcin expression was increased for TD samples at all time points when compared in all other groups. Unfortunately, this

did not translate to improvements to mineralized matrix production, as shown in the Alizarin Red staining. Interestingly, the FC samples that showed the most staining for calcium deposits only had modest increases in CBFA1 and OC expression. This could be due to the time points assessed for analysis.

9.3.4 Osteopromoters on an osteoconductive polymer

The identification of these factors is just the first step in their potential use in tissue regeneration. Specifically, these drugs may be used in conjunction with an osteoconductive matrix to be released locally to recruit native progenitor cells and stimulate osteoblast differentiation. To test the synergy between osteogenic soluble factors and an osteoconductive matrix, MSCs were cultured on thin films of a previously identified osteoconductive PBAE, A6, and grown in the OG- media plus the best case inducers (FC, TD, and Med at 100 nM).

The cell proliferation was reduced on cells grown on the A6 compare to cells grown on TCPS, though there was steady growth on the films until 14 days, then there was some cell detachment in the OG-, Med, and TD samples (Figure 9.7). The OG+ and FC cell numbers remained steady over the last week. This stability was shown with a steady rise in the ALP expression in OG+ and FC throughout the experiment, while the other samples saw a decline with detachment. The OG- ALP expression overlapped the OG+ expression up to 14 days, but this may be an artifact of the larger number of cells in the OG- samples. Normalizing the ALP expression value to the DNA, there is a clear difference between the treated groups and the negative control (OG-). The FC samples showed the largest normalized ALP values throughout the experiment.

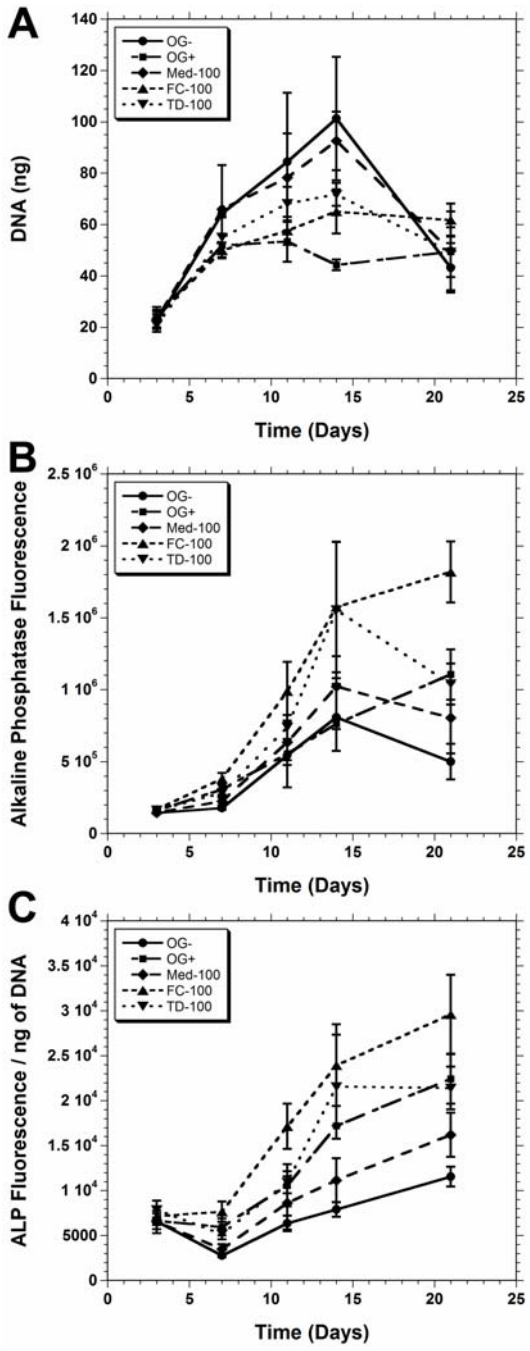

Figure 9.7 Temporal response of three of the top osteopromoters. Promoter were exposed at 100 nM to MSCs cultured on the surface of an osteoconductive PBAE, A6, and investigated for (A) cell proliferation (B) ALP activity, and (C) ALP expression normalized to amount of DNA.

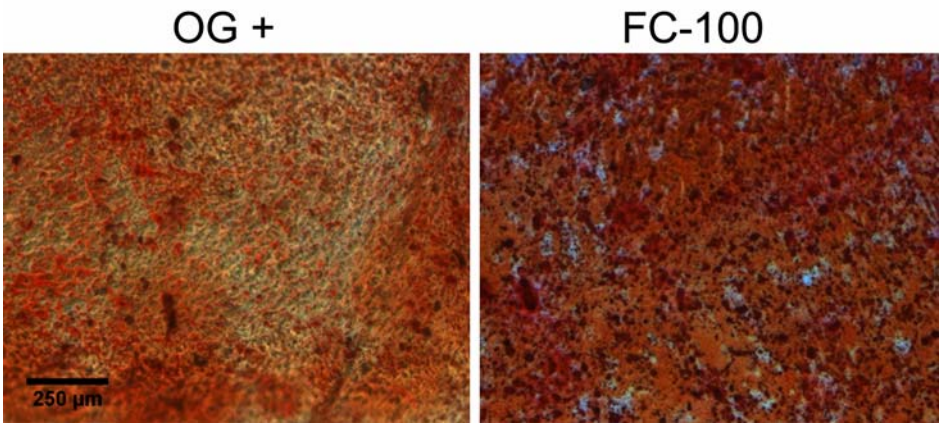

Figure 9.8 Alizarin Red staining of MSCs on A6 thin films. MSCs were grown for 21 days in OG+ and OG- media supplemented with 100 nM FC or TD and stained for calcium deposits indicating mineralized matrix production. The light orange coloring is Alizarin Red S absorbed into the polymer.

Since the FC showed continued cell growth and the highest levels of ALP activity, the mineralization on this surface was assessed. The cells were grown on thin films of A6 for 21 days and stained with Alizarin Red (Figure 9.8). The staining showed the presence of many nodules on the FC treated cells, which was comparable to the staining observed on the Dex treated MSCs on A6. FC was able to stimulate mineralized matrix on both TCPS and A6. And unlike Dex, FC is potent mineralocorticoid, which may demonstrate another pathway to stimulate osteogenic differentiation of stem cells.

9.4 Conclusions

The use of HTS techniques has long been employed by the pharmaceutical industry to more rapidly discover drugs that could be relevant to a given disease, but this

technology has only been minimally applied to tissue engineering. For this study, an assay for the osteogenic differentiation of MSCs was developed to screen a library of small molecules for their potential as promoters and inhibitors of osteogenesis. The osteopromoters from this library were further investigated using standard culture techniques to verify that these compounds drive cellular differentiation. These hits showed some improvement in the expression of ALP, osteogenic gene expression, and matrix mineralization when compared to the standard Dex. When FC was used in conjunction with the films of an osteoconductive polymer, mineralized matrix staining was observed. This work illustrates the ability of using HTS to more rapidly investigate new compounds (or new applications of old compounds) for tissue engineering purposes.

References

[1] Huang AH, Motlekar NA, Stein A, Diamond SL, Shore EM, Mauck RL. High-throughput screening for modulators of mesenchymal stem cell chondrogenesis. Annals of Biomedical Engineering 2008;36(11):1909-1921.

[2] Erickson IE, Huang AH, Chung C, Li RT, Burdick JA, Mauck RL. Differential Maturation and Structure-Function Relationships in Mesenchymal Stem Cell- and Chondrocyte-Seeded Hydrogels. Tissue Engineering Part A 2009;15(5):1041-1052.

[3] Chung C, Burdick JA. Influence of Three-Dimensional Hyaluronic Acid Microenvironments on Mesenchymal Stem Cell Chondrogenesis. Tissue Engineering Part A 2009;15(2):243-254.

[4] Benoit DSW, Schwartz MP, Durney AR, Anseth KS. Small functional groups for controlled differentiation of hydrogel-encapsulated human mesenchymal stem cells. Nature Materials 2008;7(10):816-823.

[5] Treiser MD, Yang EH, Gordonov S, Cohen DM, Androulakis IP, Kohn J, et al. Cytoskeleton-based forecasting of stem cell lineage fates. Proceedings of the National Academy of Sciences of the United States of America;107(2):610-615.

[6] Wu X, Ding S, Ding Q, Gray NS, Schultz PG. A small molecule with osteogenesis-inducing activity in multipotent mesenchymal progenitor cells. Journal of the American Chemical Society 2002;124(49):14520-14521.

[7] Brey DM, Chung C, Hankenson KD, Garino JP, Burdick JA. Identification of osteoconductive and biodegradable polymers from a combinatorial polymer library. Journal of Biomedical Materials Research Part A 2010;93A(2):807-816.

[8] Jaiswal N, Haynesworth SE, Caplan AI, Bruder SP. Osteogenic differentiation of purified, culture-expanded human mesenchymal stem cells in vitro. Journal of Cellular Biochemistry 1997;64(2):295-312.

[9] Engler AJ, Sen S, Sweeney HL, Discher DE. Matrix elasticity directs stem cell lineage specification. Cell 2006;126(4):677-689.

[10] Nuttelman CR, Tripodi MC, Anseth KS. In vitro osteogenic differentiation of human mesenchymal stem cells photoencapsulated in PEG hydrogels. Journal of Biomedical Materials Research Part A 2004;68A(4):773-782.

[11] Tao H, Rao RN, Ma DDF. Cytokine-induced stable neuronal differentiation of human bone marrow mesenchymal stem cells in a serum/feeder cell-free condition. Development Growth & Differentiation 2005;47(6):423-433.

[12] Wislet-Gendebien S, Hans G, Leprince P, Rigo JM, Moonen G, Rogister B. Plasticity of cultured mesenchymal stem cells: Switch from nestin-positive to excitable neuron-like phenotype. Stem Cells 2005;23(3):392-402.

[13] Neuhuber B, Gallo G, Howard L, Kostura L, Mackay A, Fischer I. Reevaluation of in vitro differentiation protocols for bone marrow stromal cells: Disruption of actin cytoskeleton induces rapid morphological changes and mimics neuronal phenotype. Journal of Neuroscience Research 2004;77(2):192-204.

[14] Ruiz SA, Chen CS. Emergence of Patterned Stem Cell Differentiation Within Multicellular Structures. Stem Cells 2008;26(11):2921-2927.

[15] Sasano Y, Ohtani E, Narita K, Kagayama M, Murata M, Saito T, et al. Bmps Induce Direct Bone-Formation in Ectopic Sites Independent of the Endochondral Ossification Invivo. Anatomical Record 1993;236(2):373-380.

[16] Friedman MS, Long MW, Hankenson KD. Osteogenic differentiation of human mesenchymal stem cells is regulated by bone morphogenetic protein-6. Journal of Cellular Biochemistry 2006;98(3):538-554.

[17] Viereck V, Siggelkow H, Tauber S, Raddatz D, Schutze N, Hufner M. Differential regulation of Cbfa1/Runx2 and osteocalcin gene expression by vitamin-D3, dexamethasone, and local growth factors in primary human osteoblasts. Journal of Cellular Biochemistry 2002;86(2):348-356.

[18] Li G, Cui YX, McIlmurray L, Allen WE, Wang HL. RhBMP-2, rhVEGF(165), rhPTN and thrombin-related peptide, TP508 induce chemotaxis of human osteoblasts and microvascular-endothelial cells. Journal of Orthopaedic Research 2005;23(3):680-685.

[19] Diefenderfer DL, Osyczka AM, Reilly GC, Leboy PS. BMP responsiveness in human mesenchymal stem cells. Connective Tissue Research 2003;44:305-311.

[20] Kanczler JM, Ginty PJ, White L, Clarke NMP, Howdle SM, Shakesheff KM, et al. The effect of the delivery of vascular endothelial growth factor and bone morphogenic protein-2 to osteoprogenitor cell populations on bone formation. Biomaterials;31(6):1242-1250.

[21] Shui CX, Spelsberg TC, Riggs BL, Khosla S. Changes in Runx2/Cbfa1 expression and activity during osteoblastic differentiation of human bone marrow stromal cells. Journal of Bone and Mineral Research 2003;18(2):213-221.

[22] Gruber R, Graninger W, Bobacz K, Watzek G, Erlacher L. BMP-6-induced osteogenic differentiation of mesenchymal cell lines is not modulated by sex steroids and resveratrol. Cytokine 2003;23(4-5):133-137.

[23] Osyczka AM, Diefenderfer DL, Bhargave G, Leboy PS. Different effects of BMP-2 on marrow stromal cells from human and rat bone. Cells Tissues Organs 2004;176(1-3):109-119.

[24] Kakudo N, Kusurnoto K, Wang YB, Iguchi Y, Ogawa Y. Immunolocalization of vascular endothelial growth factor on intramuscular ectopic osteoinduction by bone morphogenetic protein-2. Life Sciences 2006;79(19):1847-1855.

[25] Okubo Y, Bessho K, Fujimura K, Konishi Y, Kusumoto K, Ogawa Y, et al. Osteoinduction by recombinant human bone morphogenetic protein-2 at intramuscular, intermuscular, subcutaneous and intrafatty sites. International Journal of Oral and Maxillofacial Surgery 2000;29(1):62-66.

[26] Kakudo N, Kusumoto K, Kuro A, Ogawa Y. Effect of recombinant human fibroblast growth factor-2 on intramuscular ectopic osteoinduction by recombinant human bone morphogenetic protein-2 in rats. Wound Repair and Regeneration 2006;14(3):336-342.

[27] Okubo Y, Bessho K, Fujimura K, Kusumoto K, Ogawa Y, Tani Y, et al. Comparative study of intramuscular and intraskeletal osteogenesis by recombinant human bone morphogenetic protein-2. Oral Surgery Oral Medicine Oral Pathology Oral Radiology and Endodontics 1999;87(1):34-38.

[28] Peng HR, Usas A, Olshanski A, Ho AM, Gearhart B, Cooper GM, et al. VEGF improves, whereas sFlt1 inhibits, BMP2-induced bone formation and bone

healing through modulation of angiogenesis. Journal of Bone and Mineral Research 2005;20(11):2017-2027.

[29] Yasko AW, Lane JM, Fellinger EJ, Rosen V, Wozney JM, Wang EA. The Healing of Segmental Bone Defects, Induced by Recombinant Human Bone Morphogenetic Protein (Rhbmp-2) - a Radiographic, Histological, and Biomechanical Study in Rats. Journal of Bone and Joint Surgery-American Volume 1992;74A(5):659-670.

[30] Giannoudis PV, Einhorn TA. Bone morphogenetic proteins in musculoskeletal medicine. Injury 2009;40(Supplement 3):S1-S3.

[31] Schmidmaier G, Capanna R, Wildemann B, Beque T, Lowenberg D. Bone morphogenetic proteins in critical-size bone defects: what are the options? Injury 2009;40(Supplement 3):S39-S43.

[32] Vukicevic S, Grgurevic L. BMP-6 and mesenchymal stem cell differentiation. Cytokine & Growth Factor Reviews 2009;20(5-6):441-448.

[33] Peters A, Brey DM, Burdick JA. High-Throughput and Combinatorial Technologies for Tissue Engineering Applications. Tissue Engineering Part B-Reviews 2009;15(3):225-239.

[34] Kirton JP, Wilkinson FL, Canfield AE, Alexander MY. Dexamethasone downregulates calcification-inhibitor molecules and accelerates osteogenic differentiation of vascular pericytes implications for vascular calcification. Circulation Research 2006;98(10):1264-1272.

[35] Kuznetsov SA, Krebsbach PH, Satomura K, Kerr J, Riminucci M, Benayahu D, et al. Single-colony derived strains of human marrow stromal fibroblasts form bone

after transplantation in vivo. Journal of Bone and Mineral Research 1997;12(9):1335-1347.

[36] Meinel L, Karageorgiou V, Fajardo R, Snyder B, Shinde-Patil V, Zichner L, et al. Bone tissue engineering using human mesenchymal stem cells: Effects of scaffold material and medium flow. Annals of Biomedical Engineering 2004;32(1):112-122.

[37] Otto WR, Rao J. Tomorrow's skeleton staff: mesenchymal stem cells and the repair of bone and cartilage. Cell Proliferation 2004;37(1):97-110.

[38] Pittenger MF, Mackay AM, Beck SC, Jaiswal RK, Douglas R, Mosca JD, et al. Multilineage potential of adult human mesenchymal stem cells. Science 1999;284(5411):143-147.

[39] Adachi JD. Corticosteroid-induced osteoporosis. American Journal of the Medical Sciences 1997;313(1):41-49.

[40] Sawin PD, Dickman CA, Crawford NR, Melton MS, Bichard WD, Sonntag VKH. The effects of dexamethasone on bone fusion in an experimental model of posterolateral lumbar spinal arthrodesis. Journal of Neurosurgery 2001;94(1):76-81.

[41] Augat P, Simon U, Liedert A, Claes L. Mechanics and mechano-biology of fracture healing in normal and osteoporotic bone. Osteoporos International 2005;16(Suppl 2):S36-43.

[42] Walsh S, Jordan GR, Jefferiss C, Stewart K, Beresford JN. High concentrations of dexamethasone suppress the proliferation but not the differentiation or further

maturation of human osteoblast precursors in vitro: relevance to glucocorticoid-induced osteoporosis. Rheumatology 2001;40(1):74-83.

[43] Kim H, Suh H, Jo SA, Kim HW, Lee JM, Kim EH, et al. In vivo bone formation by human marrow stromal cells in biodegradable scaffolds that release dexamethasone and ascorbate-2-phosphate. Biochemical and Biophysical Research Communications 2005;332(4):1053-1060.

[44] Kim H, Kim HW, Suh H. Sustained release of ascorbate-2-phosphate and dexamethasone from porous PLGA scaffolds for bone tissue engineering using mesenchymal stem cells. Biomaterials 2003;24(25):4671-4679.

[45] Lounev VY, Ramachandran R, Wosczyna MN, Yamamoto M, Maidment ADA, Shore EM, et al. Identification of Progenitor Cells That Contribute to Heterotopic Skeletogenesis. Journal of Bone and Joint Surgery-American Volume 2009;91A(3):652-663.

[46] Shore EM, Xu MQ, Feldman GJ, Fenstermacher DA, Brown MA, Kaplan FS. A recurrent mutation in the BMP type I receptor ACVR1 causes inherited and sporadic fibrodysplasia ossificans progressiva. Nature Genetics 2006;38(5):525-527.

[47] Zhao YX, Ding S. A high-throughput siRNA library screen identifies osteogenic suppressors in human mesenchyrnal stem cells. Proceedings of the National Academy of Sciences of the United States of America 2007;104(23):9673-9678.

[48] Ding S, Wu TYH, Brinker A, Peters EC, Hur W, Gray NS, et al. Synthetic small molecules that control stem cell fate. Proceedings of the National Academy of Sciences of the United States of America 2003;100(13):7632-7637.

[49] Underhill GH, Bhatia SN. High-throughput analysis of signals regulating stem cell fate and function. Current Opinion in Chemical Biology 2007;11(4):357-366.

[50] Zhang JH, Chung TDY, Oldenburg KR. A simple statistical parameter for use in evaluation and validation of high throughput screening assays. Journal of Biomolecular Screening 1999;4(2):67-73.

[51] Wang YH, Liu YL, Maye P, Rowe DW. Examination of mineralized nodule formation in living osteoblastic cultures using fluorescent dyes. Biotechnology Progress 2006;22(6):1697-1701.

[52] Thornton YS BS, Lebowitz N. A viable pregnancy in a patient with myositis ossificans progressiva. Am J Obstet Gynecol 1987;156(3):577-578.

[53] Fox S KA, Mootabar H, Greenwald EF. Myositis ossificans progressiva and pregnancy. Ostet Gynecol 1987;69(3 Pt 2):453-455.

[54] Klinge CM, Blankenship KA, Risinger KE, Bhatnagar S, Noisin EL, Sumanasekera WK, et al. Resveratrol and estradiol rapidly activate MAPK signaling through estrogen receptors alpha and beta in endothelial cells. Journal of Biological Chemistry 2005;280(9):7460-7468.

[55] Solomon CG, Dluhy RG. Rethinking postmenopausal hormone therapy. New England Journal of Medicine 2003;348(7):579-580.

[56] Riggs BL, Khosla S, Melton LJ. Sex steroids and the construction and conservation of the adult skeleton. Endocrine Reviews 2002;23(3):279-302.

[57] Snyder PJ, Peachey H, Hannoush P, Berlin JA, Loh L, Holmes JH, et al. Effect of testosterone treatment on bone mineral density in men over 65 years of age. Journal of Clinical Endocrinology & Metabolism 1999;84(6):1966-1972.

[58] Riggs BL, Khosla S, Melton LJ. A unitary model for involutional osteoporosis: Estrogen deficiency causes both type I and type II osteoporosis in postmenopausal women and contributes to bone loss in aging men. Journal of Bone and Mineral Research 1998;13(5):763-773.

[59] Grossmann C, Scholz T, Rochel M, Bumke-Vogt C, Oelkers W, Pfeiffer AFH, et al. Transactivation via the human glucocorticoid and mineralocorticoid receptor by therapeutically used steroids in CV-1 cells: a comparison of their glucocorticoid and mineralocorticoid properties. European Journal of Endocrinology 2004;151(3):397-406.

[60] Rajgopal A, Young DW, Mujeeb KA, Stein JL, Lian JB, van Wijnen AJ, et al. Mitotic control of RUNX2 phosphorylation by both CDK1/cyclin B kinase and PP1/PP2A phosphatase in osteoblastic cells. Journal of Cellular Biochemistry 2007;100(6):1509-1517.

CHAPTER 10: *Summary and Future Directions*

10.1 Summary

Tissue engineering paradigms involve the combination of cells, signaling factors, and scaffold materials in order to drive the replacement or repair of damaged tissues. As discussed in Chapters 1 and 3, the development of these different components for tissue engineering has traditionally been a methodical and iterative process due to the complexity and cost of materials and factors involved. The emergence of combinatorial chemistry and HTS techniques offers opportunities to more efficiently develop new tissue engineering systems. To that end, the goal of this thesis was to use these tools to identify and develop materials from a combinatorial library of poly(β-amino ester)s (PBAEs) for application in tissue engineering, using bone tissue engineering as a representative example. Additionally, HTS techniques were used to identify new promoters and inhibitors of osteogenesis, with the goal of using the osteopromoters with the PBAE to improve mineralized matrix production.

The PBAE library of photocrosslinkable and biodegradable materials was introduced in Chapter 4. This library of commercially available monomers is formed through an addition reaction of amines and diacrylates at ratios that led to acrylated terminated molecules. These molecules could then be photopolymerized into dense networks and tested for physical properties. The degradation of these materials varied greatly with chemistry, with some materials degrading completely within 24 hours while others barely degraded over a period of 3 months. The degradation profiles also greatly

varied with chemistry, with some materials degrading rapidly at first then reaching a plateau and other demonstrating a more linear rate of degradation. Ultimately, this approach led to a library of materials with great diversity in degradation and mechanics.

In Chapters 5 and 6, specific examples of the library were chosen to further develop the library and demonstrate ways in which properties could be further tuned. By varying the ratio of diacrylates to amines, the molecular weight of the monomers could be altered. Higher ratios led to shorter macromers, and therefore more densely crosslinked networks with stronger material properties and slower degradation rates, whereas lower ratios led to higher molecular weights and opposite trends. Similarly, the addition of a triacrylate increased the branching of the macromer and led to more densely crosslinked networks. This technique was able to double the mechanical properties, which were largely decoupled from the degradation behavior. For the first time, osteoblast model cells were cultured on thin films of PBAEs and were shown to attach and proliferate. Poragen leaching techniques were also developed to produce highly porous structures that are useful as scaffolding for tissue engineering.

The library was then screened in Chapter 7 to identify an osteoconductive material. Screening parameters included the physical properties of the materials (i.e., degradation and mechanics), and *in vitro* MSC cell proliferation, ALP expression, and expression of osteogenic genes. The optimial material was identified as A6, a combination of diethylene glycol diacrylate (A) and isobutylamine (6). This material showed minimal inflammation when implanted subcutaneously into rats and tissue rapidly infiltrated into a porous scaffold; however, there was no evidence of bone formation in the pores, unless BMP-2 was introduced into the pores to induce

mineralization. These scaffolds were also implanted intramuscularly and ectopic bone was observed in samples with BMP-2, but not in samples without BMP-2. These same scaffolds were then used to fill a critical-sized cranial defect where, once again, new bone was formed throughout the scaffold that was loaded with BMP-2, but there was only minimal bone formation in the samples scaffold alone or empty defects. This information leads to the conclusion that the A6 material has osteoconductive properties, but is only inductive with the use of additional osteoinductive signals.

In Chapter 8, the same scaffolding system was used in a rat femur window defect to investigate healing in a long bone. The window defect was not critical-sized as with the cranial defect, so this made it difficult to show much improvement in the healing in the treated cases versus the natural healing of the empty defect. At 3 and 10 weeks, there was no difference in bone formation between the empty defects and the defects filled with A6 scaffold loaded with BMP-2. However, defects with unloaded scaffolds produced significantly less bone than the empty defect alone, yet was able to template bone formation better. This implicates that the scaffold may actually impede healing at this point if it degrades slower than the wound heals. Interestingly, there were no significant differences between the mechanical properties of the tested groups. There was also histological evidence that the bone matrix in the intact bone actually thickens and may compensate for the loss of material in the window defect.

The use of BMP-2 has limitations due to the high cost of production, the limitations of human sources for clinical use, and limited potency in clinical trials in humans compared to studies in rats. Therefore, new factors were explored using HTS techniques for their promotion and inhibitory effects on the osteogenesis of MSCs. This

study identified 36 potential promoters and 20 potential inhibitors of MSCs from a library of 1040 soluble compounds. Of those promoters, three of the most potent were tested using traditional cell culture techniques and several indicators of osteogenic differentiation were increased, including ALP and the gene expression of CBFA1 and OC. However, staining for mineralization showed that only FC showed consistent formation of calcium deposits. When used in conjunction with thin films of A6, calcium nodule formation was improved in the positive control and in FC supplemented media.

These studies show a process for the characterization of a combinatorial library of materials, the screening of that library to identify a material for bone tissue scaffolding, and the identification of new factors to improve osteogenic differentiation of MSCs using HTS techniques. The improvement and acceleration of these steps will be important in the future as more combinatorial libraries are formed as potential sources for scaffolding materials. The use of HTS tools will be increasingly relied upon to rapidly process factors and materials to optimize parameters for tissue engineering.

10.2 Limitations and Future Directions

10.2.1 HTS of combinatorial library of materials

While the procedures to characterize the PBAE library of materials utilized some techniques for rapid assessment, the methods for screening the materials for the identification of an osteoconductive matrix used standard, large scale (and slow) methods. The library was screened using the degradation of bulk polymers to narrow the list of candidates, then cells were grown on thin films of PBAEs on standard 12- and 24-

well plates to test cell viability and ALP activation. It would be advantageous to use a system that could more rapidly assess the cellular interactions with the materials.

To this end, some preliminary work was completed on fabricating microwells in glass slides that could similarly be lined with thin films of materials to study 2D cellular interactions. While these studies were unsuccessful for issues including nonspecific cell attachment to the well material, the development of these methods would be advantageous in screening larger libraries or modifications to the libraries. The PBAE library was shown to have a wide range of properties at one ratio of diacrylate to amine, and then we showed that these properties could be further tuned by adjusting some of the macromer characteristics. Therefore the screening of materials by degradation could have cut off more potent candidates at different ratios.

Being able to screen more materials on a smaller platform affords many more opportunities for discovery. Materials do not have to be prescreened for arbitrary reasons or gradients of copolymers and other modifications can more extensively investigated. While these materials failed to demonstrate any osteoinductive properties, several investigators have shown how the addition of tethers, such as phosphates or RGD, can influence stem cell differentiation and attachment. These modifications can be assessed in gradients or in parallel to other material changes to rapidly optimize conditions for a given application.

This work would also require different assay techniques for determination of osteogenesis. While many of these studies have used a biochemical assay of ALP, this would not be possible in a microwell array that shares common media. Plus, while ALP is an indicator of osteogenic differentiation, it is certainly not exclusive as it is also

expressed in kidney and liver cells. In our lab, we have tried inserting an OC reporter gene into cells so that they fluoresce when OC is expressed. This would allow for a noninvasive/nondestructive technique to indicate osteogenesis. Some of the limitations include that MSCs are very difficult to stably transfect, so there was much difficulty in successfully transfecting the cells. Also, while OC is much more specific to bone tissue, it is also expressed fairly late in the process of osteogenesis. This may require long incubation times that may lead to cells detaching or experiments that are no longer as rapid as desired.

Obviously, this would also help screen the same library for other applications. The use in bone tissue engineering was just a sample application picked for these studies. The material could be used in other tissue engineering applications such as tendon by using electrospun fibers, or directed neuronal growth by using patterned substrates. In each of these cases, the ideal material would likely need to be identified according to the parameters of the tissue, so this process would benefit from ways to more rapidly assess ideal candidates.

10.2.2 In vivo evaluation

For these studies, several rat animal models were used to evaluate biocompatibility and bone formation. The subcutaneous model allows for the assessment of the body's reaction to a foreign body, but there is not much assessment of the material's osteogenic properties. The use of the intramuscular implant to study ectopic bone formation was beneficial in showing that the scaffold alone would not drive osteogenesis and there was a need for an osteoinductive factor. The critical-sized cranial

defect was excellent at showing the benefits of the copolymer with BMP-2 in driving bone formation throughout the defect and the limited healing that occurs otherwise. While the femur window defect results may indicate that the degradation is too slow for certain applications of the A6 scaffold, further work needs to be performed to assess this.

To better show the difference between the healing of long bone and flat bone, it would likely have been better to use a segmental defect model instead of the window defect. This method would increase the complexity of the system due to the need for fixation of the bone, but the critical-size defect would make improvements in healing more apparent. The window defect heals rapidly on its own, so there was never a difference between natural healing and the A6 scaffold with BMP-2. Also, the segmental defect has been consistently associated with endochondral ossification, so this would satisfy the desire to investigate the effect of the scaffold on both modes of bone formation.

Methods for incorporating the identified osteopromoters into the scaffold for *in vivo* bone formation should also be explored. Some of the hits were loaded into collagen gels in the A6 copolymers and implanted into rats intramuscularly for 4 weeks. Unlike the samples implanted with BMP-2, there was no new bone formation. It is unclear whether this is due to the lack of osteogenic effect *in vivo* of these factors or if the release of the drug was not sustained long enough for the desire effect. The release of small molecules from collagen was likely very rapid, and this burst release was not enough to recruit cells and cause them to differentiate. Either swelling the drug into the hydrophobic A6 scaffolds or somehow tethering them to the structure itself may help the release to be more sustained.

Finally, in many ways, it is difficult to determine how much the presence of the A6 scaffold was beneficial in the bone regeneration. This could be related to unknowns in the design criteria used in the screening process. Ideally, selection and analysis of other PBAEs could help illustrate the importance of the A6 scaffold to the formation of this bone tissue. If there is equivalent bone growth in other cases, it calls into question whether the effects we see are specific to A6.

10.2.3 Development of HTS inhibitors

The osteopromoters found in the HTS study have a clear use in bone tissue regeneration and stem cell differentiation. The use of inhibitors may be less apparent at first. In the disease of fibrodysplasia ossificans progressiva (FOP) there is a genetic defect of a BMP receptor, ACVR-1, that causes connective tissue to spontaneously form bone. This can often lead to disastrous consequences where joints fuse or bone processes are formed that have issues including the growth of the spine and rib cage. Methods to prevent or ameliorate the amount of bone growth would be beneficial to these patients.

Therefore, we have attempted to find an ideal model of FOP cells to screen for inhibitors of this effect using the HTS process we developed. First, cell transfection using the mutated gene was attempted, but MSCs have largely been difficult to transfect. So after many failed attempts, a new cell line was explored. Stem cells from human exfoliated deciduous teeth (SHED) are one of the few cells lines that can be collected from patients with FOP. Normal extraction methods can lead to the formation of more spontaneous bone growth, so care is taken to avoid any invasive procedures. The isolation of stem cells from ‘baby’ teeth offers a source that can be used to directly study

cells with the mutated gene. Unfortunately, testing of the HTS system with healthy SHEDs was not able to show the same specificity between osteogenic positive and negative controls so that it was not possible to statistically satisfy the Z-factor score needed to demonstrate hits from noise. This could be due to the SHED cells being a more heterogeneous population of cells, and not enough were true stem cells, or that they were already predisposed to osteogenic differentiation, and populations were hard to distinguish. Clearly, more work could be pursued in this area.

10.3 Conclusions

With more combinatorial libraries and more methods for modifying material or cell behavior being developed, methods for rapid optimization will be increasing important. In this work, a new combinatorial library of PBAEs was characterized to assess how changes in chemistry, macromer length, and macromer branching affect degradation, mechanical properties, and cellular interactions. Methods were then developed to screen this library to identify an osteoconductive material. The best candidate, A6, was then shown in several animal models to support bone regeneration when used in conjunction with BMP-2. Finally, HTS techniques were used to identify new promoters and inhibitors of osteogenesis in MSCs. Overall, this work represents a process in which libraries are screened for a given application, and as combinatorial chemistry continues to be developed, these methods will be crucial in rapidly optimizing materials and conditions for stem cell differentiation towards a range of applications.